

NCC2-833

FINAL
APRIL 95

**Rotorcraft Flight Control Design Using Quantitative Feedback
Theory and Dynamic Crossfeeds**

**A Thesis Presented to the Faculty of
California Polytechnic State University
San Luis Obispo**

FINAL
10-08-00
OCT
6201
p-87

**In Partial Fulfilment
of the Requirements for the Degree of
Master of Science in Aeronautical Engineering**

**by
Rendy P. Cheng
January 30, 1995**

**Authorization for Reproduction
of Master's Thesis**

I grant permission for the reproduction of this thesis in its entirety or any of its parts,
without further authorization from me.

Randy P. Cheng
Signature

2-14-95
Date

Approval Page

Title

Rotorcraft Flight Control Design Using QFT and Dynamic Crossfeeds

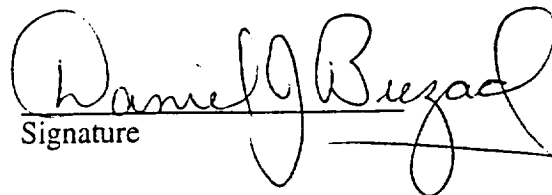
Author

Rendy P. Cheng

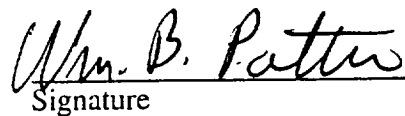
Date Submitted

January 30, 1995

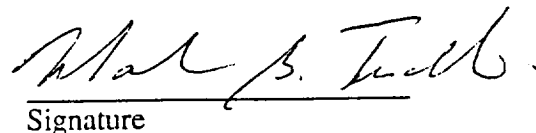
Daniel J. Biezad
Thesis Advisor
Aeronautical Engineering
Cal. Poly., San Luis Obispo


Signature

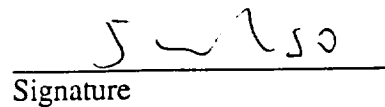
William Patterson
Committee Member
Mechanical Engineering
Cal. Poly., San Luis Obispo


Signature

Mark B. Tischler
Committee Member / Research Sponsor
U.S. Army Aeroflightdynamics Directorate
Ames Research Center, Moffett Field


Signature

Jin Tso
Committee Member
Aeronautical Engineering
Cal. Poly., San Luis Obispo


Signature

ABSTRACT**Rotorcraft Flight Control Design Using QFT and Dynamic Crossfeeds****Rendy P. Cheng****January 30, 1995**

A multi-input, multi-output controls design with robust crossfeeds is presented for a rotorcraft in near-hovering flight using Quantitative Feedback Theory (QFT). Decoupling Criteria are developed for dynamic crossfeed design and implementation. Frequency dependent performance metrics focusing on piloted flight are developed and tested on 23 flight configurations. The metrics show that the resulting design is superior to alternative control system designs using conventional fixed-gain crossfeeds and to feedback-only designs which rely on high gains to suppress undesired off-axis responses. The use of dynamic, robust crossfeeds prior to the QFT design reduces the magnitude of required feedback gain and results in performance that meets current handling qualities specifications relative to the decoupling of off-axis responses. The combined effect of the QFT feedback design following the implementation of low-order, dynamic crossfeed compensator successfully decouples ten of twelve off-axis channels. For the other two channels it was not possible to find a single, low-order crossfeed that was effective. This is an area to be investigated in future research.

ACKNOWLEDGMENTS

This research was funded by NASA Grant NCC 2-833. I am grateful for the support and facilities of the Rotorcraft and Powered Lift Branch for accomplishing my work. Special thanks to Dr. Mark Tischler for his guidance and insight which gave me great appreciation for the research process.

I would also like to thank the faculty of Cal. Poly. San Luis Obispo for their traditional quality engineering education, which allowed me to experience a great spectrum of possible career opportunities in between the years of classes. I especially am grateful to Dr. Daniel Bieczad for his experience and enthusiasm in research work which inspired me to find the same spirit in myself.

I dedicate this research to my dear friend Justine who is always helping me to view my life from a different perspective. As my goal to be an aeronautical engineer, I am trained not only to see what is on the surface but also to understand the inner working principles behind it. One thing she had taught me is that it is normal not to be too analytical. Sometimes, life is prettier this way.

TABLE OF CONTENTS

CHAPTER 1. INTRODUCTION	1
Background	1
Problem Definition	4
Organization	5
CHAPTER 2. LITERATURE REVIEW	6
Coupling Numerator Theory	6
Crossfeed Design: D. R. Catapang	7
Digital Control of Highly Augmented Combat Rotor: M. B. Tischler	8
H_∞ Helicopter Flight Control Law Design: M. D. Takahashi	9
QFT Rotorcraft Control System Design (No Crossfeeds) : R. A. Hess	10
Quantitative Feedback Theory	11
CHAPTER 3. AIRCRAFT & SYSTEMS MODELS	12
Helicopter Mathematical Model: "FORECAST"	12
Variation of configurations	13
Digital control system Emulation	15
CHAPTER 4. CROSSFEED ANALYSIS	17
Frequency Range of Interest for Heave & Rate Responses	17
Uncompensated Responses	17
Bare-Airframe Decoupling Performance Metrics	19
Ideal Crossfeed	20
Low-Order Approximation of the Ideal Crossfeed	21
Compensated Responses	30
CHAPTER 5. QFT DESIGN	41
Design Point Selection	41

Tracking Performance Specification & Responses Types	42
Controller Design	44
Prefilter Design	51
CHAPTER 6. FLIGHT CONTROL SYSTEM ANALYSIS	57
Decoupling Performance Metrics of Opened-Loop System (Review)	57
Decoupling Performance Metrics of Closed-Loop System	57
Effect of Dynamic Crossfeed on a Closed-Loop System	58
Handling Quality Analysis	59
Small-Amplitude Attitude Change	60
Moderate-Amplitude Attitude Change	61
Large-Amplitude Attitude Change	63
Collective-to-Yaw Coupling Requirement	64
Disturbance Rejection Performance	65
CHAPTER 7. CONCLUSIONS & RECOMMENDATIONS	66
REFERENCES	68
APPENDIX A.	
List of Model State Vector and Control Vector in Forecast Program	70
APPENDIX B.	
Variation of Flight Configurations	72
APPENDIX C.	
Derivation of Coupling Numerator For Pitch-from-Aileron Coupling	73

LIST OF FIGURES

Figure 1.1 UH-60 Black Hawk Three-View Configurations	2
Figure 1.2 RASCAL Development Program	3
Figure 1.3 System Model	4
Figure 2.1 Attitude Channel of ADOCS Control System Structure	8
Figure 2.2 H_{∞} Controls System Structure	9
Figure 2.3 Nichols Chart, Multi-Input Single-Output (MISO) Design	10
Figure 3.1 General 4x4 Control System Structure	14
Figure 3.2 Digital Control System Structure	15
Figure 4.1 Decoupling Performance Metrics of UH-60 Bare-Airframe	20
Figure 4.2 Sample Equations of the Ideal Crossfeed	21
Figure 4.3 Low-Order Fit to Ideal Crossfeed	22
Figure 4.4 Templates of Influential Ideal Crossfeeds, Roll-from-Elevator	25
Figure 4.5 Templates of Influential Ideal Crossfeeds, Pitch-from-Elevator	26
Figure 4.6 Templates of Influential Ideal Crossfeeds, Roll-from-Collective	26
Figure 4.7 Templates of Influential Ideal Crossfeeds, Pitch-from-Collective	27
Figure 4.8 Templates of Influential Ideal Crossfeeds, Yaw-from-Collective	27
Figure 4.9 Templates of Influential Ideal Crossfeeds, Roll-from-Rudder	28
Figure 4.10 Templates of Influential Ideal Crossfeeds, Pitch-from-Rudder	28
Figure 4.11 Low-Order Dynamic Crossfeeds Block Diagram	29
Figure 4.12 Decoupling Performance Metrics of Compensated System	29
Figure 4.13 Frequency Envelop Plot of Roll-from-Elevator Channel	30
Figure 4.14 Scatter Plot of Roll-from-Elevator Channel	31
Figure 4.15 Frequency Envelop Plot of Pitch-from-Elevator Channel	32
Figure 4.16 Scatter Plot of Pitch-from-Elevator Channel	32

Figure 4.17 Frequency Envelop Plot of Roll-from-Collective Channel	33
Figure 4.18 Scatter Plot of Roll-from-Collective Channel	34
Figure 4.19 Frequency Envelop Plot of Pitch-from-Collective Channel	35
Figure 4.20 Scatter Plot of Pitch-from-Collective Channel	35
Figure 4.21 Frequency Envelop Plot of Yaw-from-Collective Channel	36
Figure 4.22 Scatter Plot of Yaw-from-Collective Channel	37
Figure 4.23 Frequency Envelop Plot of Roll-from-Rudder Channel	38
Figure 4.24 Scatter Plot of Roll-from-Rudder Channel	38
Figure 4.25 Frequency Envelop Plot of Pitch-from-Rudder Channel	39
Figure 4.26 Scatter Plot of Pitch-from-Rudder Channel	40
Figure 5.1 Design Point Selection	42
Figure 5.2 Tracking Bounds of Roll, Pitch Axis	43
Figure 5.3 Tracking Bounds of Heave Axis	43
Figure 5.4 Tracking Bounds of Yaw Axis	44
Figure 5.5 SISO QFT Problem	44
Figure 5.6. Controller Structure	46
Figure 5.7 Roll Axis QFT Controller	47
Figure 5.8 Pitch Axis QFT Controller	48
Figure 5.9 Heave Axis QFT Controller	49
Figure 5.10 Yaw Axis QFT Controller	50
Figure 5.11 Roll Axis QFT Prefilter Frequency Plot	52
Figure 5.12 Pitch Axis QFT Prefilter Frequency Plot	53
Figure 5.13 Heave Axis QFT Prefilter Frequency Plot	54
Figure 5.14 Yaw Axis QFT Prefilter Frequency Plot	55
Figure 5.15 QFT Control System Block Diagram	56
Figure 6.1 Decoupling Metric of Closed-Loop System	58

Figure 6.2 Effect of the Low-Order Dynamic Crossfeeds	59
Figure 6.3 Definitions of Bandwidth and Phase Delay	60
Figure 6.4 Requirements for Small-Amplitude Attitude Changes	61
Figure 6.5 Requirements for Moderate- & Large-Amplitude Roll Attitude Changes	62
Figure 6.6 Collective-to-Yaw Coupling Requirements	64
Figure 6.7 Response to a Pulse Disturbance.	65

LIST OF TABLES

Table I	Variation of Configurations	13
Table II	Digital Control System Component Time-Delay	16
Table III	Lateral Cyclic, δ_a , Input Responses	18
Table IV	Longitudinal Cyclic, δ_e , Input Responses	18
Table V	Tail Rotor Collective, δ_r , Input Responses	18
Table VI	Main Rotor Collective, δ_c , Input Responses	19
Table VII	Low-Order Dynamic Crossfeeds	24
Table VIII	Features of Crossfeed Templates	24
Table IX	Tracking Performance Transfer Functions	42
Table X	QFT Controllers	45
Table XI	QFT Prefilters	51
Table XII	Requirements for Large-Amplitude Attitude Changes	63

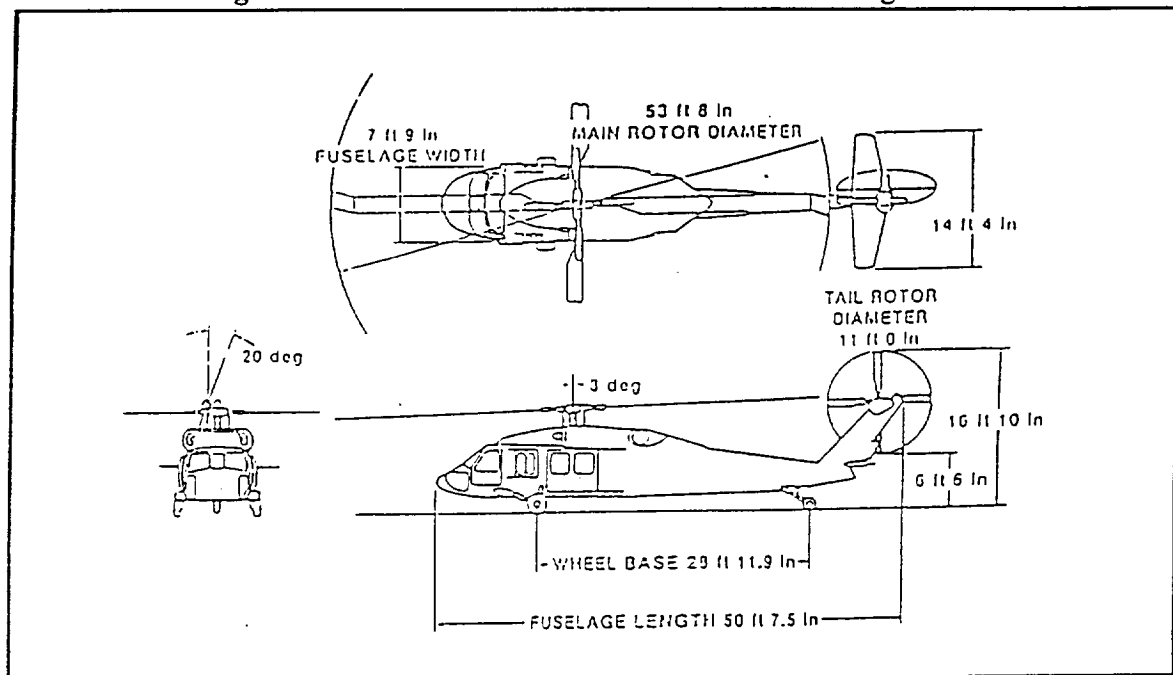
CHAPTER I INTRODUCTION

Background

Cross-coupling in near-hover condition is a characteristic problem for a helicopter. Cross-coupling occurs when an off-axis response develops as a result of an on-axis command. The UH-60 Black Hawk (see Figure 1.1) is representative of a helicopter with highly coupled motion because of its canted tail rotor that is located above the center of gravity. The Black Hawk will be used as the Rotorcraft Aircrew Systems and Controls Airborne Laboratory (RASCAL, see Figure 1.2), a joint U. S. Army / NASA program to evaluate proposed controls and systems concepts (ref. 2). One of the proposed control concepts is a robust hover control to be designed using Quantitative Feedback Theory (QFT) (ref. 3). QFT is a classical feedback control design method for robust compensation of uncertain plant transfer functions. This design method is suitable to the hover condition because the rotorcraft transfer function can change due to wind speed and direction, weight at hover, center of gravity location, and main rotor speed. QFT can be used on a multiple-input, multiple-output (MIMO) system if the system can be decoupled into several single-input, single-output (SISO) systems. Therefore, the precursor to QFT robust feedback design is a robust crossfeed design. The classical approach to crossfeed design is the use of coupling numerator theory, which has been explained in detail in literature by McRuer(ref.4,5). An important conclusion of coupling numerator theory is that an ideal crossfeed can be calculated with constrained variables to decouple the degrees of freedom of a coupled system. Coupling numerator theory has been successfully applied in the YF-

16 Control Configured Vehicle (CCV) program (ref. 6) and the UH-60 Black Hawk Advanced Digital Optical Control System (ADOCS) program (ref.2). However, crossfeeds for these programs were calculated only for a nominal condition. Using a strategy called Mean Square Weighting (ref. 1), it has been possible in this research to determine dynamic crossfeeds for a large set of hovering flight conditions. Metrics developed in Reference 1 suggested when decoupling specified degrees of freedom were beneficial. The strategy and

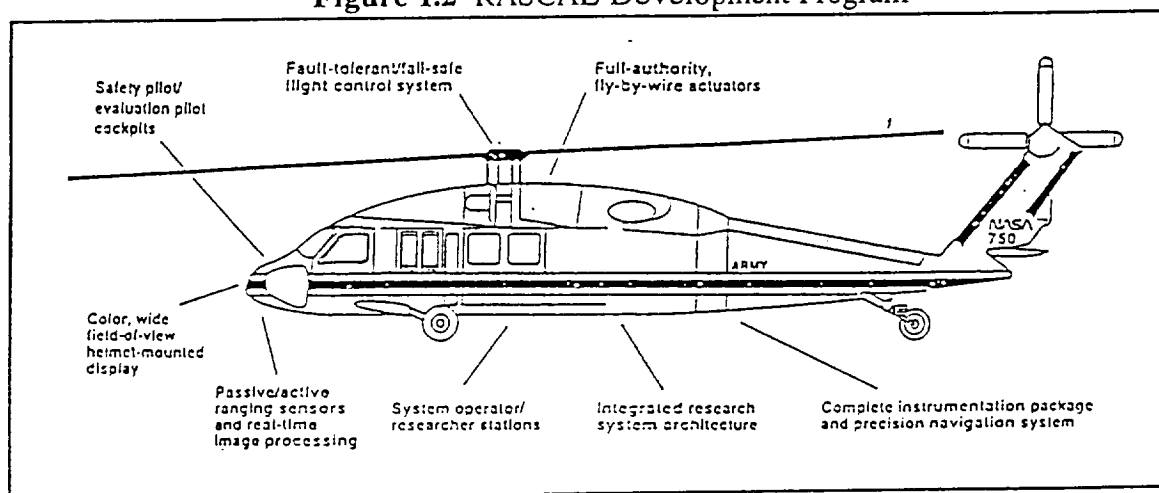
Figure 1.1 UH-60 Black Hawk Three-View Configuration



tests proved effective on preliminary, linearized models of the RASCAL helicopter in hovering flight. Decoupled performance was evaluated by comparing off-axis responses with current handling quality specifications (ref. 7). Decoupling could have been achieved with high gain feedback, which as a plus adds robustness and disturbance rejection, but as a minus would have required high bandwidth systems that may excite structural modes and result in control limiting or even closed-loop instability. The use of crossfeeds, when properly applied, is shown here to relax the high gain required for decoupling without sacrificing performance or robustness. The general technique uses crossfeeds to cancel

off-axis outputs in the off-axis control channels. The concept of "constrained variables" (ref. 2) takes the approximate effects of the feedback loops not yet synthesized into account in the crossfeed design. The rotorcraft configurations representing a 4x4 decoupling problem for approximately 23 near-hover conditions were generated on FORECAST, the mathematical model for the Black Hawk that originated at Ames Research Center and modified at the University of Maryland (ref. 8). The configurations were weighted based on likelihood of occurrence. The models were then being calibrated with flight test data to obtain correct off-axis responses. The frequency range of interest for piloted angle rate commands was 1.0 to 10.0 rad/sec and for heave command from 0.2 to

Figure 1.2 RASCAL Development Program



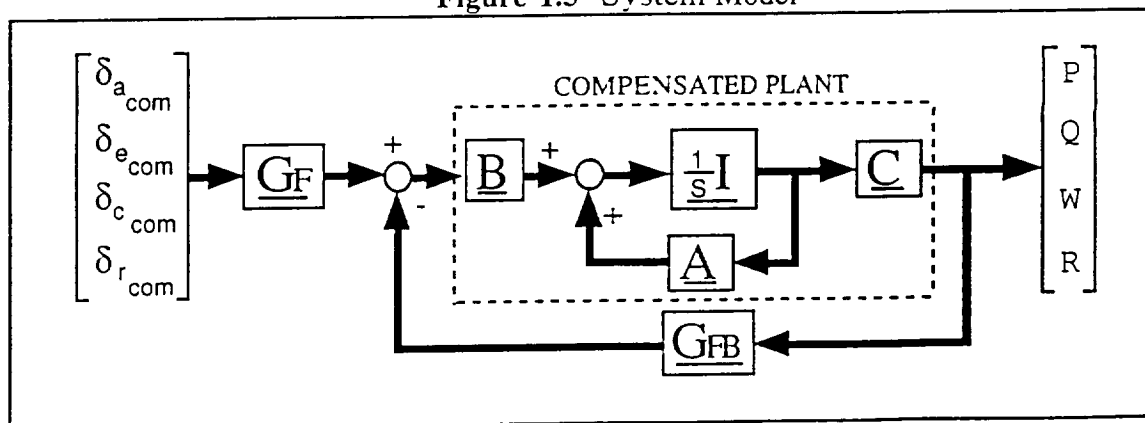
2.0 rad/sec. The effectiveness of the crossfeeds in decoupling was measured with the analysis tools developed in References 1 and 9. When the open-loop, off-axis average decoupling metric was greater than 20 dB, a crossfeed was not considered necessary since this represents significant attenuation (by a factor of 10) that already exists for that axis. A QFT controller was designed for the baseline model using the CAD package of Reference 13. A general application of this procedure without using crossfeeds may be found in Reference 14 (see Reference 15 for the most complete development of QFT). The robust

decoupling metric was used to compare and evaluate system performance with and without feedback.

Problem Definition

The focus of this study is to reduce the off-axis coupled responses through the crossfeed design and to improve the on-axis channels to achieve desirable handling qualities in 23 near-hovering flights using QFT control law design. The full-order helicopter dynamics such as engine model, rotor flapping mode, rotor lagging mode, dynamic inflow model, tail downwash, and tail sidewash are included to represent the cross-coupling more accurately. Cross-coupling characteristics are expected to vary greatly with range of flight conditions; therefore, the main purpose of this research is to achieve acceptable decoupling characteristics for flight speed of 15 knots around a nominal hovering point (0 knots). The final crossfeed design is then included in the UH-60 dynamic response as a pre-compensator for a RASCAL QFT control law design (see Figure 1.3). The additional feedbacks (G_{FB}) and filters (G_F) will shape the responses to meet a tracking performance and result desirable flying handling qualities.

Figure 1.3 System Model



Organization

This study is organized as follows. Chapter II is a review of literature containing coupling numerator theory and quantitative feedback theory including a brief summary of previous researchers. Chapter III contains the aircraft modeling, systems modeling, and range of flight configurations. Chapter IV contains the research procedures describing the robust crossfeed design. Chapter V concentrates on QFT design. In that chapter, the design point and tracking performance are specified, and the controllers and prefilters are designed to meet these specifications. Chapter VI is a decoupling performance analysis comparing the effectiveness of feedbacks and crossfeeds. The handling qualities analysis is also study in this chapter. The handling qualities and disturbance rejections were evaluated according to military rotorcraft specifications (ADS-33C). Chapter VII contains conclusions and recommendations for future research.

CHAPTER II LITERATURE REVIEW

Coupling Numerator Theory

The classical approach to crossfeed design is the use of coupling numerator theory, which has been explained in detail in literature by McRuer (ref. 4,5). Coupling numerator theory has been successfully applied in the YF-16 Control Configured Vehicle (CCV) program (ref. 6) and the UH-60 Black Hawk Advanced Digital Optical Control System (ADOCS) program (ref.2). However, crossfeeds for these programs were calculated only for a nominal condition. The concept of "constrained variables" (ref. 2) is an important aspect of this approach. This concept allows the crossfeed design to consider the approximate effects of the feedback loops not yet synthesized at this stage of the control system formulation. In the cited reference, coupling numerator techniques were applied either to obtain crossfeeds for single design point models or to gain schedule as a function of key flight condition variables (e.g., airspeed, air density, gross weight, and vertical velocity as in ref. 10) but did not consider the problem of crossfeed design for highly uncertain systems. An important conclusion of coupling numerator theory is that an ideal crossfeed can be calculated with constrained variables to decouple the degrees of freedom of a coupled system. The current study combines coupling numerator theory with the QFT concept of uncertainty templates to yield an approach for robust crossfeed design.

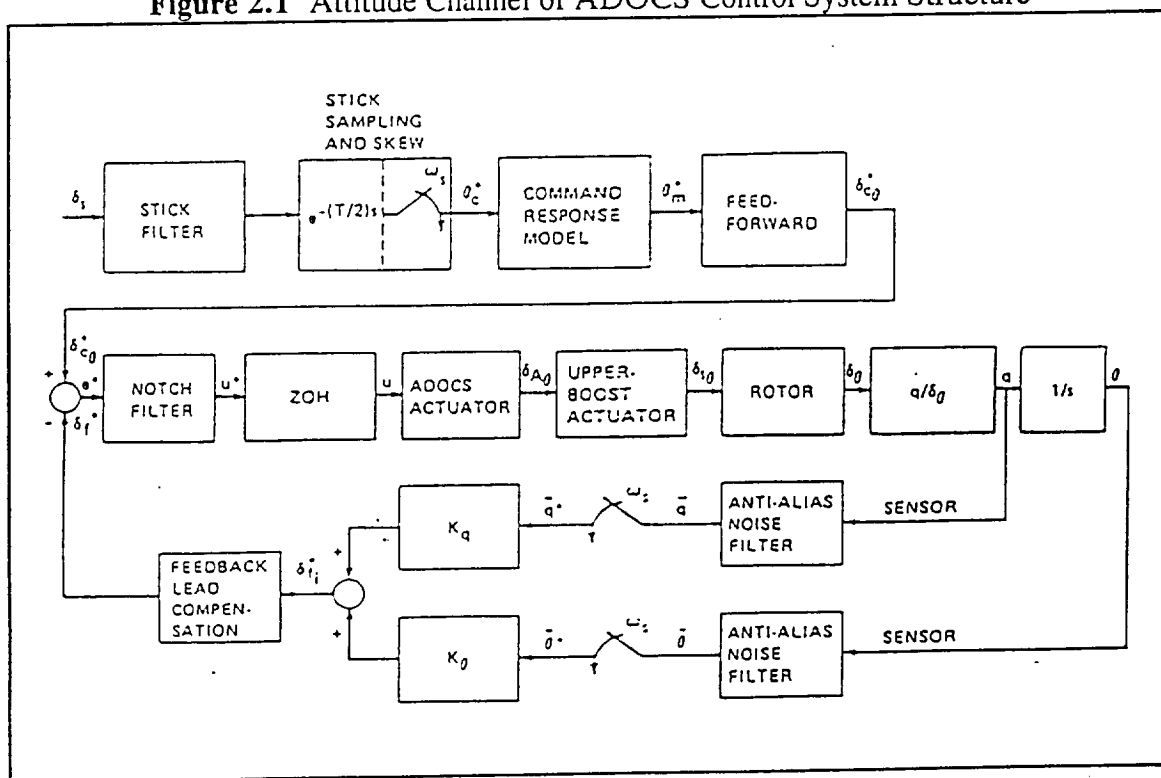
Crossfeed Design : D. R. Catapang

Robust crossfeeds using the Mean Square Weighting (MSW) strategy were obtained using the process described in Reference 1. Analytical derivation of the crossfeeds for this system can be found in Reference 9 (page 10-14) and Reference 10. Templates illustrating model variation were generated on LCAP, a linear controls analysis program well suited for order reduction and graphical display of transfer functions (ref. 11). "Ideal" analytical crossfeeds were approximated using NAVFIT, a program that finds the best fit to magnitude and phase angle data using a transfer function of fixed order (ref. 12). Application of the MSW strategy to the set of hovering flight conditions resulted in two important outcomes. First, a "target" set of frequency dependent gains and phase angles was found, along with a NAVFIT transfer function approximation to those values, that favored clusters of points within frequency templates. The purpose of this "target" set is to ensure robust decoupling over the set of hover trim conditions. Second, "most influential" points were identified (see page 23 of Reference 9) for each template frequency that had the most effect on the "target" points at that frequency. The templates for the "most influential" points determined if a crossfeed is advisable between two channels (indicated by non-overlapping templates) and, if so, whether or not it should be a dynamic or a static crossfeed (large vs. small variance in "target" points within the templates). The final, robust crossfeed between two channels (i.e., the NAVFIT approximate transfer function) was designed the "achievable" crossfeed. The set of "achievable" transfer functions, added as dynamic crossfeeds into the original hovering flight models, constituted the design baseline for the application of Quantitative Feedback Theory (QFT).

Digital Control of Highly Augmented Combat Rotorcraft : M. B. Tischler

The ADOCS, which was a demonstrator system (Figure 2.1) being tested on the UH-60 Black Hawk aircraft, is the first attempt to develop a full-flight-envelope, full-authority, digital fiber-optic flight control system (ref. 2). A high-bandwidth, model-following control system design is used to provide task-tailored handling qualities for a variety of missions. The attainable bandwidth of high-gain flight control systems has consistently been overestimated in design studies; this overestimation is generally not exposed until after hardware implementation and flight test. Equivalent time delays can be rapidly accumulated in the actuator/rotor system, filters, and software architecture used in modern combat rotorcraft. Therefore, careful design and analyses are needed to anticipate and minimize unnecessarily long delays. ADOCS architecture is redundant, and it lacks contribution to loop design.

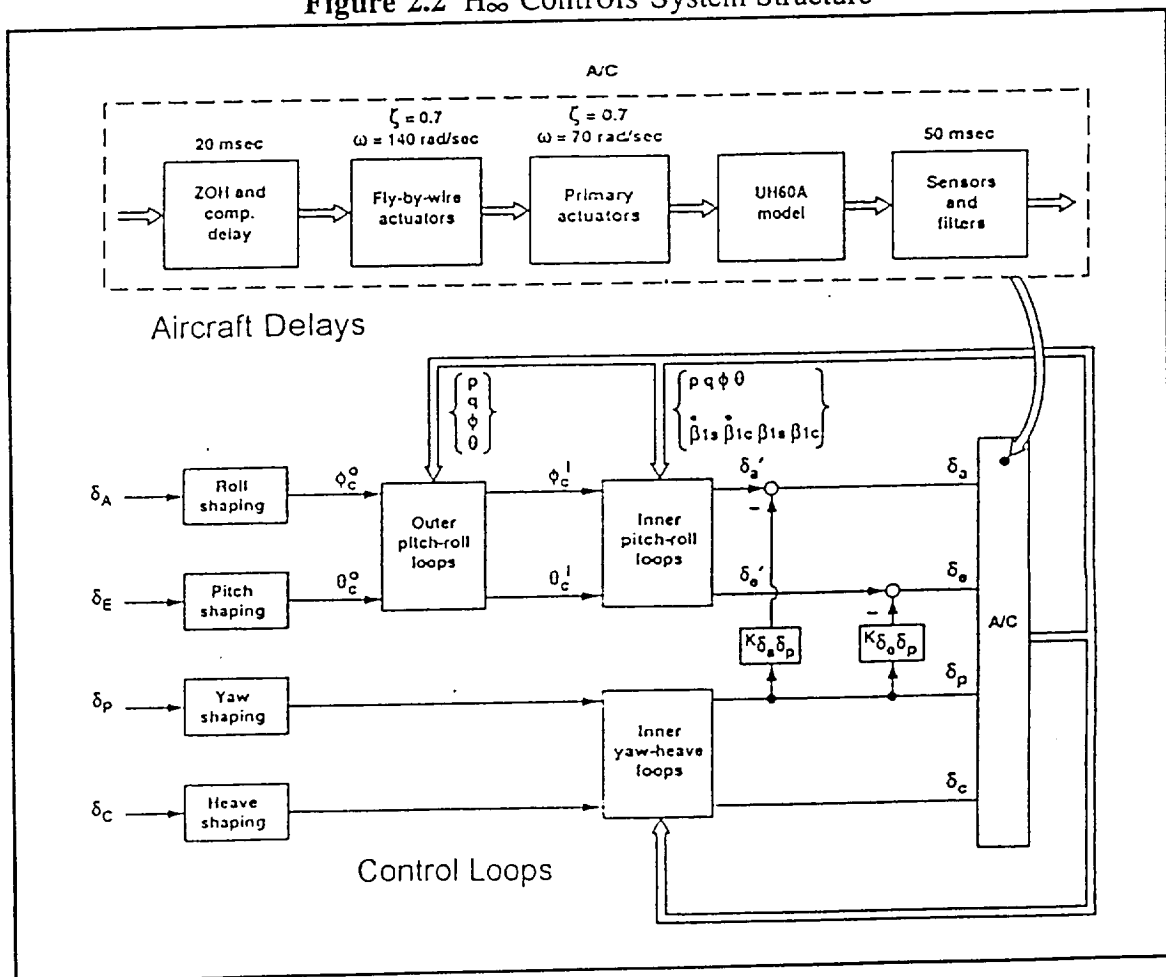
Figure 2.1 Attitude Channel of ADOCS Control System Structure



H_∞ Helicopter Flight Control Law Design : M. D. Takahashi

The H_∞ formulation allows somewhat straightforward adjustment of the weight functions to meet design goals (ref. 18). The crossover frequency is determined by the sensitivity weight function, while the closed-loop robustness is determined by the complementary sensitivity weight function, and the control weight function determines the relative size of the feedback gains. This framework facilitates design to the quantitative low speed requirements of the modern combat rotorcraft handling qualities specification, ADS-33C.

Figure 2.2 H_∞ Controls System Structure

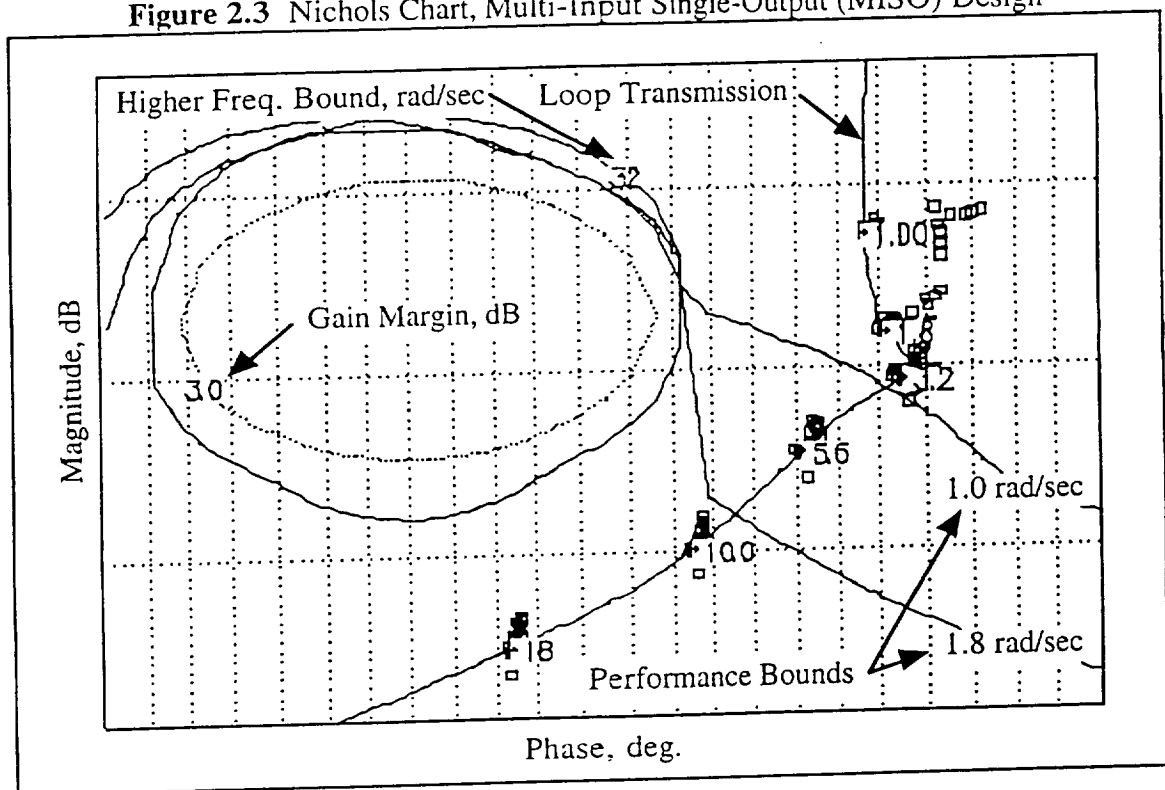


The inner loop manages the disturbance rejection requirements through the adjustment of the high frequency crossover behavior. The low-gain outer-loop feedbacks (Figure 2.2) manage the low frequency pole-placement requirements. Feedforward shaping allows the response requirements to be met.

QFT Rotorcraft Control System Design (No Crossfeeds) : R. A. Hess

The QFT control system design has developed, and it provided a flight control system which meets specified quantitative performance criteria. The optimum QFT design is one in which the loop transmission lies on the appropriate boundary on a Nichols Chart at each frequency (ref. 14). These boundaries (Figure 2.3) are the combination results of tracking, disturbance rejection requirements, and stability margins. In QFT design, control cross-couplings are considered as the disturbances which are minimized by QFT design process.

Figure 2.3 Nichols Chart, Multi-Input Single-Output (MISO) Design



In Hess's study, the rotorcraft model does not include the rotor and actuator dynamics, and it has shown the flight control system of a BO-105C rotorcraft for an airspeed range from 0 to 100 kts. Since this QFT design does not have the dynamic crossfeeds, Hess's QFT controllers tend to have higher-order (second- & third-order) comparing to the simple constant gain implemented in this research.

Quantitative Feedback Theory

QFT is a classically based feedback control design method for robust compensation of uncertain plant transfer functions (ref.3, 15, 16). The method is well suited to the rotorcraft flight control problems because it directly addresses costs including actuator limiting, sensor noise amplification, and loss of stability robustness. The benefits of feedback are performance robustness, stability, and disturbance rejection.

In QFT, aircraft dynamics uncertainties are modeled in direct terms of gain and phase response variation ("uncertainty templates") associated with the family of design points to be included. As such, the QFT problem formulation is very well suited to the helicopter problem, where sophisticated simulations provide a large family of single point dynamic models as a function of physical parameters such as wind speed and direction, weight at hover, center of gravity location, moments of inertia, main rotor speed, and aircraft turn rate. It is impractical to gain schedule the control system compensation as a function of the many parameters that affect aircraft dynamics; also many of these parameters are not measurable in-flight. Therefore, a large degree of uncertainty of aircraft dynamic will exist that must be included in the design. Dynamics variations are generally most significant for helicopter near-hovering flight, while control power is generally at a minimum level due to the lack of airspeed. These factor combine to make the hover condition flight control design a most challenging problem for the application of QFT techniques.

CHAPTER III AIRCRAFT & SYSTEMS MODELS

Helicopter Mathematical Model : "FORECAST"

The configuration used here is a UH-60 Black Hawk, which is a four-blade, articulated rotor, utility helicopter. The linear mathematical models are generated from the model described in Reference 19. This model represents the helicopter as a six degrees-of-freedom rigid fuselage with rigid rotor blades each with a flap and lag degree of freedom. No forward velocity, lateral velocity, and yaw angle are included in this model since they have low frequency responses which are not within frequency of interest.

The linear design model has 45 states that 6 states are attributable to the body motion, 16 states define the flap and lag motions of the rotor (collective, sine, and cosine), 2 states describe the dynamic twist, 4 states represent the dynamic inflow, 6 states define the engine dynamics, 8 states describe the primary servo dynamic, 2 states define the downwash, sidewash of the tail rotor, and one state defines the blade azimuth error. The details of the linear model states are presented in the Appendix A. Because of the software limitation, 26 out of 45 states are linearized using average linearization method (ref. 20). Although these 26 states have been linearized, the effect of these states is shown through remain 19 states.

The nominal flight condition is in hover at a gross weight of 16,825 lb with the air density at a standard sea level value of $0.002377 \text{ slug/ft}^3$ and the rotor speed set at 27 rad/sec. Other flight conditions near hovering are explained in next section.

Variation of Configurations

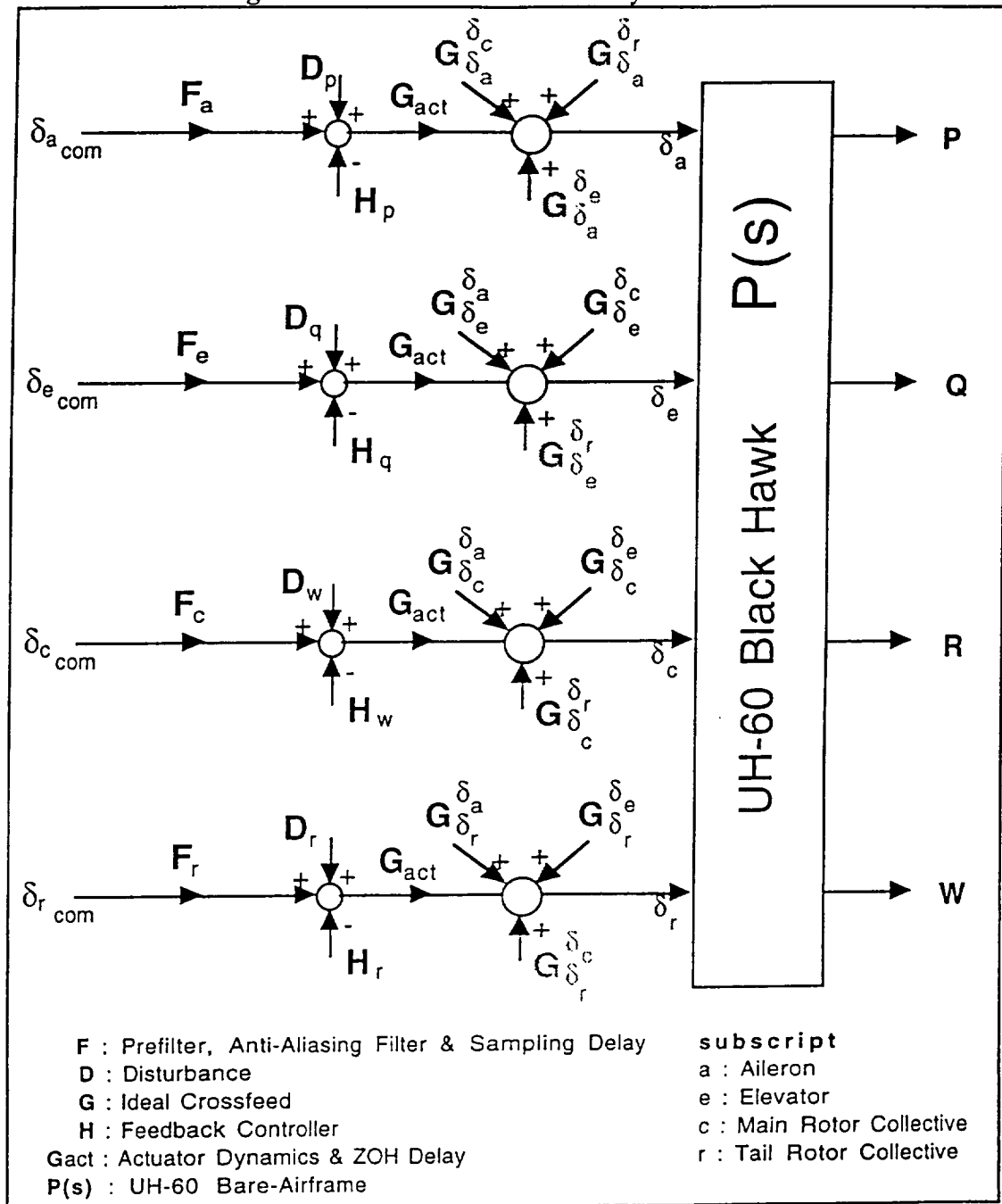
The "Forecast" simulation is capable of generating large families of linear models over a wide range of flight and configuration conditions. The current study includes the nominal hover operating point plus 22 off-nominal points. The 23 configurations include variations in trim airspeed (longitudinal and lateral), rotor RPM, aircraft weight, center of gravity, turning rate, climb speed, and descending speed. For this study, the configurations considered are shown in Appendix B. The configurations were put into groups. Each group was given a weighting to signify the influence of each configuration in the group on crossfeed design and decoupling evaluation as shown in Table I.

Table I. Variation of Configurations

Groups	Configurations	Weighting
I : Most Probable	1, 2, 3, 7, 9	1.0
II : Less Probable	6, 8, 14, 15	1.0
III : Least Probable	4, 5, 10, 12, 13, 16, 18~25	0.3

The final flight control system design will be based on the FORECAST model using the entire family of 23 configurations. The 4x4 control system for 23 near-hover conditions was investigated, and its general control system structure is shown in Figure 6. In this diagram, G 's are representing the crossfeeds where $G_{\delta_c}^{\delta_a}$ is the roll-from-heave ideal crossfeed, H 's are the feedback controllers, D 's are the disturbances, and F 's are the prefilters. It is possible to design 12 crossfeeds for the 4x4 system as shown in Figure 3.1; however, it is desired to identify which crossfeeds are necessary or possible to design. Analysis of bare-airframe coupling assisted in this identification process. The detail of this identification process will shown in Chapter IV.

Figure 3.1 General 4x4 Control System Structure



With the cross-coupling now effectively suppressed by the crossfeeds, this multiple-input, multiple-output (MIMO) system is then decoupled into four single-input, single-output (SISO) systems. QFT techniques can be applied to the compensated SISO system to synthesize feedback H , controller G , and prefilter F elements of the control system that satisfy the design specifications.

Digital Control System Emulation

The framework and the aircraft dynamics are shown in Figure 3.2. A common method in digital flight control system design is to select the compensation based on an equivalent analog block diagram. Approximating effects of the digital-to-analog converter (ZOH), signal sampler, anti-aliasing filter, and computational delay form the basis of this emulation method (see Figure 3.2, bold frame). The most important contributions to the time-delay for a digital system and their approximated transfer functions are shown in Table II. The aircraft dynamic include the UH-60 dynamics and two sets of actuator dynamics, which represent the fly-by-wire driver actuators and UH-60 primary actuator. The total loop time delay of system is 145 msec.

Figure 3.2 Digital Control System Structure

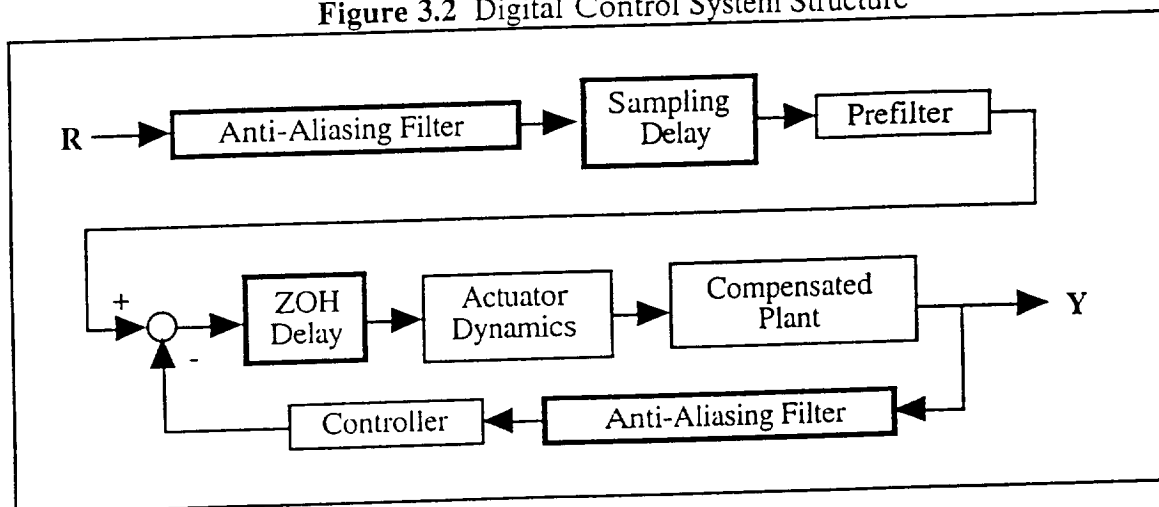


Table II. Digital Control System Component Time-Delay

Time-Delay Types	Time-Delay Periods, msec	Transfer Functions
Actuator Dynamics	36	$\frac{1521}{[0.7, 39]}^1$
Computation Delay & ZOH	15	$\frac{-(-133.33)}{(133.33)}^2$
Anti-Aliasing Filter	18	$\frac{6084}{[0.7, 78]}$
Sampler Delay	10	$\frac{-(-200)}{(200)}$
Rotor Dynamics	66	3

There are three advantages (ref. 2) of this emulation approach:

- (1) Emulation yields a flyable, continuous controller.
- (2) Structural and stability properties of the controller dynamics are invariant with respect to the sample-time parameter.
- (3) Sample rate estimates based on this approach are conservative, and the resulting digital control software is generally flyable.

The limitations of the emulation approach are as follows:

- (1) There is no way of detecting when the time-delay and analog-to-discrete transformations are beginning to introduce significant errors into the analysis and design.
- (2) There is no information on actuator responses to the zero-order-hold command signal.
- (3) No information is available on the effects of aliasing.
- (4) Design by emulation yields a conservative choice of sample rate in order to validate the continuous-to-discrete approximations.
- (5) There is no information on the sensitivity of the z-plane performance characteristics to changes in timing and word length.

¹ $[\xi, \omega] = [s^2 + 2\xi\omega s + \omega^2]$

² $(a) = (s + a)$

³ Rotor dynamics time delays have included in the Forecast helicopter model.

CHAPTER IV CROSSFEED ANALYSIS

Frequency Range of Interest for Heave & Rate Responses

The frequency range of interest for piloted angle rate commands (δ_a , δ_e , δ_r) was 1.0 to 10.0 rad/sec and for heave command (δ_c) from 0.2 to 2.0 rad/sec. These ranges were determined experimentally from the autospectrum of pilot inputs during the ADOCS study (ref. 20). Note that 2 to 10 rad/sec was used in Reference 1; however, 1 to 10 rad/sec was used in this study.

Uncompensated Responses

The uncompensated responses are responses of the bare-airframe dynamics which included the original mechanical control mixer box of the UH-60. The equations (Table III, IV, V, VI) shown the uncompensated and compensated rotorcraft responses in form of coupling numerator. In these equations, the symbol N and G represent the coupling numerator and crossfeed element respectively. The constrained variables (ref. 2) takes the approximate effects of the feedback loops not yet synthesized into account in the crossfeed design. The uncompensated solutions can be obtained simply set the crossfeed element G equal to zero. As discuss in previous chapter , 23 configurations were linearized. These linearizations result in a unique characteristic equation for each type of constrain. These characteristic equation and their respective coupling numerators may be found using software for control system analysis such as LCAP (ref. 11)

Table III. Lateral Cyclic, δ_a , Input Responses

Control Coupling	Off-Axis	On-Axis
Pitch / Roll (Yaw constrained)	$\left[\frac{q}{\delta_a} \right]_r = \frac{N_{\delta_a \delta_r}^q + G_{\delta_a}^{\delta_e} N_{\delta_e \delta_r}^q + G_{\delta_a}^{\delta_c} N_{\delta_c \delta_r}^q}{N_{\delta_r}^r}$	$\left[\frac{p}{\delta_a} \right]_r = \frac{N_{\delta_a \delta_r}^p}{N_{\delta_r}^r}$
Yaw / Roll (Pitch constrained)	$\left[\frac{r}{\delta_a} \right]_q = \frac{N_{\delta_a \delta_e}^r + G_{\delta_a}^{\delta_e} N_{\delta_e \delta_e}^r + G_{\delta_a}^{\delta_c} N_{\delta_c \delta_e}^r}{N_{\delta_e}^q}$	$\left[\frac{p}{\delta_a} \right]_q = \frac{N_{\delta_a \delta_e}^p}{N_{\delta_e}^q}$
Heave / Roll (Pitch & Yaw constrained)	$\left[\frac{w}{\delta_a} \right]_{qr} = \frac{N_{\delta_a \delta_e \delta_r}^{wq} + G_{\delta_a}^{\delta_c} N_{\delta_c \delta_e \delta_r}^{wq}}{N_{\delta_e \delta_r}^q}$	$\left[\frac{p}{\delta_a} \right]_{qr} = \frac{N_{\delta_a \delta_e \delta_r}^{pq}}{N_{\delta_e \delta_r}^q}$

Table IV. Longitudinal Cyclic, δ_e , Input Responses

Control Coupling	Off-Axis	On-Axis
Roll / Pitch (Yaw constrained)	$\left[\frac{p}{\delta_e} \right]_r = \frac{N_{\delta_e \delta_r}^p + G_{\delta_e}^{\delta_a} N_{\delta_a \delta_r}^p + G_{\delta_e}^{\delta_c} N_{\delta_c \delta_r}^p}{N_{\delta_r}^r}$	$\left[\frac{q}{\delta_e} \right]_r = \frac{N_{\delta_e \delta_r}^q}{N_{\delta_r}^r}$
Yaw / Pitch (Roll constrained)	$\left[\frac{r}{\delta_e} \right]_p = \frac{N_{\delta_e \delta_a}^r + G_{\delta_e}^{\delta_a} N_{\delta_a \delta_a}^r + G_{\delta_e}^{\delta_c} N_{\delta_c \delta_a}^r}{N_{\delta_a}^p}$	$\left[\frac{q}{\delta_e} \right]_p = \frac{N_{\delta_e \delta_a}^q}{N_{\delta_a}^p}$
Heave / Pitch (Roll & Yaw constrained)	$\left[\frac{w}{\delta_e} \right]_{pr} = \frac{N_{\delta_e \delta_a \delta_r}^{wp} + G_{\delta_e}^{\delta_c} N_{\delta_c \delta_a \delta_r}^{wp}}{N_{\delta_a \delta_r}^p}$	$\left[\frac{q}{\delta_e} \right]_{pr} = \frac{N_{\delta_e \delta_a \delta_r}^{qp}}{N_{\delta_a \delta_r}^p}$

Table V. Tail Rotor Collective, δ_r , Input Responses

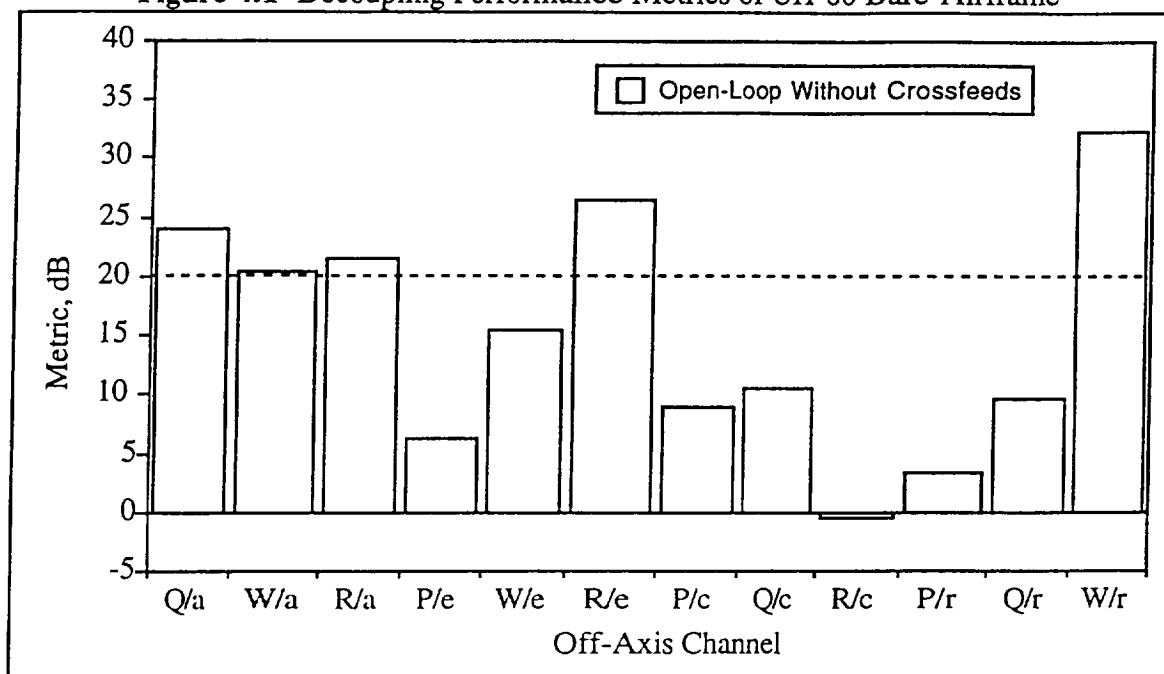
Control Coupling	Off-Axis	On-Axis
Pitch / Yaw (Roll constrained)	$\left[\frac{q}{\delta_r} \right]_p = \frac{N_{\delta_r \delta_a}^q + G_{\delta_r}^{\delta_e} N_{\delta_e \delta_a}^q + G_{\delta_r}^{\delta_c} N_{\delta_c \delta_a}^q}{N_{\delta_a}^p}$	$\left[\frac{r}{\delta_r} \right]_p = \frac{N_{\delta_r \delta_a}^r}{N_{\delta_a}^p}$
Roll / Yaw (Pitch constrained)	$\left[\frac{p}{\delta_r} \right]_q = \frac{N_{\delta_r \delta_e}^p + G_{\delta_r}^{\delta_a} N_{\delta_a \delta_e}^p + G_{\delta_r}^{\delta_c} N_{\delta_c \delta_e}^p}{N_{\delta_e}^q}$	$\left[\frac{r}{\delta_r} \right]_q = \frac{N_{\delta_r \delta_e}^r}{N_{\delta_e}^q}$
Heave / Yaw (Roll & Pitch constrained)	$\left[\frac{w}{\delta_r} \right]_{pq} = \frac{N_{\delta_r \delta_a \delta_e}^{wp} + G_{\delta_r}^{\delta_c} N_{\delta_c \delta_a \delta_e}^{wp}}{N_{\delta_a \delta_e}^q}$	$\left[\frac{r}{\delta_r} \right]_{pq} = \frac{N_{\delta_r \delta_a \delta_e}^{rp}}{N_{\delta_a \delta_e}^q}$

Table VI. Main Rotor Collective, δ_c , Input Responses

Control Coupling	Off-Axis	On-Axis
Pitch / Heave (Roll & Yaw constrained)	$\left[\frac{q}{\delta_c} \right] p r = \frac{N_{\delta_c \delta_a \delta_r}^{q p r} + G_{\delta_c}^{\delta_c} N_{\delta_c \delta_a \delta_r}^{q p r}}{N_{\delta_a \delta_r}^{p r}}$	$\left[\frac{w}{\delta_c} \right] p r = \frac{N_{\delta_c \delta_a \delta_r}^{w p r}}{N_{\delta_a \delta_r}^{p r}}$
Roll / Heave (Pitch & Yaw constrained)	$\left[\frac{p}{\delta_c} \right] q r = \frac{N_{\delta_c \delta_e \delta_r}^{p q r} + G_{\delta_c}^{\delta_a} N_{\delta_c \delta_e \delta_r}^{p q r}}{N_{\delta_e \delta_r}^{q r}}$	$\left[\frac{w}{\delta_c} \right] q r = \frac{N_{\delta_c \delta_e \delta_r}^{w q r}}{N_{\delta_e \delta_r}^{q r}}$
Yaw / Heave (Roll & Pitch constrained)	$\left[\frac{r}{\delta_c} \right] p q = \frac{N_{\delta_c \delta_a \delta_e}^{r p q} + G_{\delta_c}^{\delta_r} N_{\delta_c \delta_a \delta_e}^{r p q}}{N_{\delta_a \delta_e}^{p q}}$	$\left[\frac{w}{\delta_c} \right] p q r = \frac{N_{\delta_c \delta_a \delta_e \delta_r}^{w p q r}}{N_{\delta_a \delta_e \delta_r}^{p q r}}$

Bare-Airframe Decoupling Performance Metrics

Analysis of bare-airframe coupling based on coupling numerator method assisted in this identification process. Metrics developed in Reference 1 indicated when decoupling specified degrees of freedom was beneficial. It is possible to design 12 crossfeeds for the 4x4 system; however, it is desired to identify which crossfeeds are necessary or possible to design. The average results of the bare-airframe coupling for all 23 configuration evaluated by program "Metric" is shown in Figure 8. As shown in Figure 4.1, Pitch Rate-, Heave-, Yaw Rate-from-aileron command (denoted as Q/a, W/a, R/a), Yaw Rate-from-elevator command (denoted as R/c), and Heave-from-rudder command (denoted as W/r) all have the decoupling metric of 20 dB or above, which means that a crossfeed is not considered necessary for this channel since this represents significant attenuation (by a factor of 10) which already exists for that axis. Therefore, the crossfeed design will proceed without these 5 channels.

Figure 4.1 Decoupling Performance Metrics of UH-60 Bare-Airframe

Ideal Crossfeed

The ideal crossfeed is a mathematical solution (see Figure 4.2) solved directly from the equations in Table III, IV, V, VI for 23 configurations which were obtained using the LCAP (Linear Control Analysis Program). Study done in Reference 9 indicated that the "ideal" crossfeeds are unstable, high-order transfer functions which are not practical. Practical, stable, dynamic crossfeeds are obtained by approximating the ideal crossfeeds with low-order equivalent transfer function over the frequency range of interest. The low-order crossfeed fit results obtained from NAVFIT (ref. 12) and the tail works about low-order crossfeeds are discussed in next section.

Figure 4.2 Sample Equations of the Ideal Crossfeed

Ideal Heave-from-Roll Crossfeed

$$N_{\delta_a \delta_r \delta_e}^{w r q} + G_{\delta_a}^{\delta_c} N_{\delta_c \delta_r \delta_e}^{w r q} = 0$$

$$\Rightarrow G_{\delta_a}^{\delta_c} N_{\delta_c \delta_r \delta_e}^{w r q} = -N_{\delta_a \delta_r \delta_e}^{w r q} \Rightarrow G_{\delta_a}^{\delta_c} = -\frac{N_{\delta_a \delta_r \delta_e}^{w r q}}{N_{\delta_c \delta_r \delta_e}^{w r q}}$$

Ideal Pitch-from-Roll Crossfeed

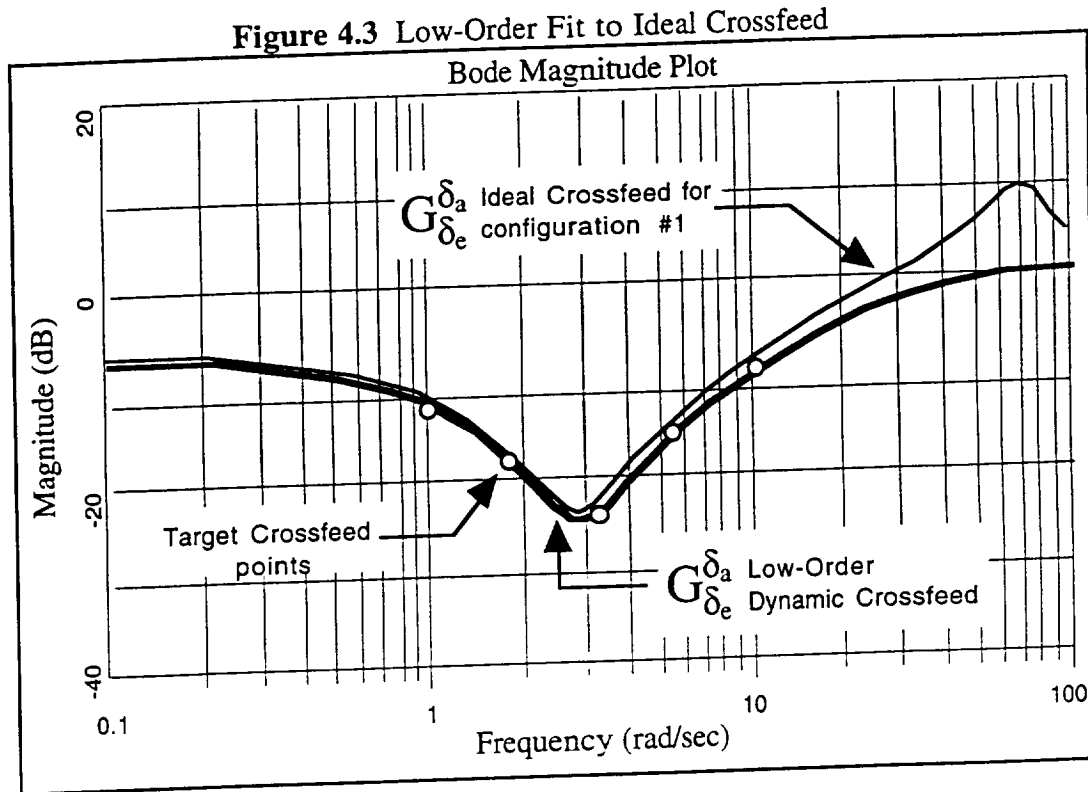
$$N_{\delta_a \delta_r}^{q r} + G_{\delta_a}^{\delta_e} N_{\delta_e \delta_r}^{q r} + G_{\delta_a}^{\delta_c} N_{\delta_c \delta_r}^{q r} = 0$$

$$\Rightarrow G_{\delta_a}^{\delta_e} N_{\delta_e \delta_r}^{q r} = -N_{\delta_a \delta_r}^{q r} - G_{\delta_a}^{\delta_c} N_{\delta_c \delta_r}^{q r} \Rightarrow G_{\delta_a}^{\delta_e} = \frac{-N_{\delta_a \delta_r}^{q r} - G_{\delta_a}^{\delta_c} N_{\delta_c \delta_r}^{q r}}{N_{\delta_e \delta_r}^{q r}}$$

$$= \frac{-N_{\delta_a \delta_r}^{q r} - \left[-\frac{N_{\delta_a \delta_r \delta_e}^{w r q}}{N_{\delta_c \delta_r \delta_e}^{w r q}} \right] N_{\delta_c \delta_r}^{q r}}{N_{\delta_e \delta_r}^{q r}} = \frac{-N_{\delta_a \delta_r}^{q r} N_{\delta_c \delta_r \delta_e}^{w r q} + N_{\delta_a \delta_r \delta_e}^{w r q} N_{\delta_c \delta_r}^{q r}}{N_{\delta_e \delta_r}^{q r} N_{\delta_c \delta_r \delta_e}^{w r q}}$$

Low-Order Approximation of the Ideal Crossfeed

In QFT loop-shaping terminology, the performance characteristics of a crossfeed apply not only to a single design configuration but to a "specified set" of configurations. This single crossfeed, appropriately selected for a set of configurations, is called the "target" compensation, and the low-order approximation to this "target" is called the "achieved" compensation (ref. 9). The selection of target points for all 23 configurations are based on MSW strategy and coupling variance (ref. 9). Figure 4.3 is a frequency plot for configuration #1 (hover) showing the accuracy of the low-order dynamic approximation to the roll-from-elevator target points. The simple low-order roll-from-elevator dynamic crossfeed ($G_{\delta_e}^{\delta_a}$, the bold curve) which generated from NAVFIT matches the ideal result (the thin curve) well within the frequency range of interest (1 to 10 rad/sec).



All 7 low-order dynamic crossfeed are obtained in similar method and their results are shown in Table VII. Notice that all but one of the resulting crossfeeds were implemented using transfer functions instead of fixed-gains to ensure robust decoupling. Figure 4.4~4.10 shows the templates analysis for necessary crossfeeds. Frequency templates, low-order crossfeed fit, and ideal crossfeed is shown on a Nichols Chart of each crossfeed analysis. The frequency templates are constructed by connecting the influential points. Influential points are identified by evaluating the sensitivity of the MSW target crossfeed for a certain template by moving an ideal crossfeed points ± 1 dB or ± 10 deg. and then recalculating the MSW target crossfeed (ref. 9). If the MSW target crossfeed moves ± 0.05 dB or ± 0.5 deg. the ideal crossfeed point is considered influential. Notice that neither the target points nor the low-order crossfeed is calculated base on the influential points. Influential points are only used to illustrate the templates. Table VIII identifies features of the crossfeed templates in Figure 4.4~4.10.

Figure 4.4 is the plot of templates for roll-from-elevator crossfeed and the thick black curve represents the low-order approximation of the target crossfeeds. The ideal crossfeed points at frequency of 3.162 rad/sec. has very large scatter which significantly affects the accuracy of the low-order roll-from-elevator crossfeed fit. Figure 4.6 is the plot of templates containing ideal crossfeed point for roll-from-collective crossfeed. Similar to roll-from-elevator crossfeed, it has a large scatter ideal crossfeed points at frequency of 1.125 rad/sec.

Figure 4.5 is the plot of templates containing ideal crossfeed point for heave-from-elevator crossfeed. There is no practical effective low-order transfer function for this set of templates because the template shapes are large in relation to the small dispersion of the target crossfeed which indicating excessive variance in the ideal crossfeed data. Although the target points can be fit with a low-order crossfeed, the target crossfeeds do not fully represent the ideal crossfeeds; therefore, the effectiveness of this low-order crossfeed is reduced.

Figure 4.8 is the plot of templates containing ideal crossfeed point for yaw-from-collective crossfeed. This channel has the worse off-axis response that is directly related to the engine dynamics. In the Figure 4.8, all 23 flight configurations have very small variations in both magnitude and phase. The advantage of use dynamic crossfeed has successfully demonstrated in this channel. The decoupling performance metric for this channel without the crossfeed is -0.46 which means the average magnitude of off-axis responses are stronger than the on-axis responses. The effectiveness of this crossfeed is discuss in next section.

Figure 4.9 is the plot of templates containing ideal crossfeed point for roll-from-rudder crossfeed. A low-order transfer function can be fit through the templates, but a static crossfeed is sufficient because the target crossfeeds vary little in magnitude.

The final seven resultant low-order dynamic crossfeeds are implemented in program MATLAB, and its simulation block diagram is shown in Figure 4.11. The results of the compensated open-loop system is discussed in next section.

Table VII. Low-Order Dynamic Crossfeeds

Off-Axis	Transfer Function
$G_{\delta_c}^{\delta_a}$	$\frac{1.1829 [0.3, 3.0]}{(0.6812)(30)}$
$G_{\delta_c}^{\delta_c}$	$\frac{6.5032}{(1.5712)(6.9965)}$
$G_{\delta_c}^{\delta_a}$	$\frac{0.01536 [0.9487, 4.5915]}{[0.5475, 1.7705]}$
$G_{\delta_c}^{\delta_e}$	$\frac{0.1688 [0.3519, 1.0825]}{(0.4834)(3.0)}$
$G_{\delta_c}^{\delta_r}$	$\frac{-0.1827 (6.0)}{[0.3120, 2.3669]}$
$G_{\delta_r}^{\delta_a}$	0.3377
$G_{\delta_r}^{\delta_e}$	$\frac{4.2087}{(9.4877)}$

Table VIII. Features of Crossfeed Templates

Symbol	Feature	Frequency, rad/sec	
		P, Q, R Channel	Heave Channel
□	ω_1	1.000	0.200
△	ω_2	1.778	0.356
◇	ω_3	3.162	0.623
○	ω_4	5.623	1.125
+	ω_5	10.000	2.000
⊕	Target Crossfeed		
⊗	Static Crossfeed		

Figure 4.4 Templates of Influential Ideal Crossfeeds

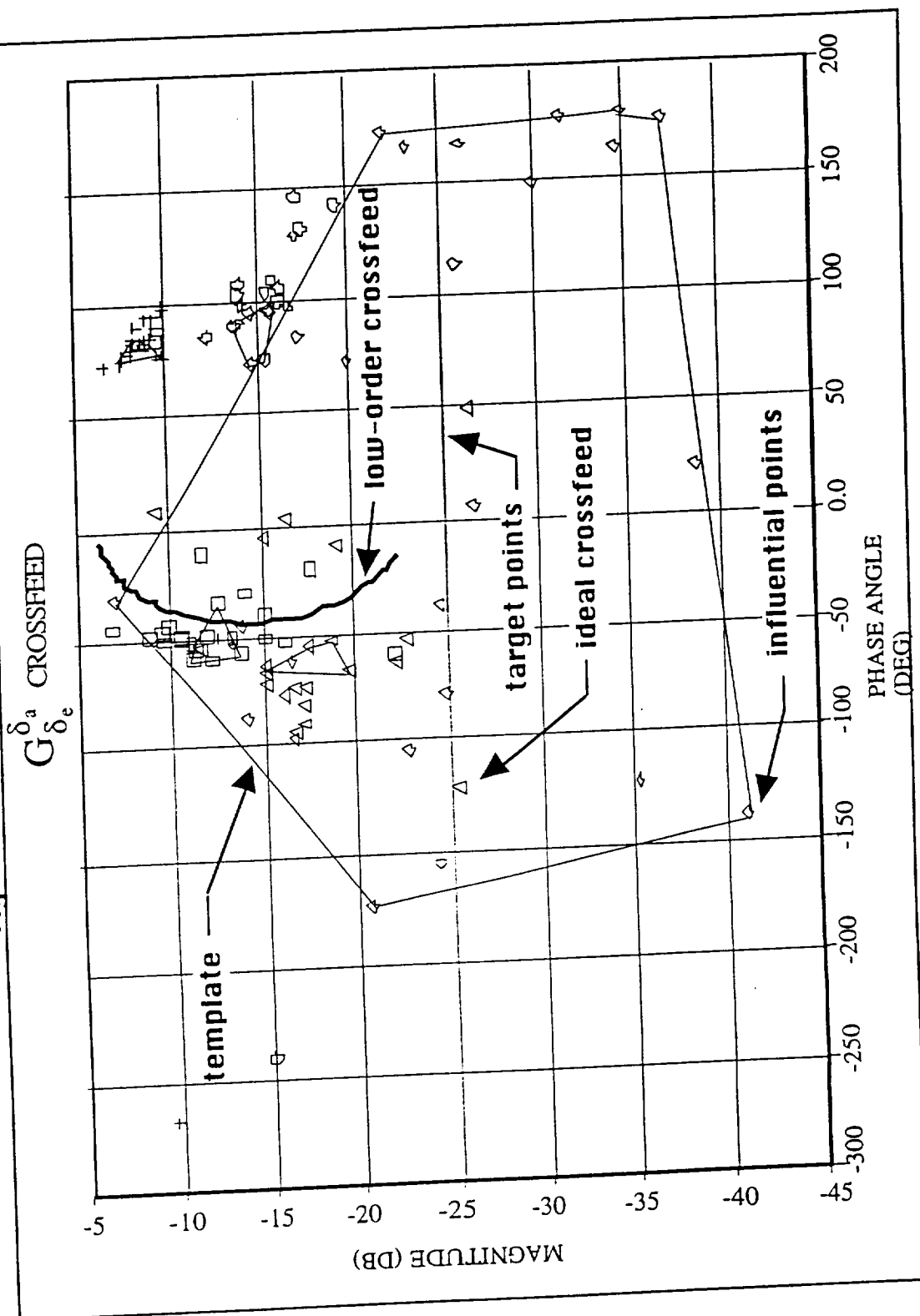


Figure 4.5 Templates of Influential Ideal Crossfeeds

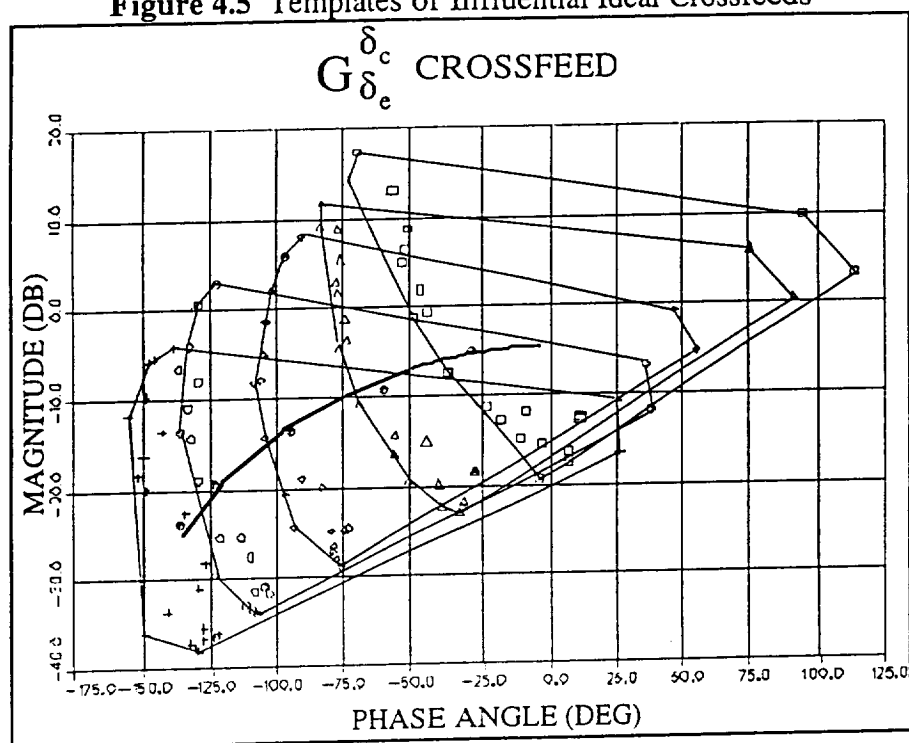


Figure 4.6 Templates of Influential Ideal Crossfeeds

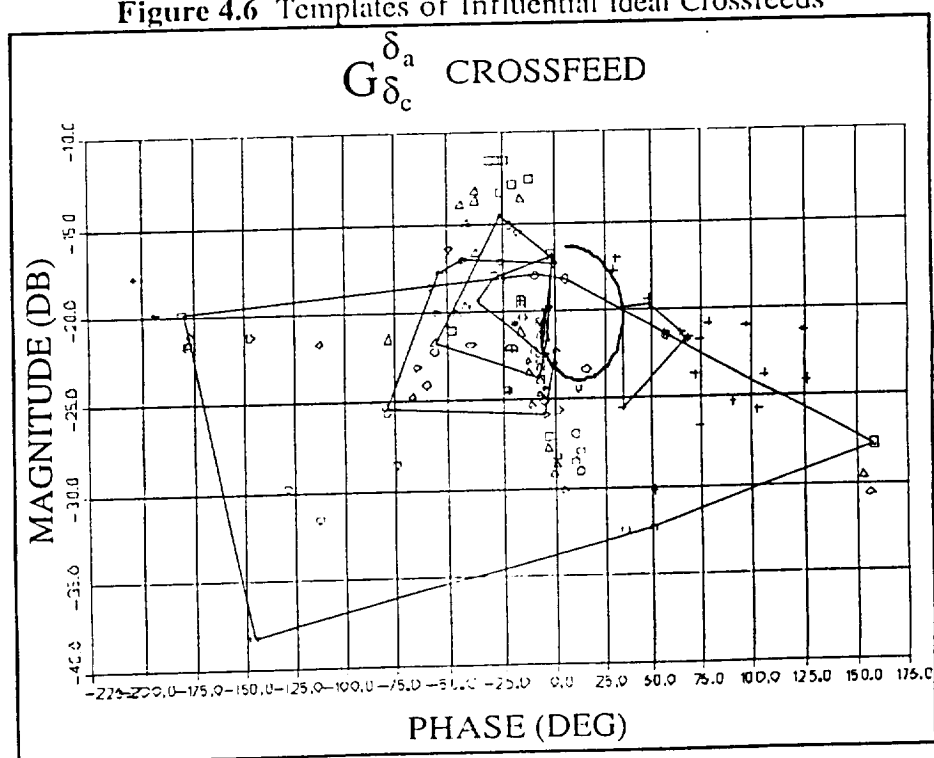


Figure 4.7 Templates of Influential Ideal Crossfeeds

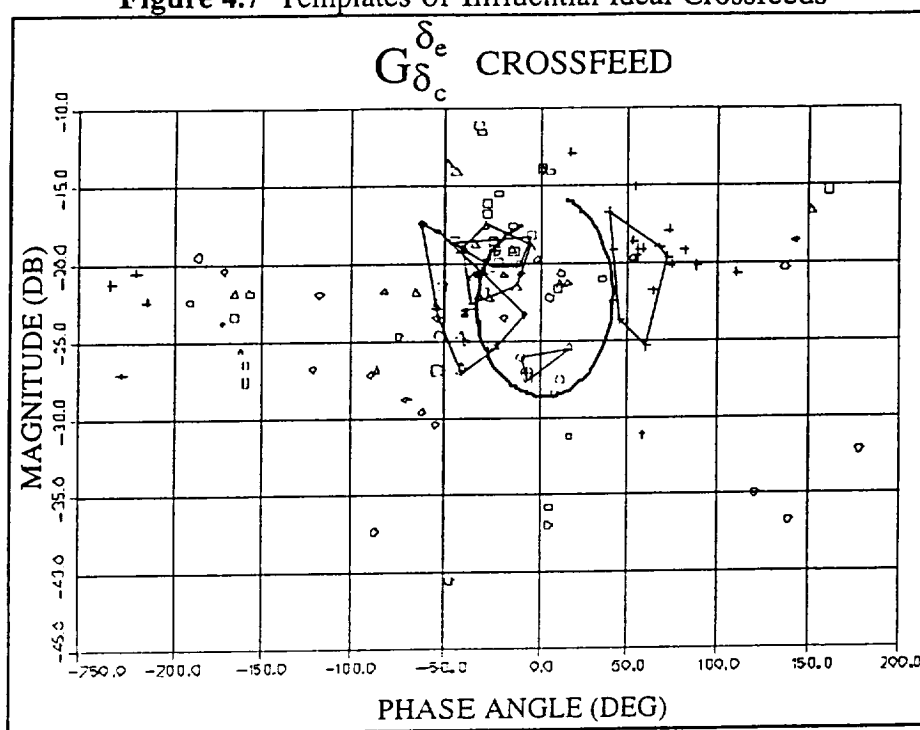


Figure 4.8 Templates of Influential Ideal Crossfeeds

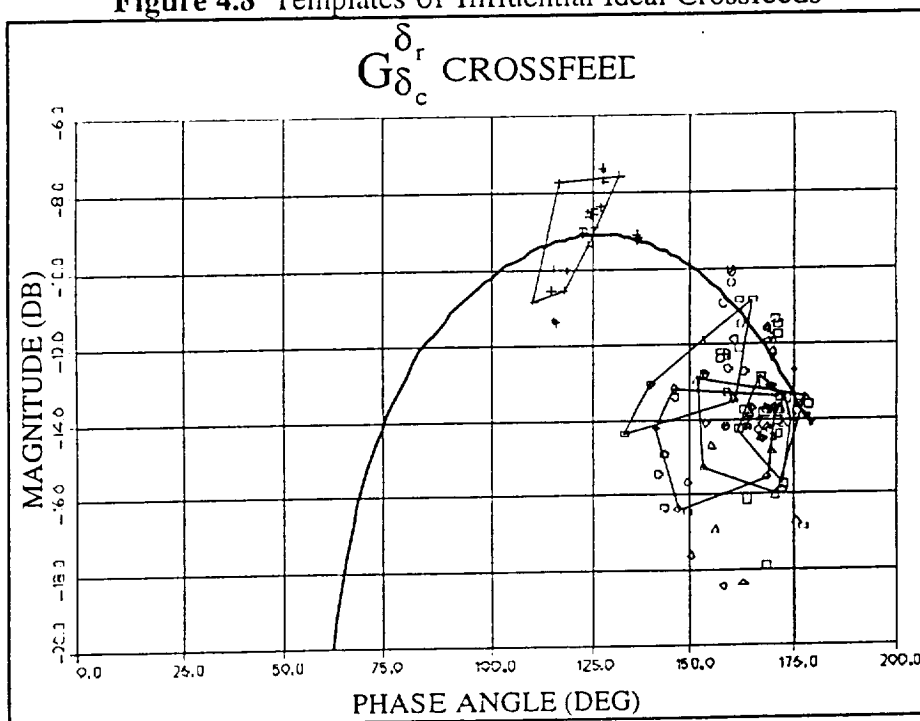


Figure 4.9 Templates of Influential Ideal Crossfeeds

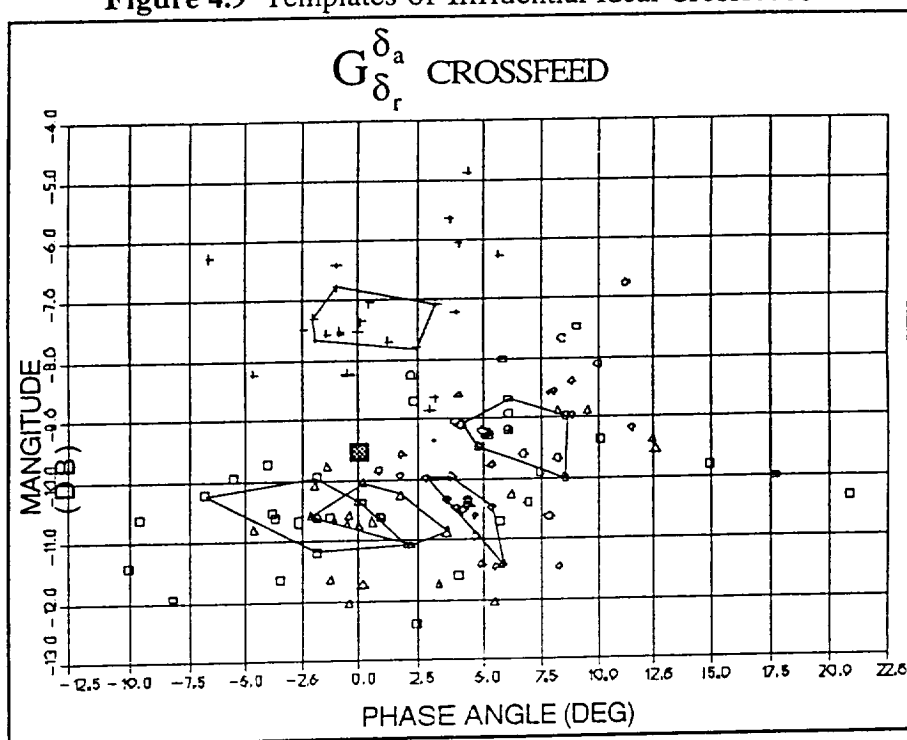


Figure 4.10 Templates of Influential Ideal Crossfeeds

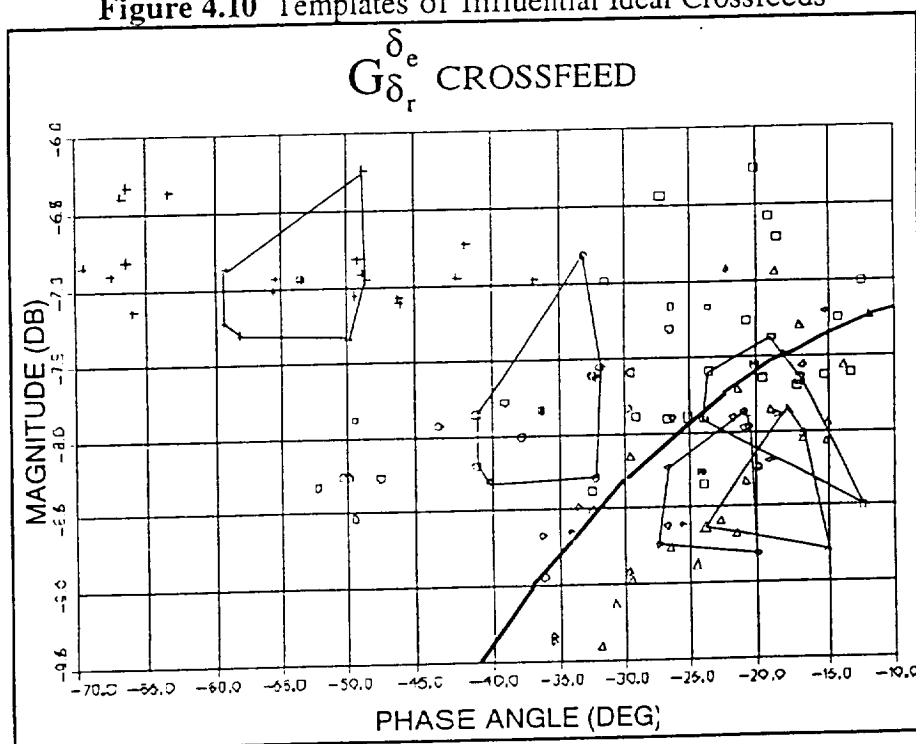


Figure 4.11 Low-Order Dynamic Crossfeeds Block Diagram

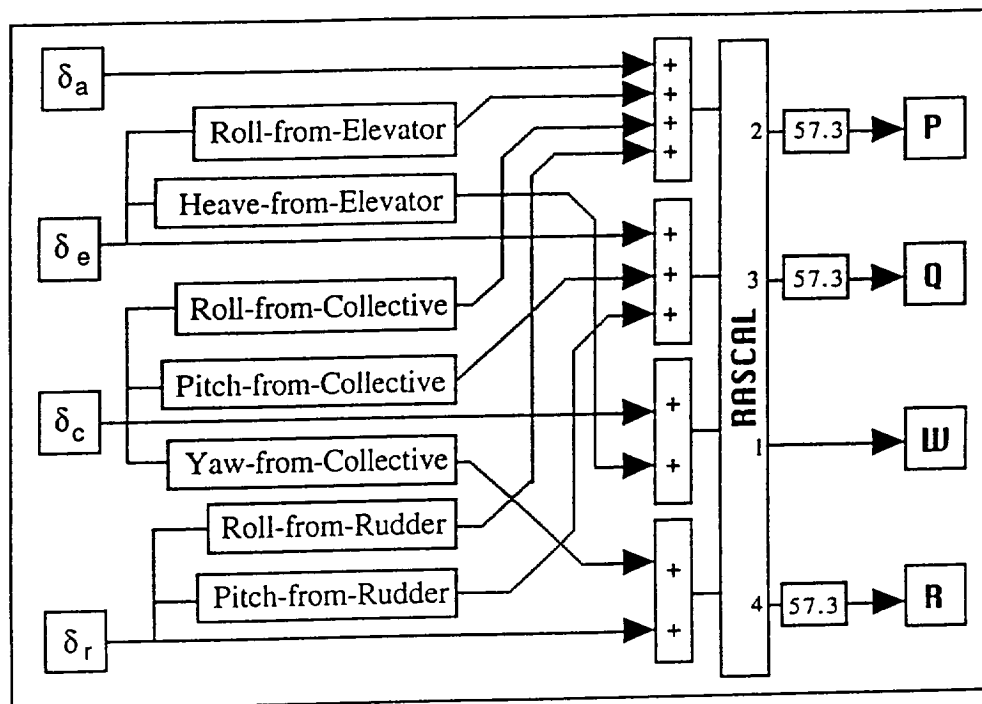
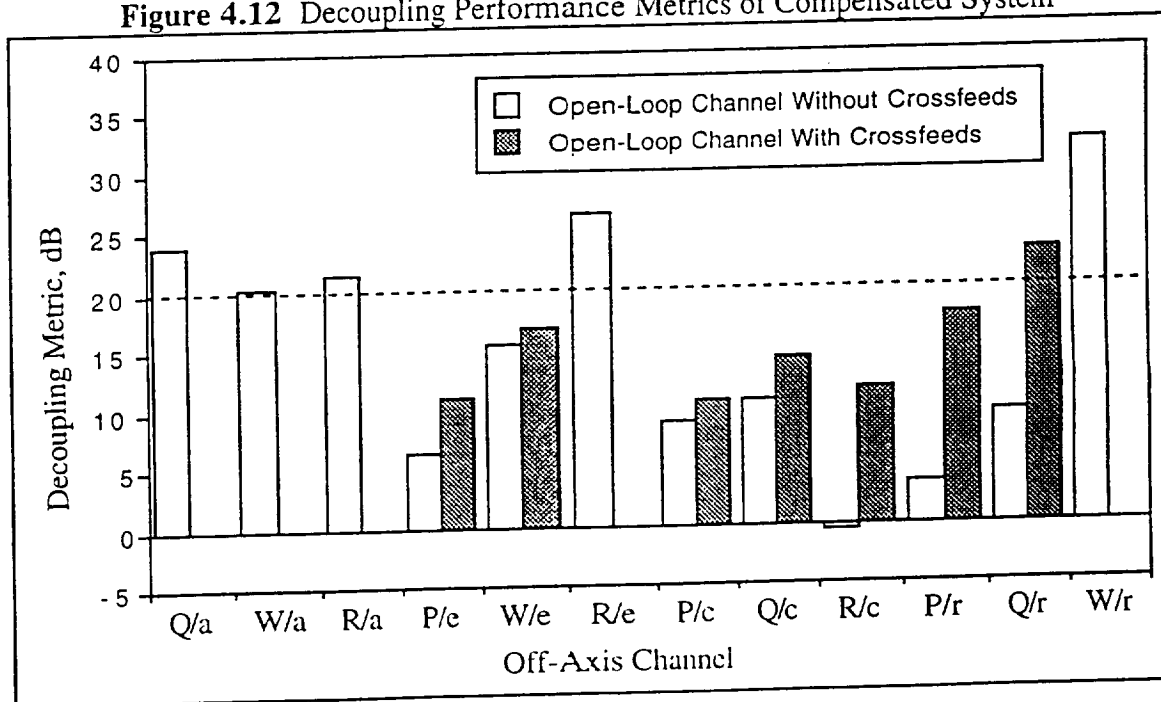


Figure 4.12 Decoupling Performance Metrics of Compensated System



Compensated Responses

The decoupling performance metrics of the open-loop system with crossfeeds is shown in Figure 4.12. Notice that very little improvement in heave-from-elevator, roll-from-elevator crossfeeds and dramatic improvement in yaw-from-collective, roll-from-rudder, pitch-from-rudder crossfeeds. The frequency envelope plot of roll-from-elevator channel (Figure 4.13) shows the average decoupling improvement over entire frequency range of interest (1~10 rad/sec) except at 3.162 rad/sec. In template analysis discuss in previous section, the problem at frequency of 3.162 has foreseen. Since the frequency envelope plot only display the average decoupled magnitude, the difference in standard deviation between uncompensated, nominal, and MSW response can best be visualized on scatter plots (Figure 4.14). In Figure 4.14, it shows the decoupling metric of all 23 configurations have been improved.

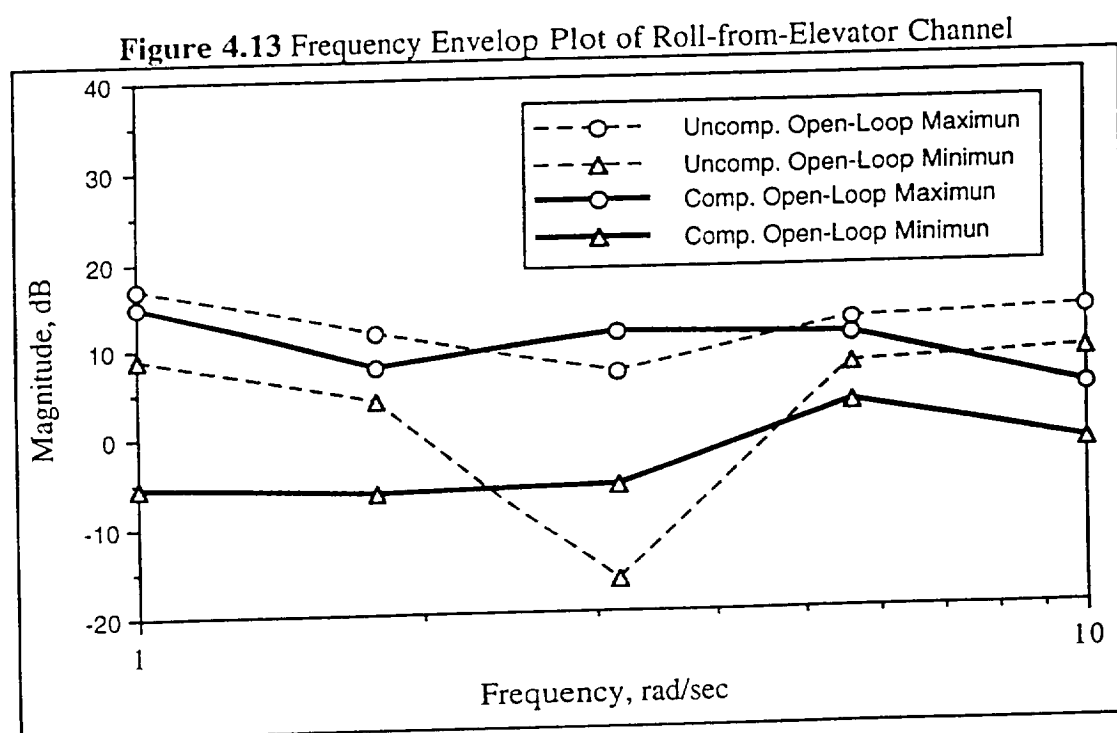
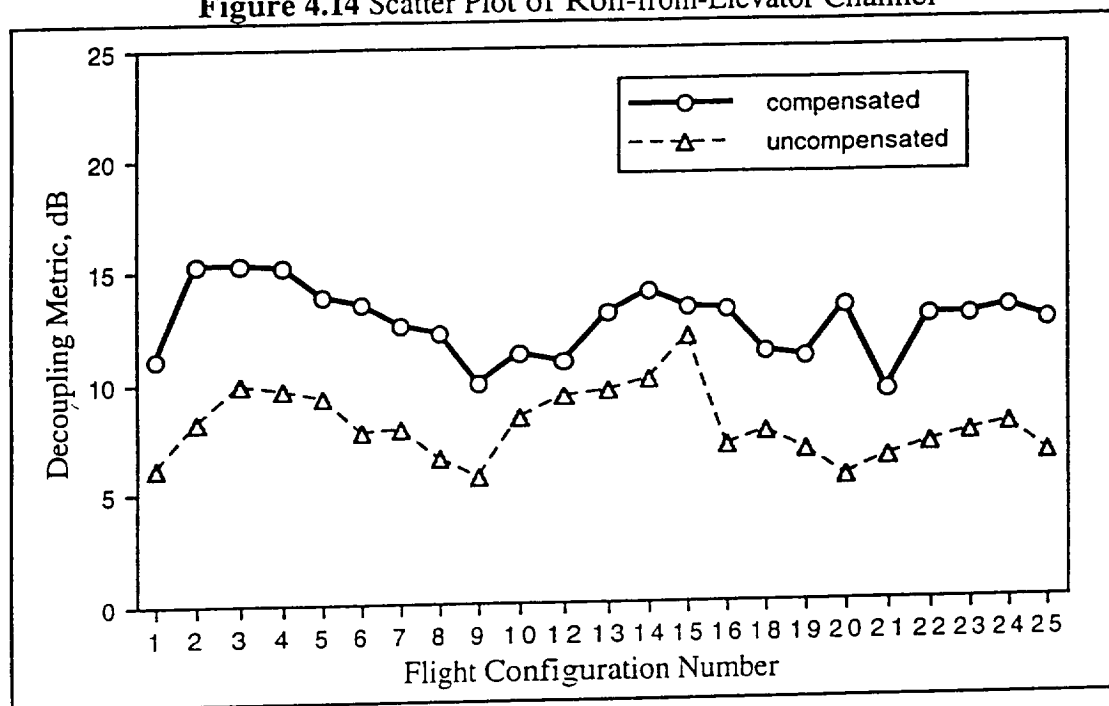


Figure 4.14 Scatter Plot of Roll-from-Elevator Channel



In Figure 4.15, the frequency envelope plot of heave-from-elevator channel shows little improvement in the upper bound and it has worsen in the lower bound. The scatter plot (Figure 4.16) also presents little improvement for most of cases. The main reason of this low-order crossfeed inefficiency is caused by the huge templates which can not represented thoroughly by the target points. Although a low-order crossfeed can be fit through the target points, it does not mean this crossfeed will work since the target points does not fully representing all 23 configurations. As a new agent for next research study, an new method of calculating the target points for the huge template channels should be developed. One benefit can be gain from this new method is a larger set of plant selection can be incorporate into the study to cover a wider spectrum of flight conditions.

Figure 4.15 Frequency Envelop Plot of Heave-from-Elevator Channel

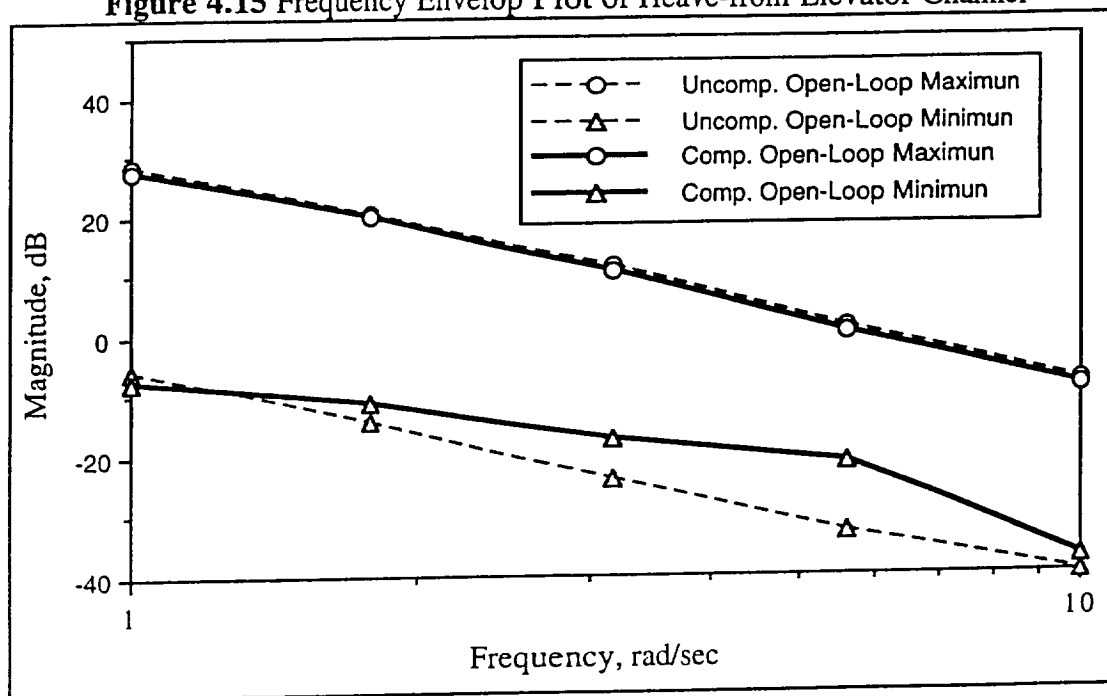
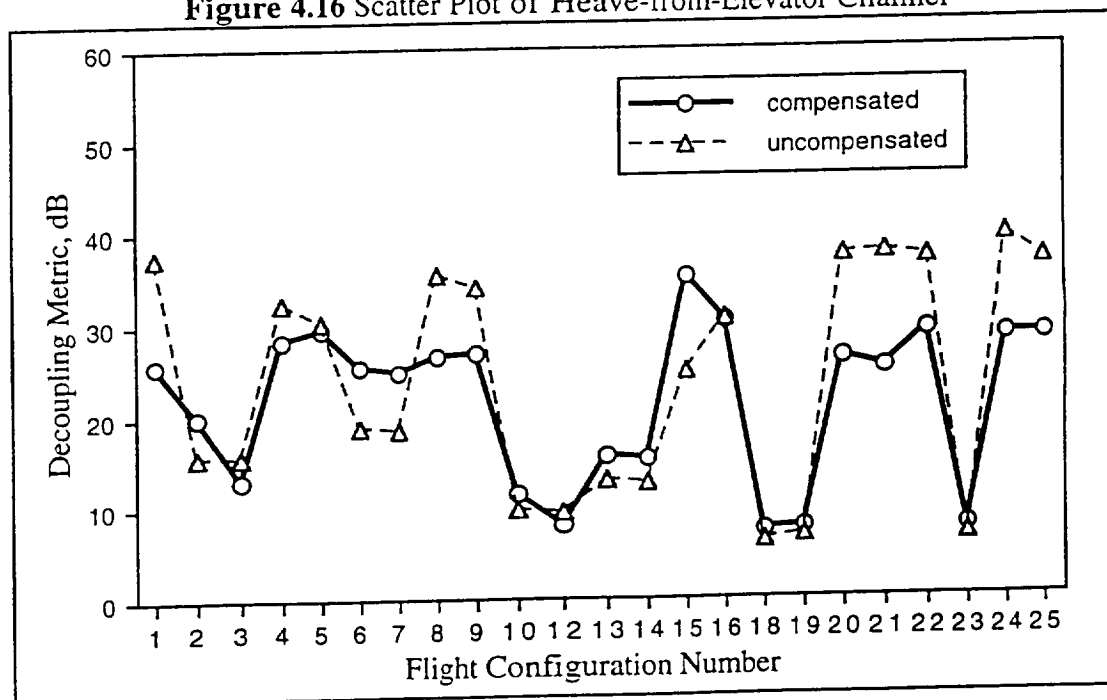


Figure 4.16 Scatter Plot of Heave-from-Elevator Channel



Similar to heave-from-elevator channel, the frequency envelope plot of roll-from-collective channel (Figure 4.17) also shows little improvement. The main reason for this insufficiency is not all caused by the poor representation of target points but mostly caused by the over-lapping of the templates. One can say a simple fixed gain can be used since most of the target points are cluster in a small zone. This observation is inaccurate. It is true that most of the target points are in cluster, but phase shift in the template variation are too much for a simple fixed gain to handle. The scatter plot (Figure 4.16) also indicates a little improvement for most of cases.

Figure 4.17 Frequency Envelop Plot of Roll-from-Collective Channel

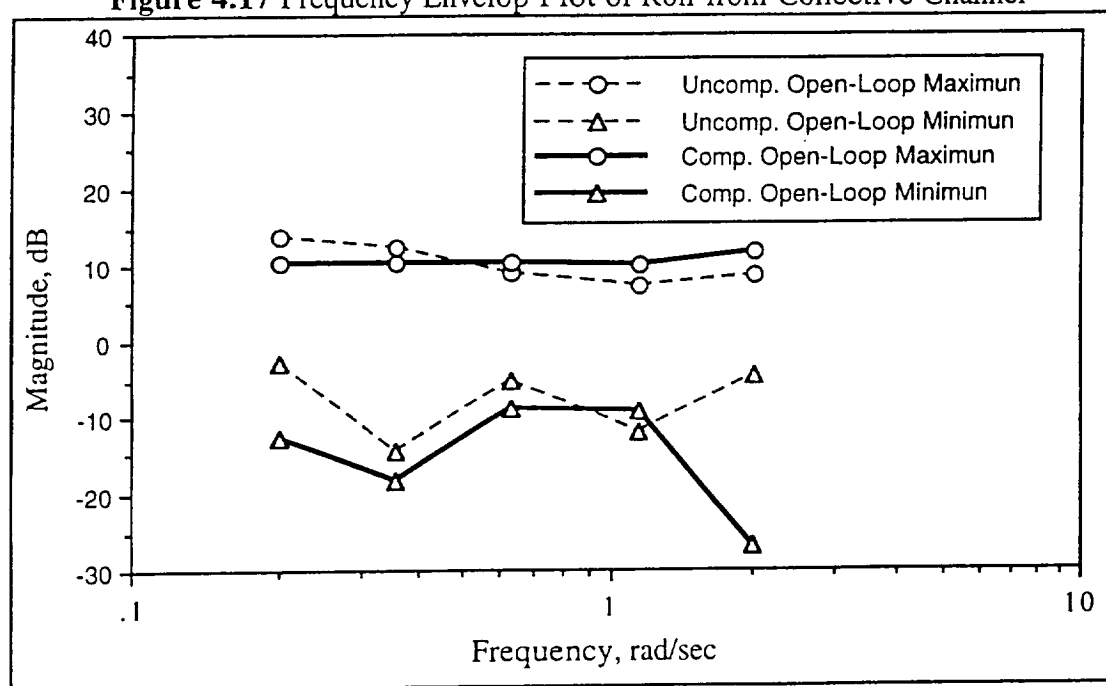
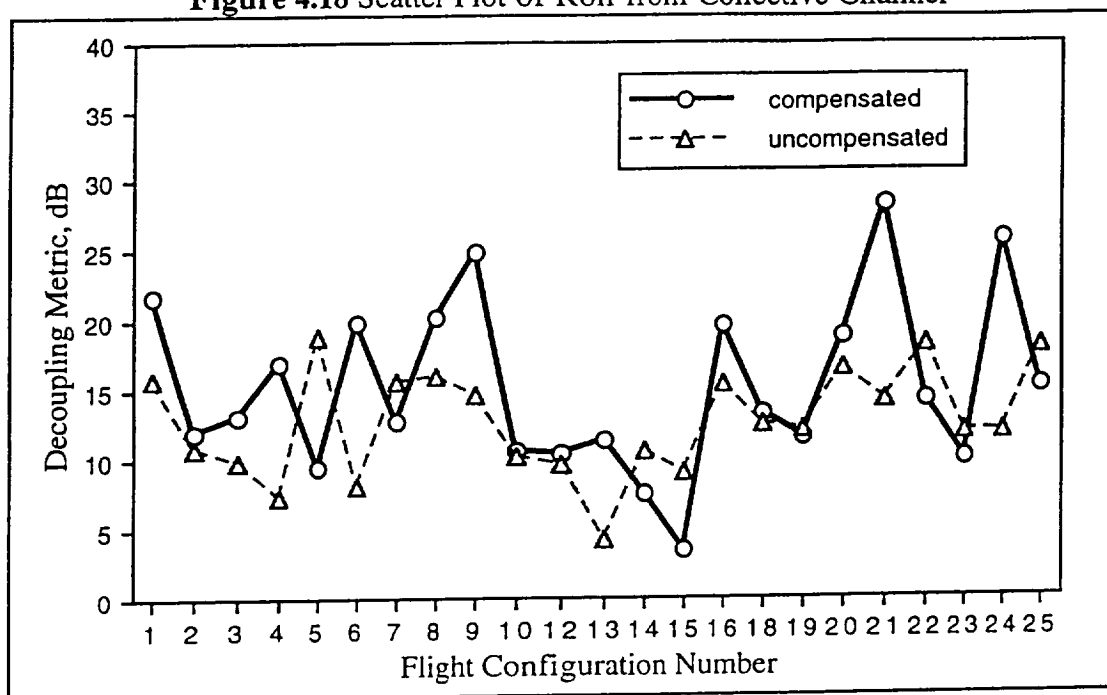


Figure 4.18 Scatter Plot of Roll-from-Collective Channel



The frequency envelope plot of pitch-from-collective channel (Figure 4.19) only show small improvement over entire frequency range but the scatter plot shows otherwise. In Figure 4.20, the scatter plot shows that the low-order crossfeed has successfully decoupled both Group I and Group II configuration. The reason for frequency envelope plot and decoupling performance metrics shows only little improvement is because of the unsuccessfully decoupling in Group III configurations.

Figure 4.19 Frequency Envelop Plot of Pitch-from-Collective Channel

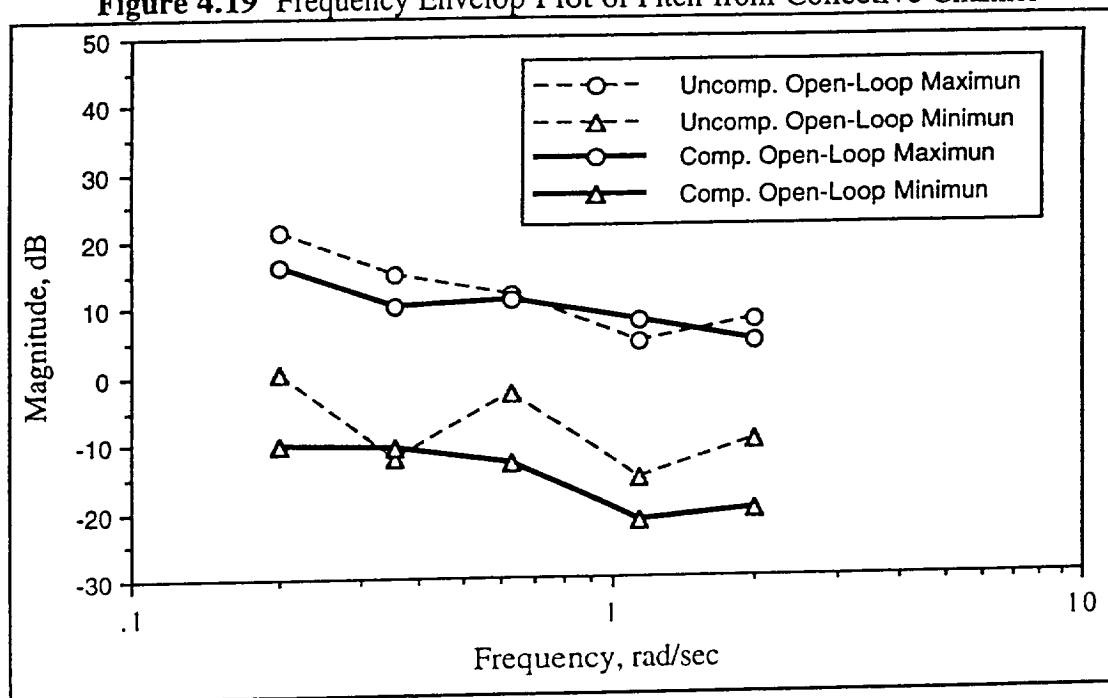
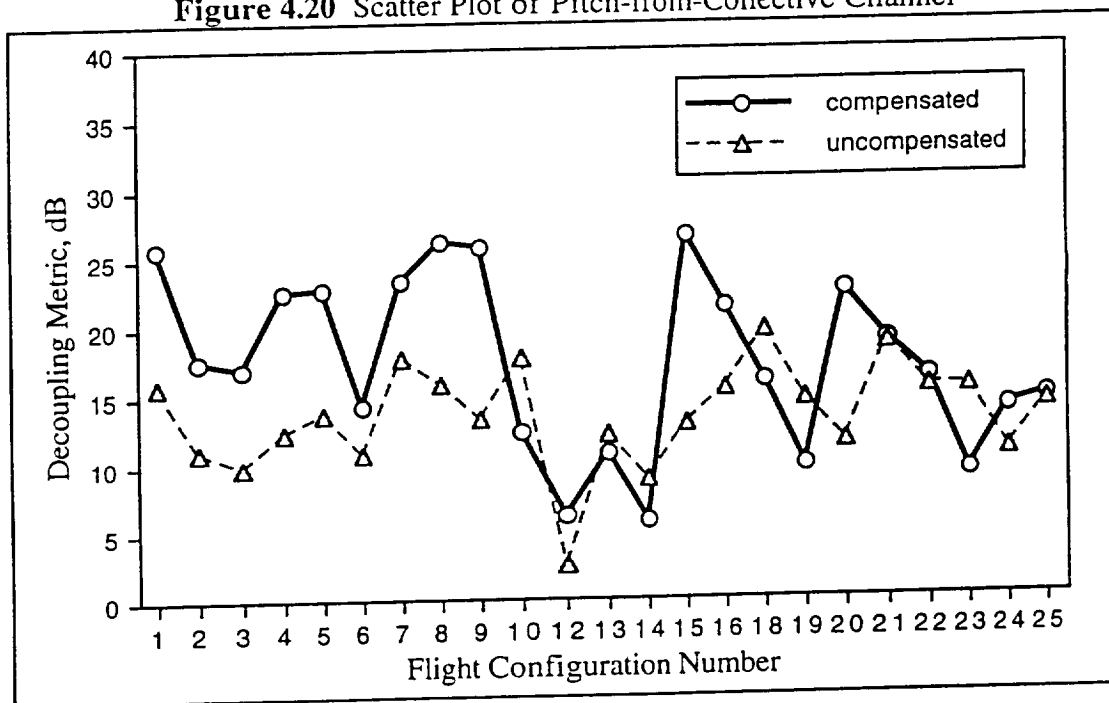


Figure 4.20 Scatter Plot of Pitch-from-Collective Channel



In Figure 4.21, the frequency envelope plot of yaw-from-collective channel has illustrated the heavily coupled response that is caused by the engine dynamic. By implementing a second order transfer function as the dynamic crossfeed, the off-axis response has reduced 14 dB (reduces 75% coupling). The scatter plot in Figure 4.22 display how this simple low-order crossfeed decoupled all 23 flight configurations.

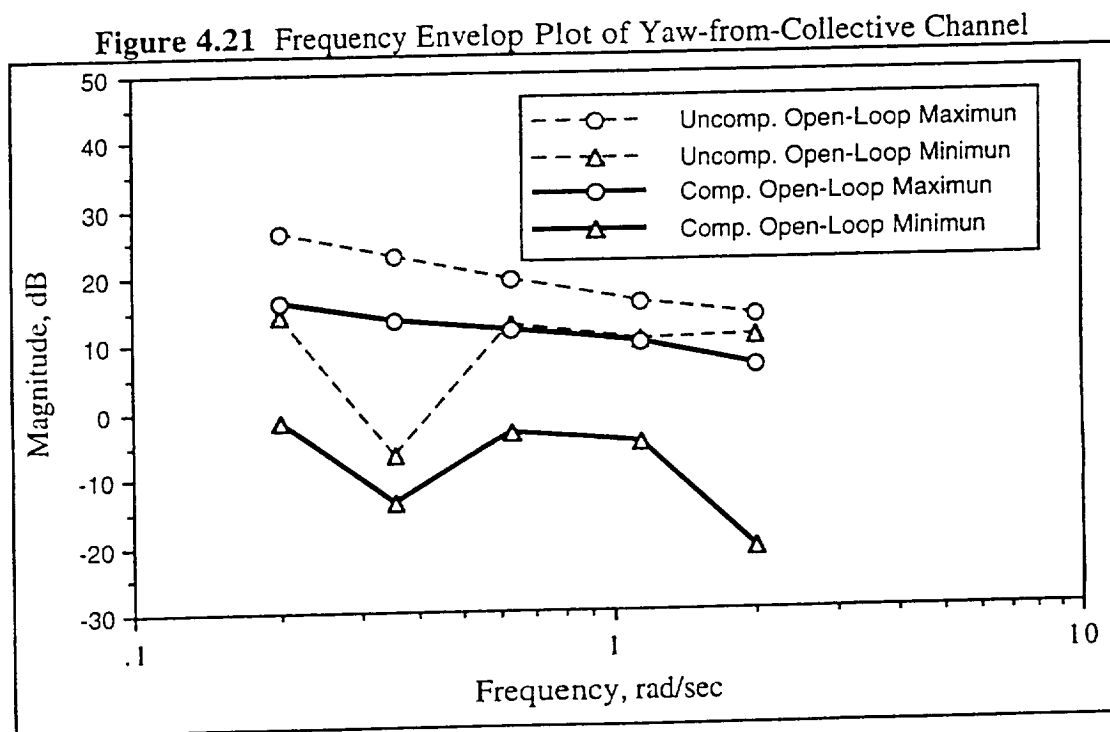
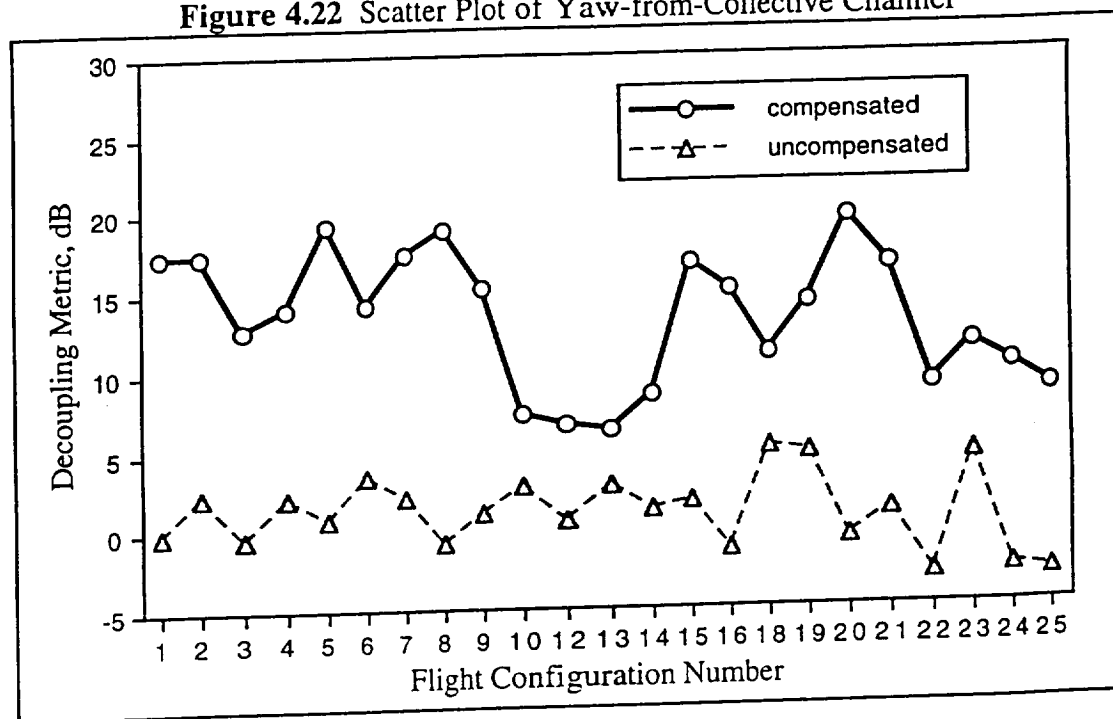


Figure 4.22 Scatter Plot of Yaw-from-Collective Channel



In the roll-from-rudder crossfeed frequency envelope plot (Figure 4.23), the magnitude responses illustrate nearly flat curve that indicates a simple fixed gain should be able to reduce these off-axis responses. The template analysis in last section also points out this observation. This simple fixed gain crossfeed has successfully reduced the off-axis responses by average of 15 dB. The scatter plot (Figure 4.24) also shows improvement in decoupled performance metrics for all flight configurations.

Figure 4.23 Frequency Envelop Plot of Roll-from-Rudder Channel

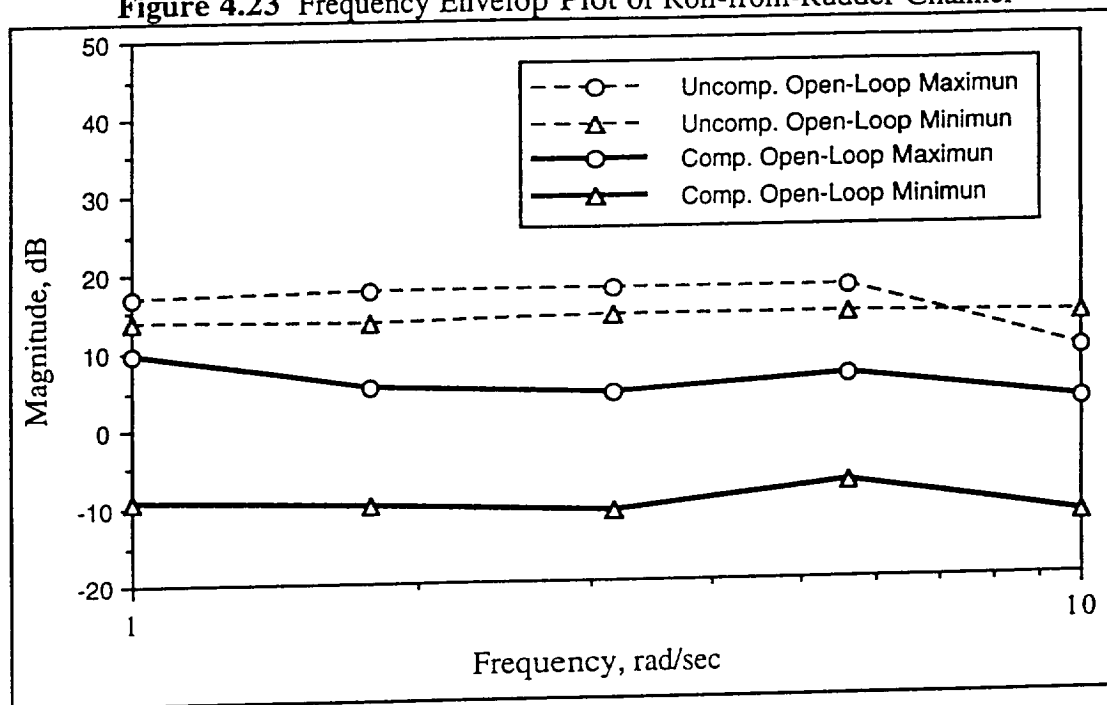
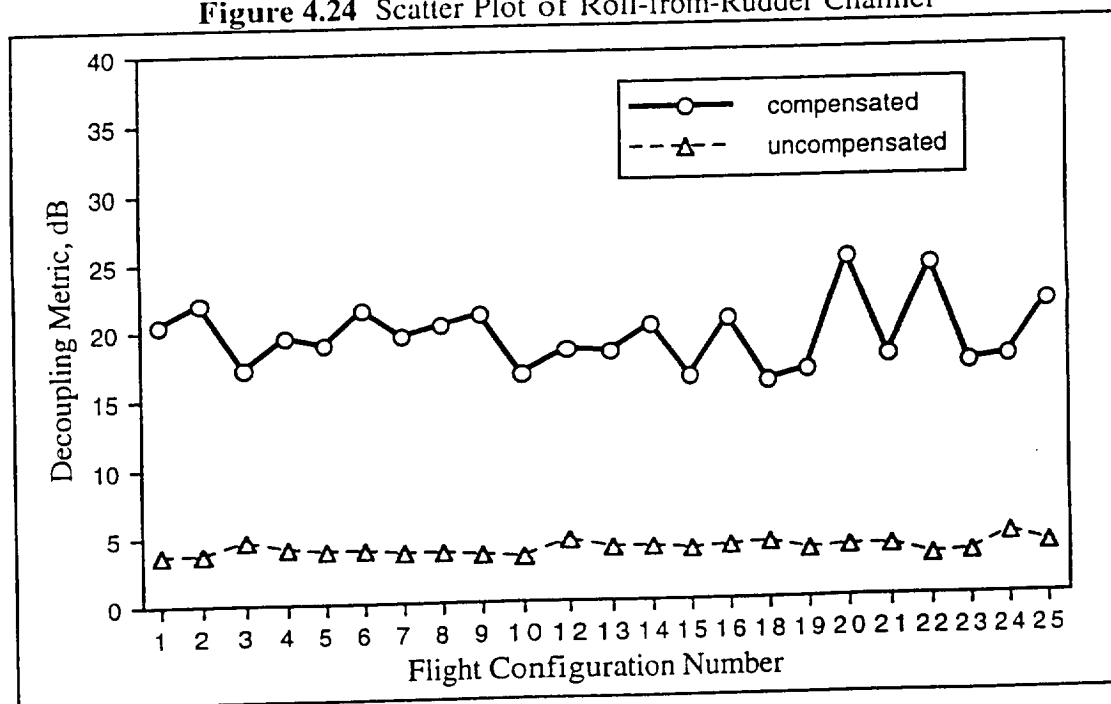
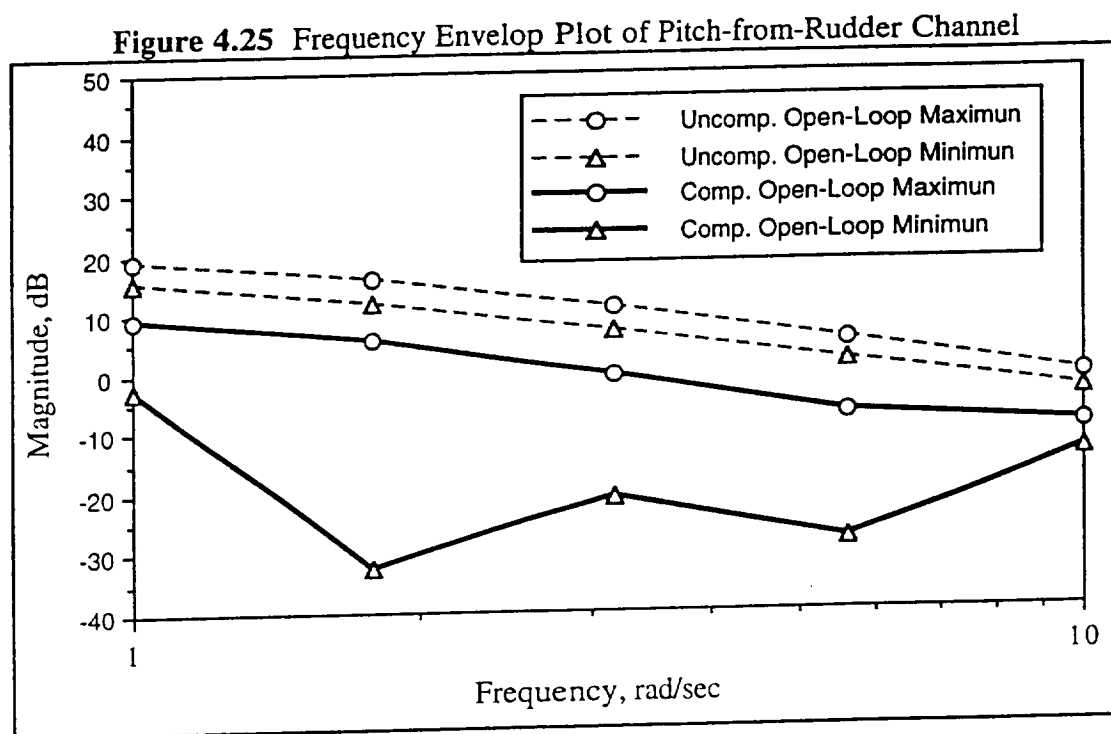


Figure 4.24 Scatter Plot of Roll-from-Rudder Channel

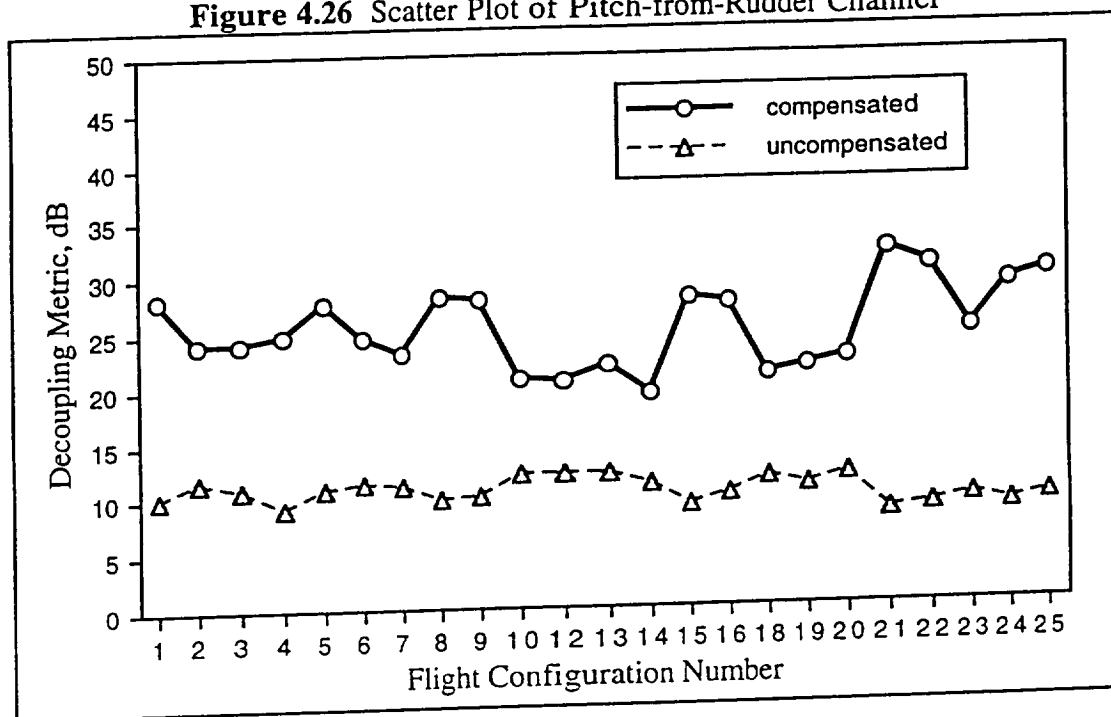


The frequency envelope plot (Figure 4.25) shows that the low-order pitch-from-rudder crossfeed reduces average of 15 dB. In the scatter plot (Figure 4.26), the low-order crossfeed has improved the decoupling performance metrics for all flight configuration.



All seven crossfeed channels' decoupling performance have improved but only the pitch-from-rudder low-order crossfeed has successfully decoupled its channel more than 20 dB (10% coupling). Although the remained six off-axis channels are still below the decoupling specification set in this study, but they have relaxed the high gain required for decoupling without sacrificing performance and robustness. The additional feedback from QFT design should decouple the off-axis channel even more.

Figure 4.26 Scatter Plot of Pitch-from-Rudder Channel



CHAPTER V QFT DESIGN

Design Point Selection

The design point selection was chosen to meet the requirement in ADS-33C⁴ for small-amplitude change of hover and low speed flight configurations. Most of these requirements can be achieved by using response shaping which does not affect the feedback properties of control law. The only requirement in the specification need to be addressed by feedback is the disturbance rejection requirement. The disturbance rejection properties are determined by crossover frequency, which affects the higher frequency pitch-roll attitude modes. The ADS-33C lacks the robust requirement, but an implicit assumption that the performance should be maintained for all flight conditions. In Takahashi's H_∞ Helicopter Controls Study, it has shown that a high level of feedback was set, 5 rad/sec crossfeed, and a requirement was imposed to have at least 45° of phase margin and 6 dB of gain margin.⁵

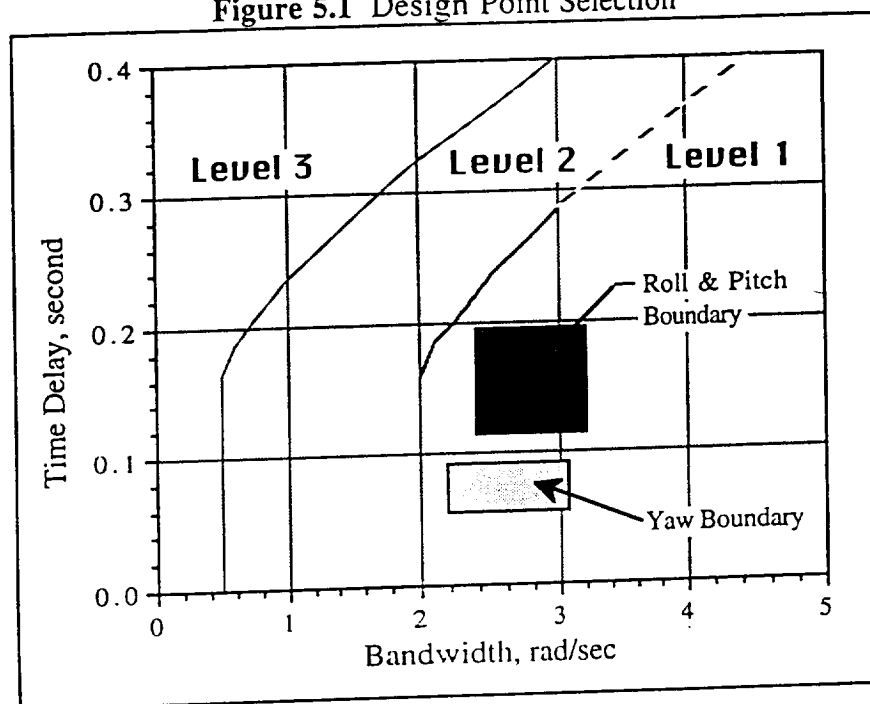
The QFT control law design (as it mentioned in Chapter II) inherent ability is to reject disturbance, and the control cross-couplings are considered as the disturbances which are minimized by this design process. Since the controls have been decoupled and the feedback gain has been conserved, a low level of feedback, crossover of 2.5 rad/sec is selected for roll, pitch, and yaw axes. In Figure 5.1, the rectangular shaded box shows

⁴ Handling Qualities Requirements for Military Rotorcraft, ADS-33C, page 18

⁵ Takahashi, M. D. , H_∞ Helicopter Flight Control Law Design With and Without Rotor State Feedback.

nominal plant and its variation bound which determine the tracking performance specifications in time domain. These specifications included stability margin of 2.3 dB, bandwidth of 3 rad/sec, and gain margin of 6 dB.

Figure 5.1 Design Point Selection



Tracking Performances Specifications & Response Types

Based on the time domain specification, tracking performance bounds are determined by using second order transfer functions which have been selected to meet the handling qualities specification plus 10% overshoot for a step input. The transfer functions are listed in Table IX.

Table IX. Tracking Performance Transfer Functions

Control Axis	Upper Bound	Lower Bound	Frequency Range
Roll, Pitch Axis	$\frac{8.3190 e^{-0.143s}}{[0.45, 2.75]}$	$\frac{27.34 e^{-0.143s}}{[0.75, 2.25] (6.0)}$	1 ~ 10 rad/sec
Yaw Axis	$\frac{5.5 e^{-0.077s}}{(0) (5.0)}$	$\frac{36 e^{-0.050s}}{(0) (5.0) (8.0)}$	1 ~ 10 rad/sec
Heave Axis	$\frac{2.2 e^{-0.077s}}{(0) (2.0)}$	$\frac{6.3 e^{-0.050s}}{(0) (1.0) (7.0)}$	0.2 ~ 2.0 rad/sec

In Figure 5.2~5.4, the roll and pitch responses are design for attitude command-attitude hold system (ACAH), and the heave and yaw responses are rate command-attitude hold (RCAH). For example, in Figure 5.2, the solid lines are the magnitude curves, and the dashed lines are the phase curves. The final frequency responses of all flight configurations for roll and pitch axis must fall within the bounds in frequency of range of 1 to 10 rad/sec. Falling outside bounds at frequency lower than 1 rad/sec will not provide desired steady state responses and falling outside bounds at frequencies higher than 10 rad/sec will not provide desired transient response.

Figure 5.2 Tracking Bounds of Roll, Pitch Axis

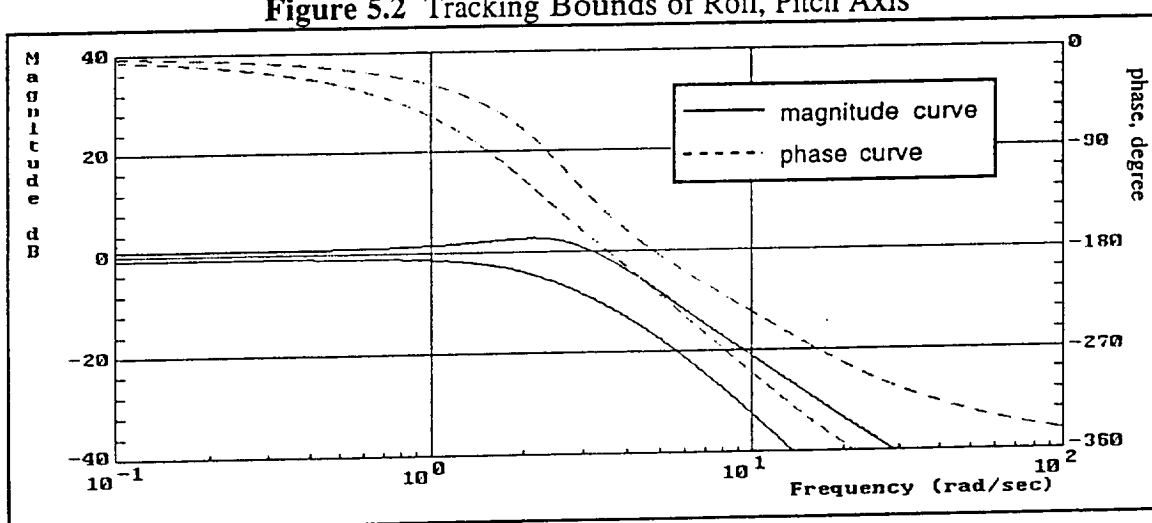


Figure 5.3 Tracking Bounds of Heave Axis

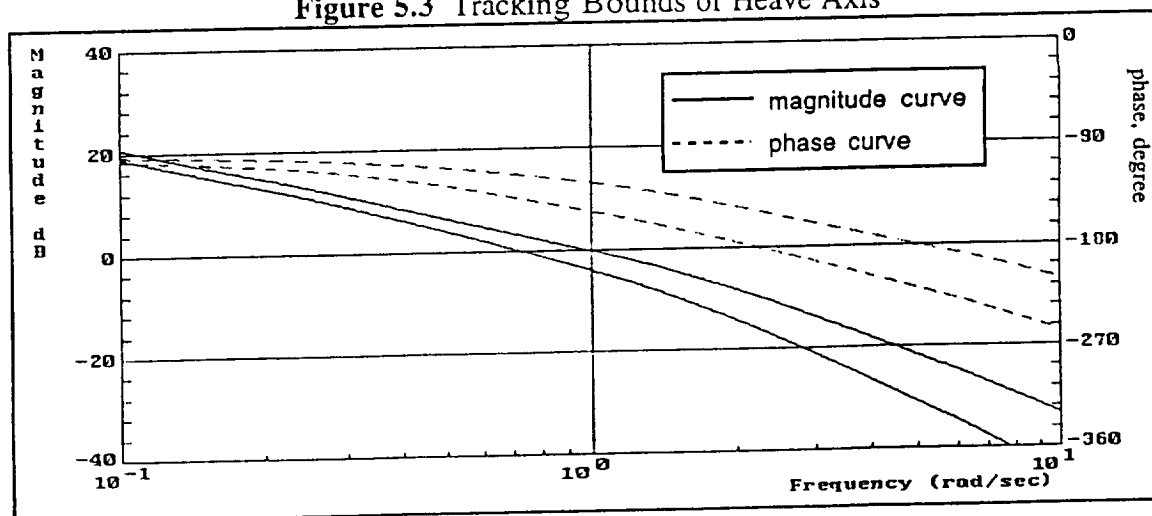
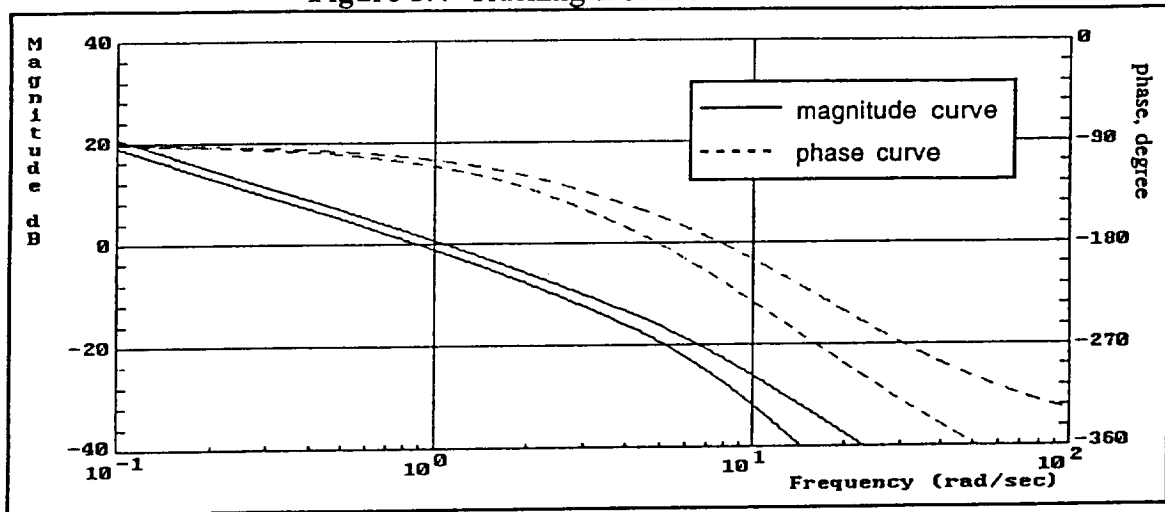


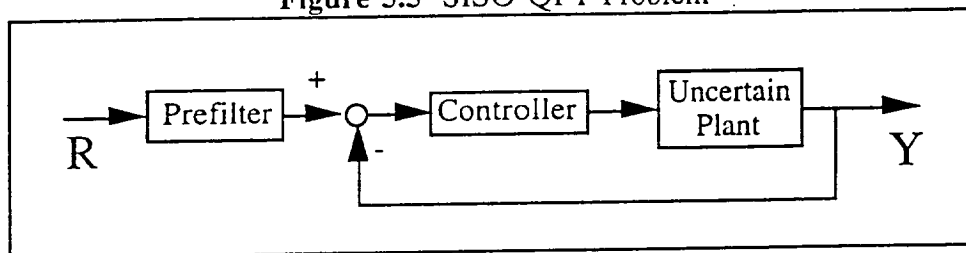
Figure 5.4 Tracking Bounds of Yaw Axis



Controller Design

The low-order crossfeeds designed so far have decoupled the multi-input multi-output (MIMO) system into four single-input single-output control systems (SISO) shown in Figure 5.5.

Figure 5.5 SISO QFT Problem



In QFT design, the purpose of the controller is to obtain the loop transmission so the "magnitude variation" of closed-loop frequency response over the frequency range of interest does not exceed the tracking bound specifications (discussed in previous section). No actual loop-shaping of frequency response is concerned at this point, only the variations over frequency with uncertainty. The loop-shaping of the closed-loop frequency responses is done by the prefilter which is discussed in next section. In the design of the controller, a high-order transfer function can be implemented, but only the constant gains were used in this study for the demonstration of QFT control design. All four axis were using same

controller structure; however, only the roll axis is shown in Figure 5.6 as example. Since the QFT CAD package (ref. 13) only allow unit feedback, a block diagram algebra demonstrates conversion between two structures, where **P** and **ACT** represent the decoupled compensated plant and actuator dynamic, respectively. The **ZOH** and **AA** are added for digital control system emulation. The **ZOH** is used here to simulate computational and zero-order-hold time delay and the **AA** is implemented to reduce the sensor noise. A study done by Dr. Tischler in Reference 2 was using similar control structure which incorporating a lead compensator in its feedback loop addition to the feedback gains. A QFT controller was designed for the baseline model using the CAD package of Reference 13 and resultant controllers are shown in Table X.

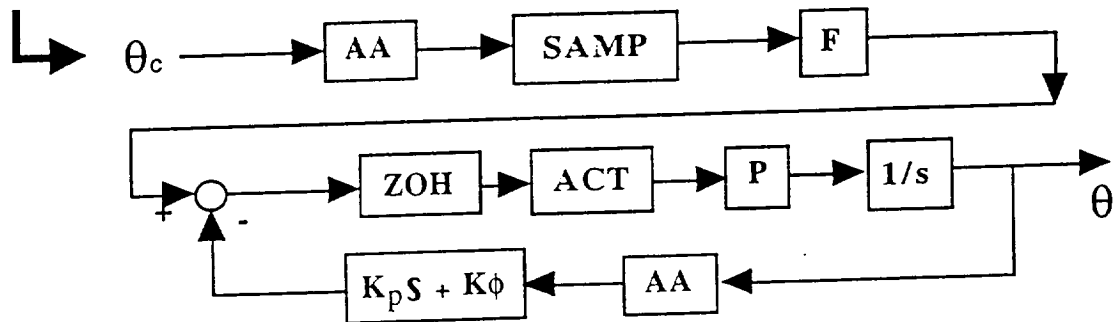
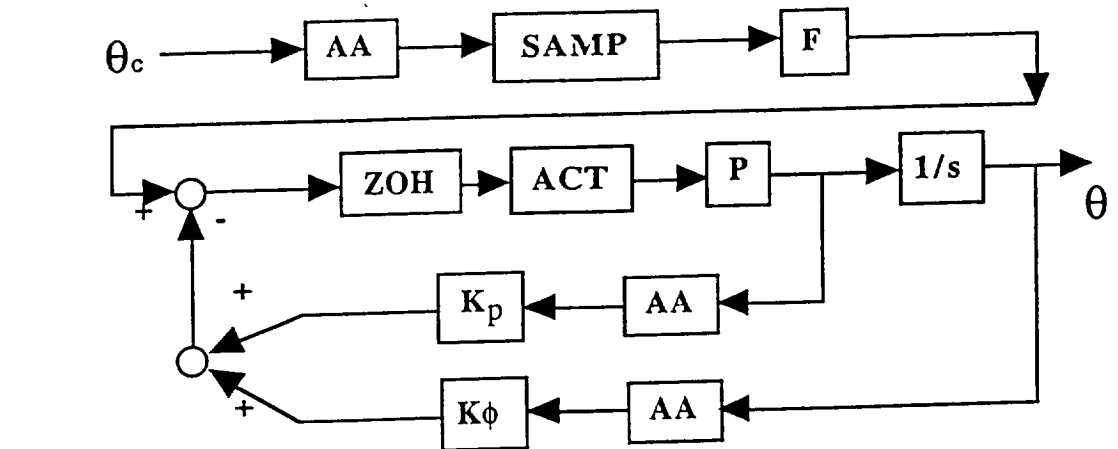
Table X. QFT Controllers

	Rate Feedback Gain	Attitude Feedback Gain	Crossover Freq.
Roll Axis	0.0222	0.1111	2.57
Pitch Axis	0.1089	0.0653	2.56
Heave Axis	0.1759	0.0633	1.05
Yaw Axis	0.1064	0.0255	2.42

The CAD program enables the user to design the QFT controller in graphical method. By changing the controller, the CAD program automatically re-calculates and re-plots the loop transmission on screen. The screen displays the tracking boundaries, high frequency bound, template points at each frequency, and the loop transmission on Nichols Chart as shown in Figure 5.7~5.10. In the Figure 5.7, the loop-transmission in roll axis has a crossover frequency of 2.57 rad/sec which fall within boundary of design bounds in Figure 5.2. Similar to roll axis, pitch and yaw axis also has a crossover frequency within bounds.

Figure 5.6. Controller Structure

Structure used in Matlab Simulink Program



Structure used in QFT CAD Package

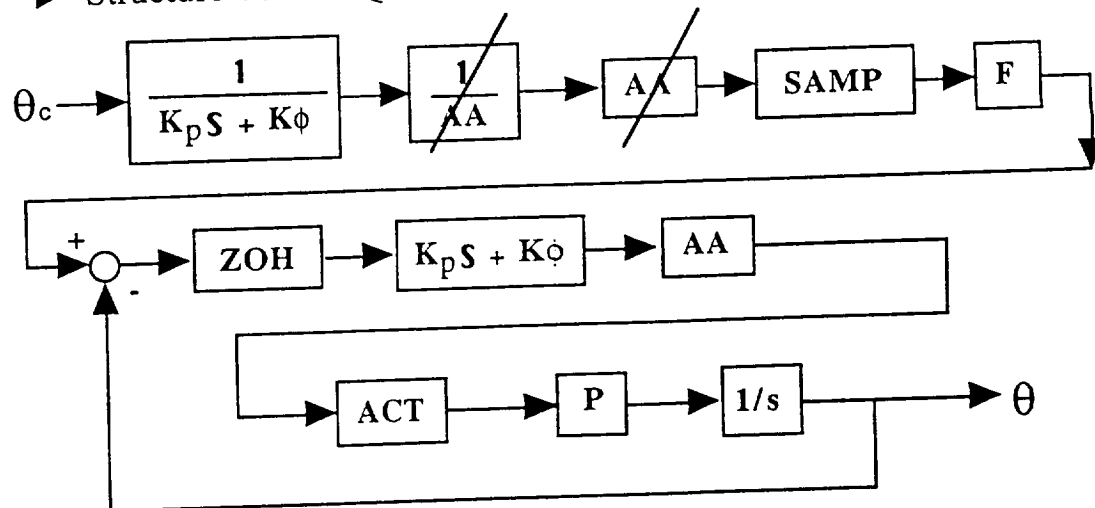


Figure 5.7 Roll Axis QFT Controller

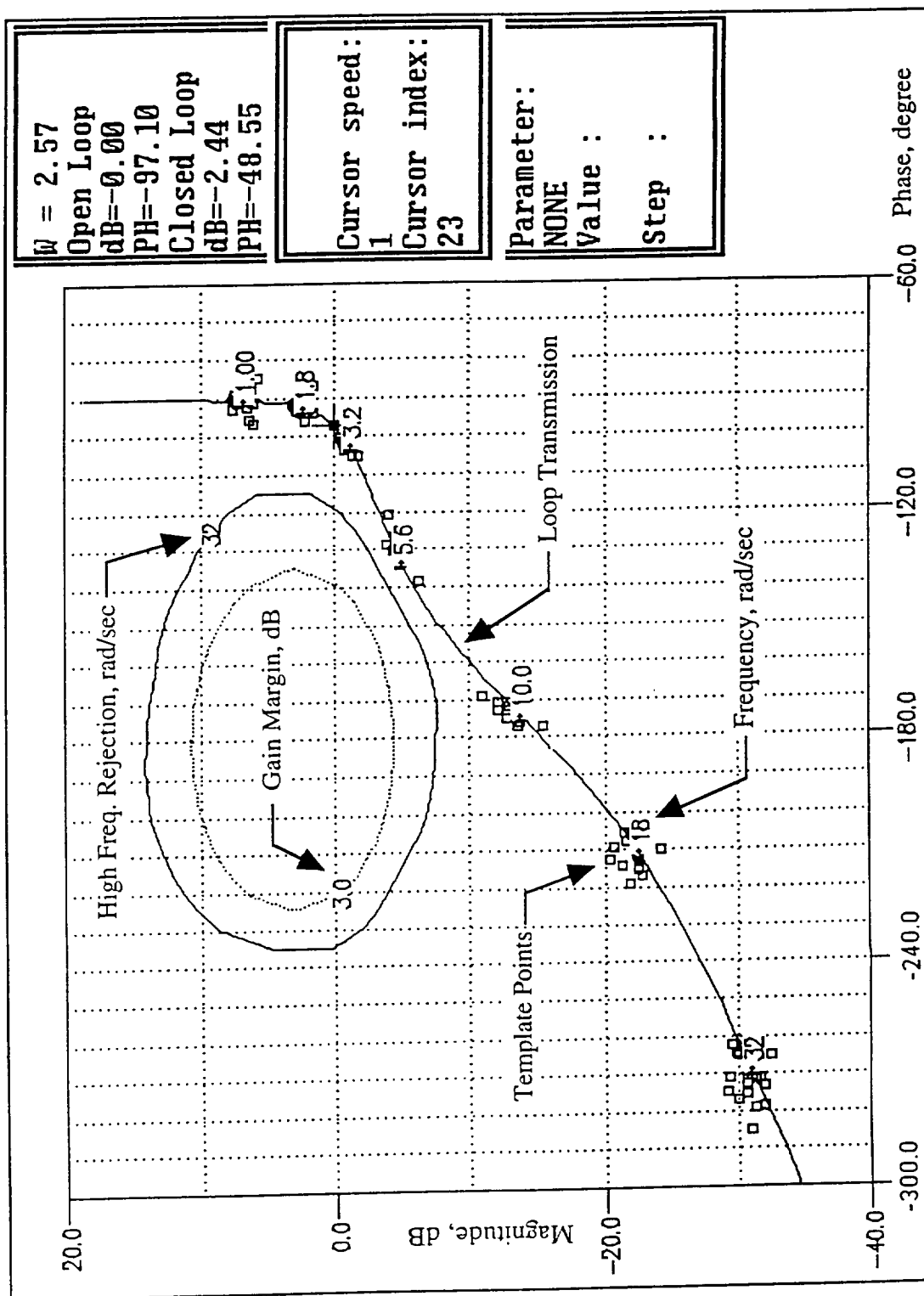


Figure 5.8 Pitch Axis QFT Controller

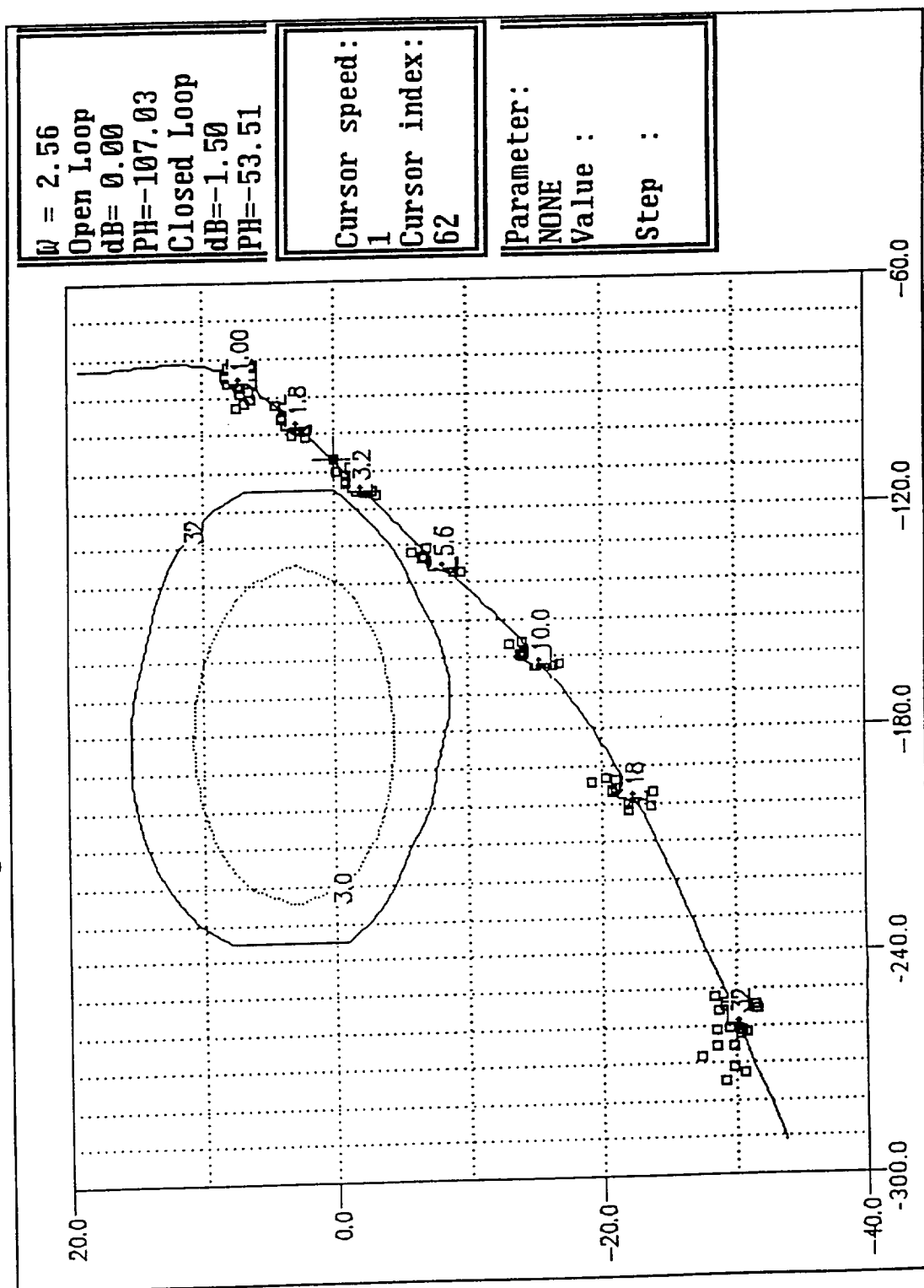


Figure 5.9 Heave Axis QFT Controller

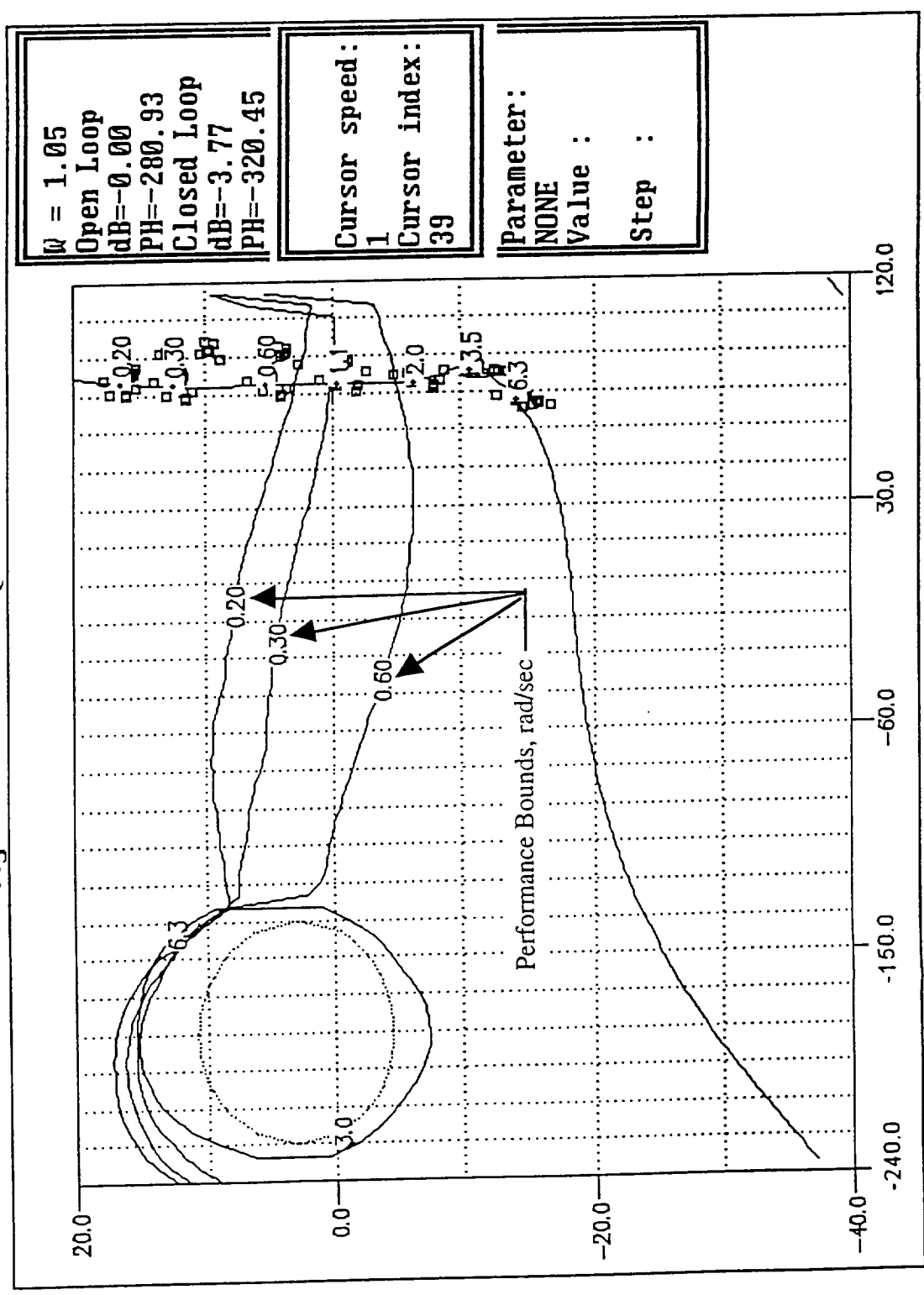
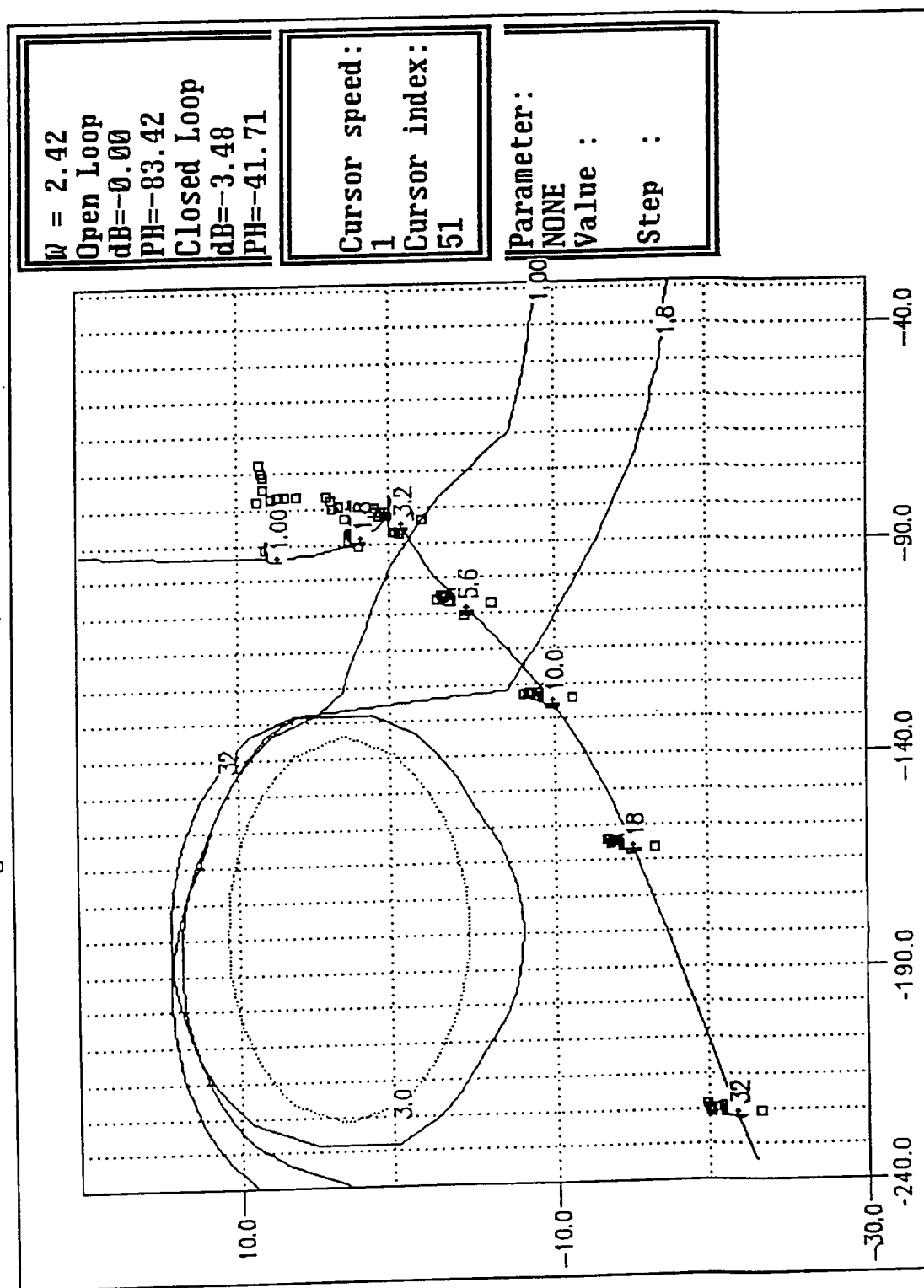


Figure 5.10 Yaw Axis QFT Controller



Prefilter Design

The purpose of prefilter in QFT design is to ensure the resulting frequency response lies within tracking bounds (Figure 5.2~5.4) which are determined from Figure 5.1. The basic prefilter block diagram is shown Figure 5.5 where **SAMP** is used to simulate the sampling time delay of digital system in analog system, and **F** is the prefilter of the QFT design. Since both heave and yaw axis are RCAH system, an integrator is added to the prefilter design which is shown in Table XI. The pole at -100 rad/sec is added to the roll axis prefilter to make it realizable. The frequency plots of the final QFT control system are shown in Figure 5.11~5.14, and the QFT control system block diagram is in Figure 5.15. The most outer pair curves are the performance bounds. The next pair curves are the template variations, and the most center curve is the nominal plant. Note that the template variation of all 23 flight configurations stay within their tracking performance bounds in the frequency range of interest.

Table XI QFT Prefilter

Control Axis	Transfer Function
Roll Axis	$\frac{0.2248 [0.7, 5.6] (10)}{[0.64, 2.52] (100)}$
Pitch Axis	$\frac{0.2942 (0.45)}{(2.0)}$
Heave Axis	$\frac{0.2748 (0.296) (2.0)}{(0) (2.58)}$
Yaw Axis	$\frac{0.1179 (0.220)}{(0)}$

Figure 5.11 Roll Axis QFT Prefilter Frequency Plot

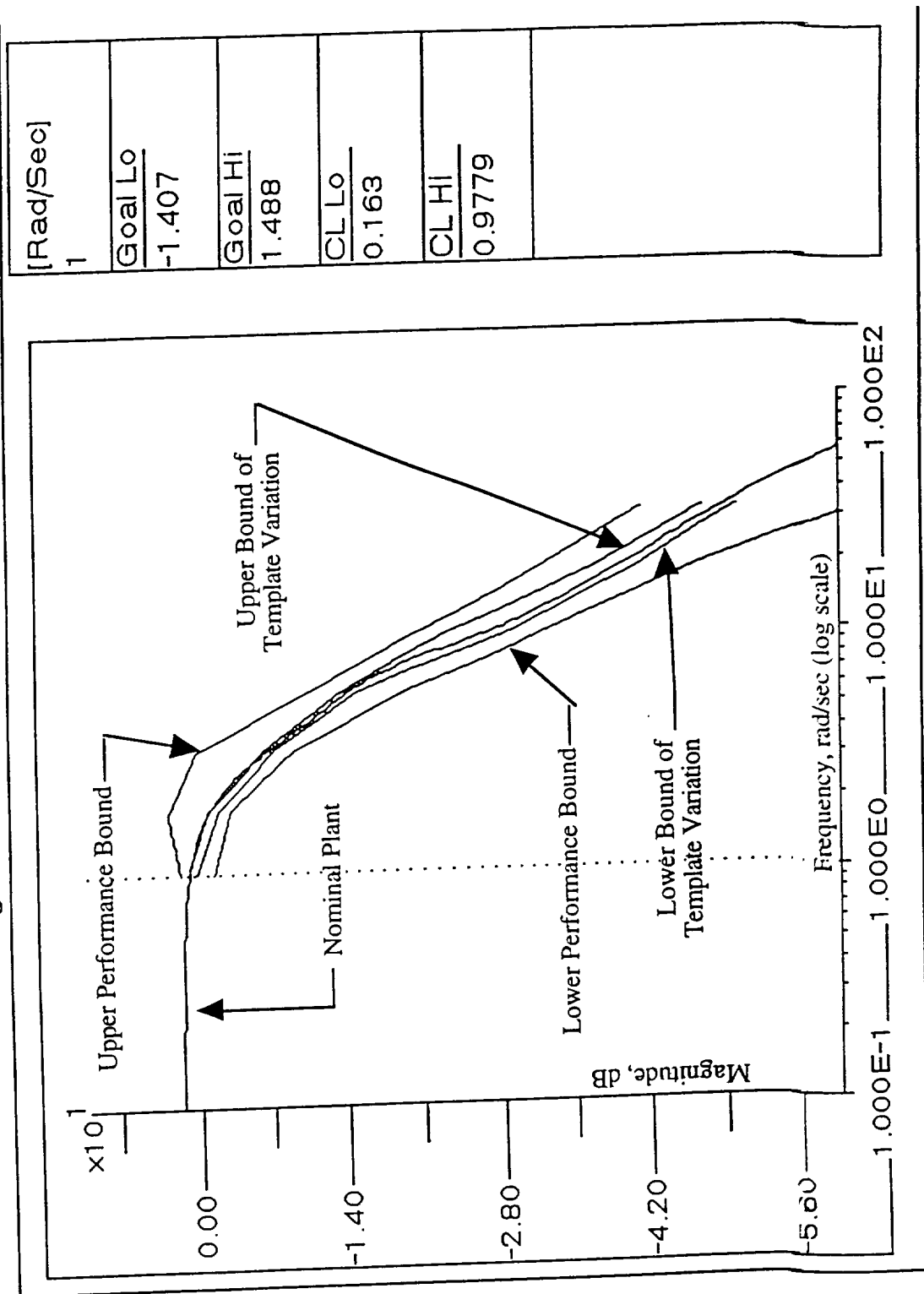


Figure 5.12 Pitch Axis QFT Prefilter Frequency Plot

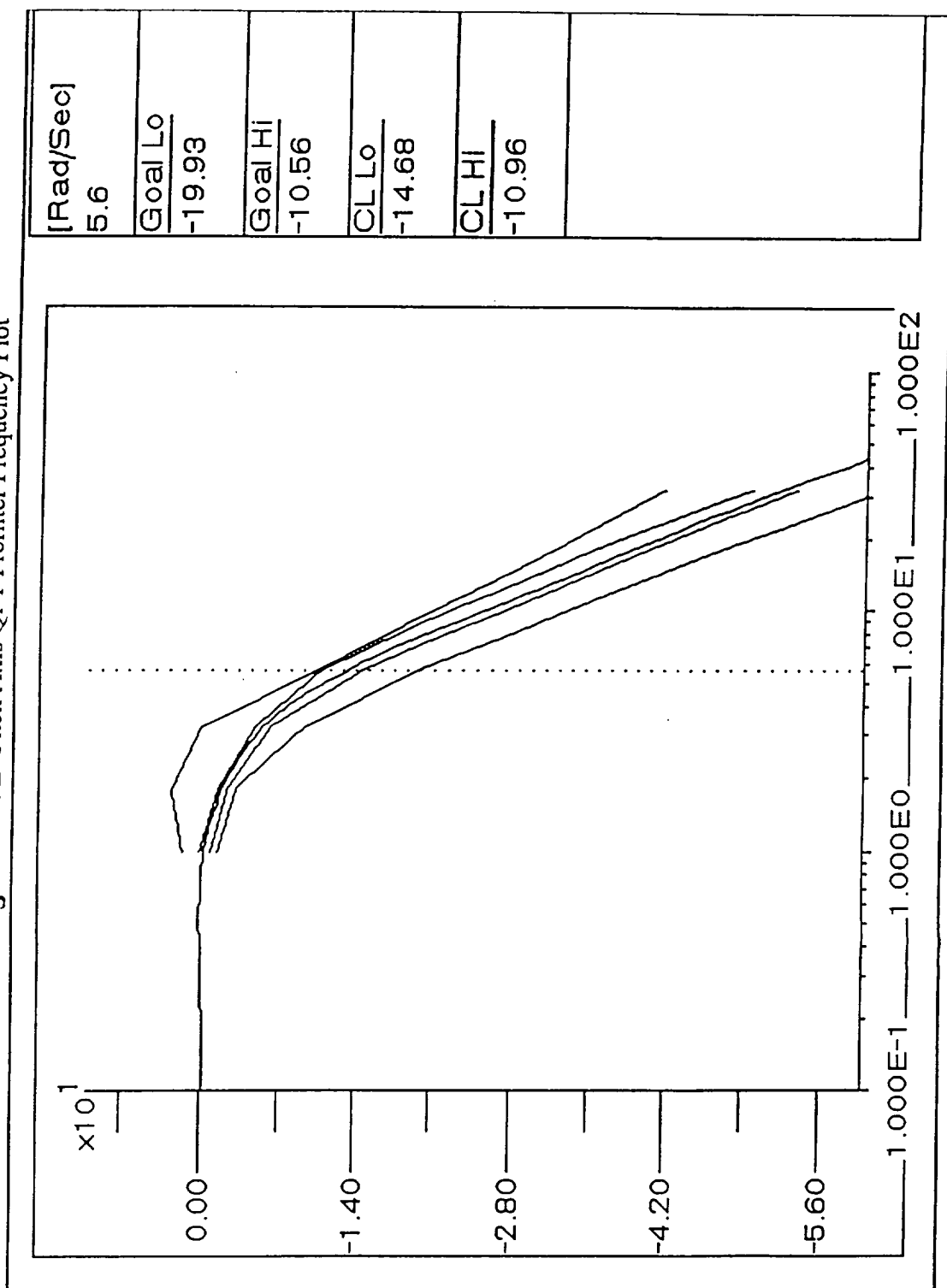


Figure 5.13 Heave Axis QFT Prefilter Frequency

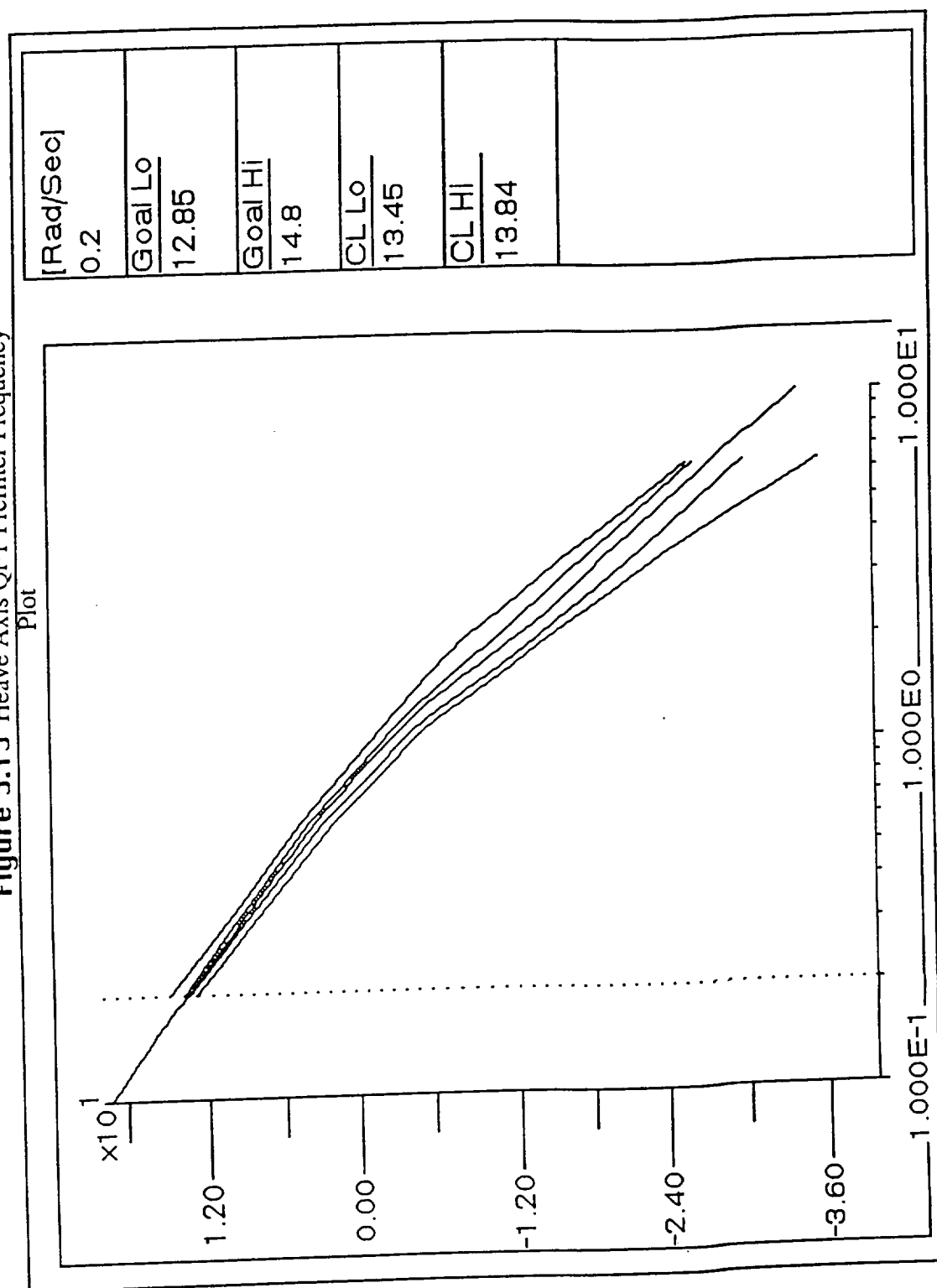


Figure 5.14 Yawl Axis QFT Prefilter Frequency

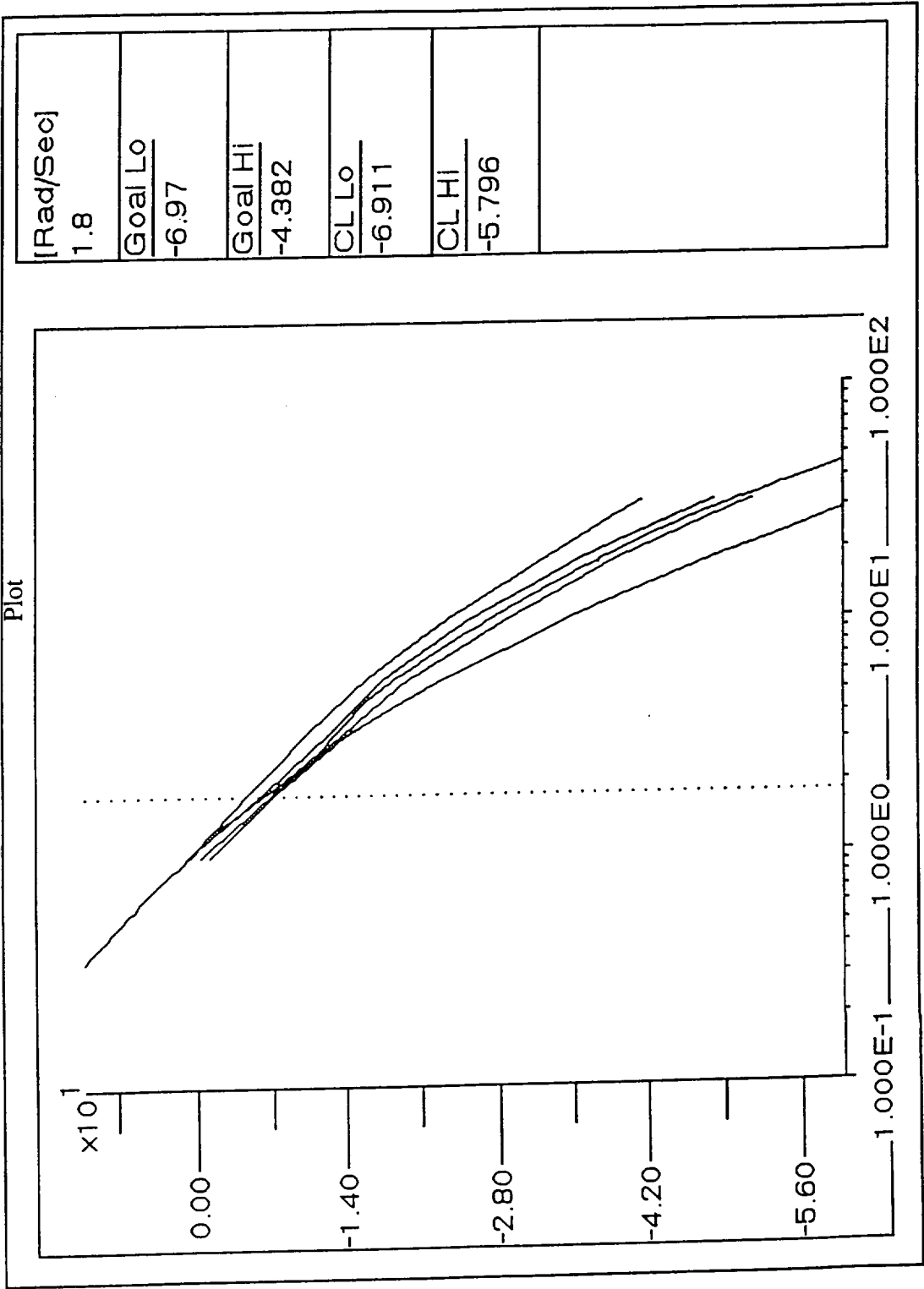
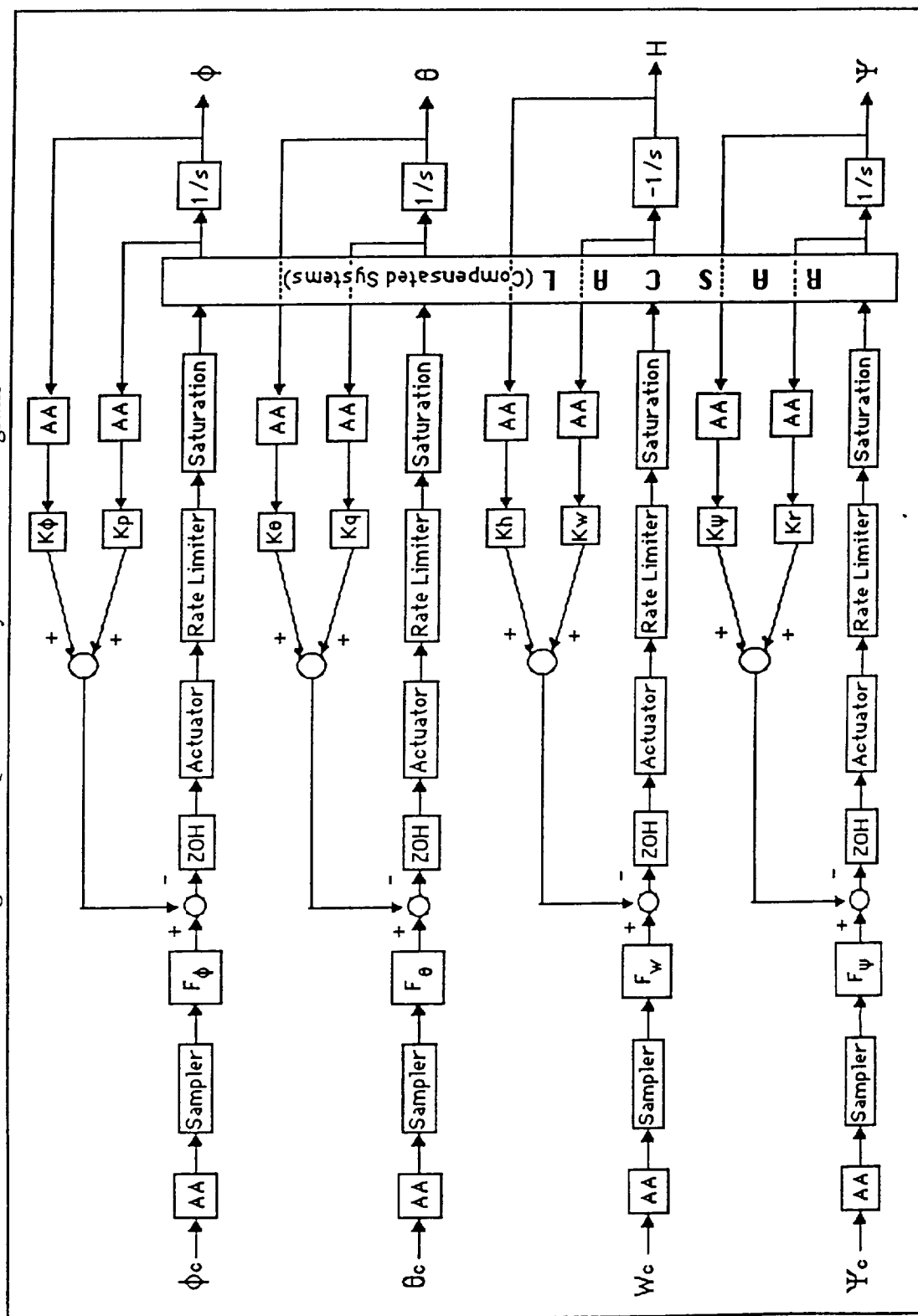


Figure 5.15 QFT Control System Block Diagram



CHAPTER VI

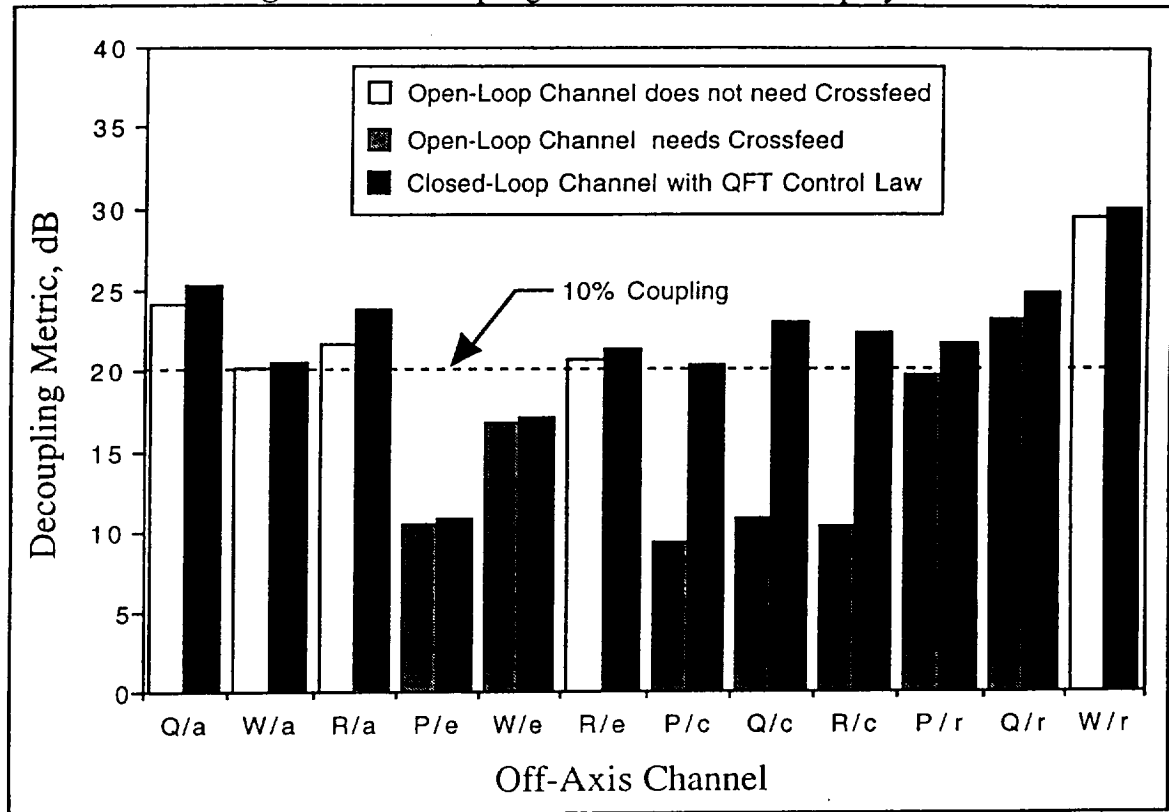
FLIGHT CONTROL SYSTEM ANALYSIS

Decoupling Performance Metrics of Open-Loop Control System (Review)

In this research, the control system design consists of two stages: crossfeed design and QFT design. The performance of the low-order crossfeeds has evaluated in Chapter IV. In the crossfeed design, Seven out of twelve off-axis channels required the low-order dynamic crossfeeds, and only the pitch-from-rudder channel has achieved the desired decoupling performance metric above 20 dB.

Decoupling Performance Metrics of Closed-Loop Control System

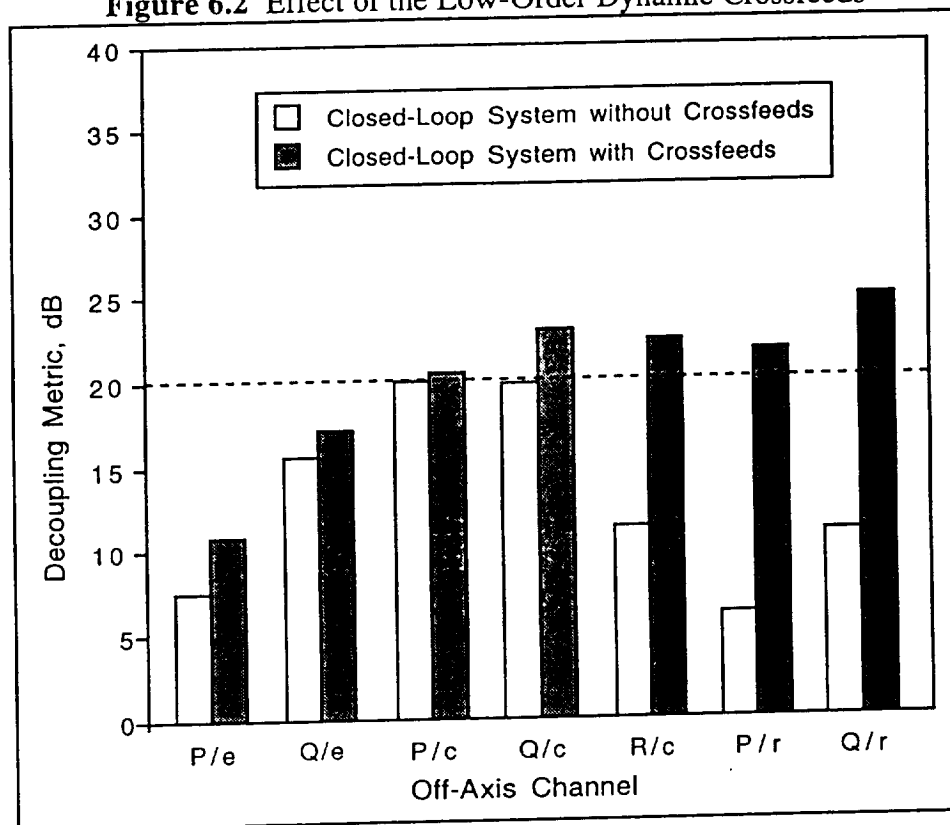
The decoupling performance metrics of closed-loop system is evaluated, and their results is shown in Figure 6.1. Notice in this chart, only the heave channels (P/c , Q/c , R/c) improved most by the QFT feedback design. The average increase in decoupling metrics is 11.7 dB, which in term of decoupling percentage is 74% improvement. Other four channels also have small increase of the decoupling metric, but they are not as much as the heave channel. All channels have achieved the decoupling metric of 20 dB or better except the roll-from-elevator (P/e) and the pitch-from-elevator (Q/e).

Figure 6.1 Decoupling Metric of Closed-Loop System

Effect of Dynamic Crossfeed on a Closed-Loop System

The effect of the crossfeeds on a closed-loop system is shown in Figure 6.2. In this figure, the decoupling crossfeeds improved the decoupled metric most on the yaw-from-collective (R/c) channel and yaw channel (P/r, Q/r). by 13.5 dB or 79% improvement. On the other hand, the effectiveness of the crossfeeds (P/e, Q/e, P/c, and Q/c) on remainder four channels seem to be limited. Refer back to Figure 4.4~4.7, these template plots point out why the low-order dynamic crossfeed does not function well on these channels. From Figure 4.4 to 4.6, they all have large, over-lay templates which cannot be represented properly by the target points. In case of Figure 4.7, the size of the template is not enormous, but there is too much scatter in each frequency such that the templates are poorly represented by the small template shown on Figure 4.7.

Figure 6.2 Effect of the Low-Order Dynamic Crossfeeds

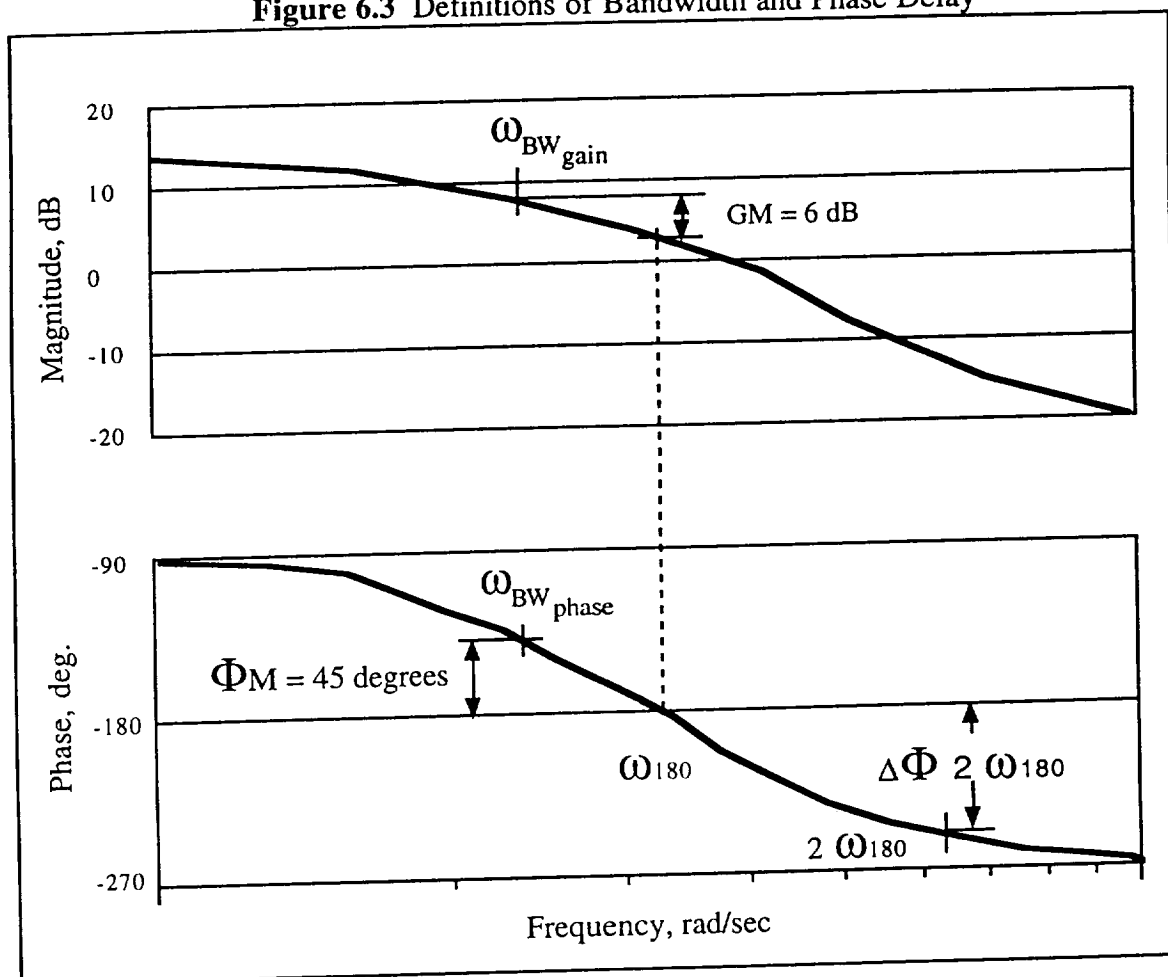


Handling Quality Analysis

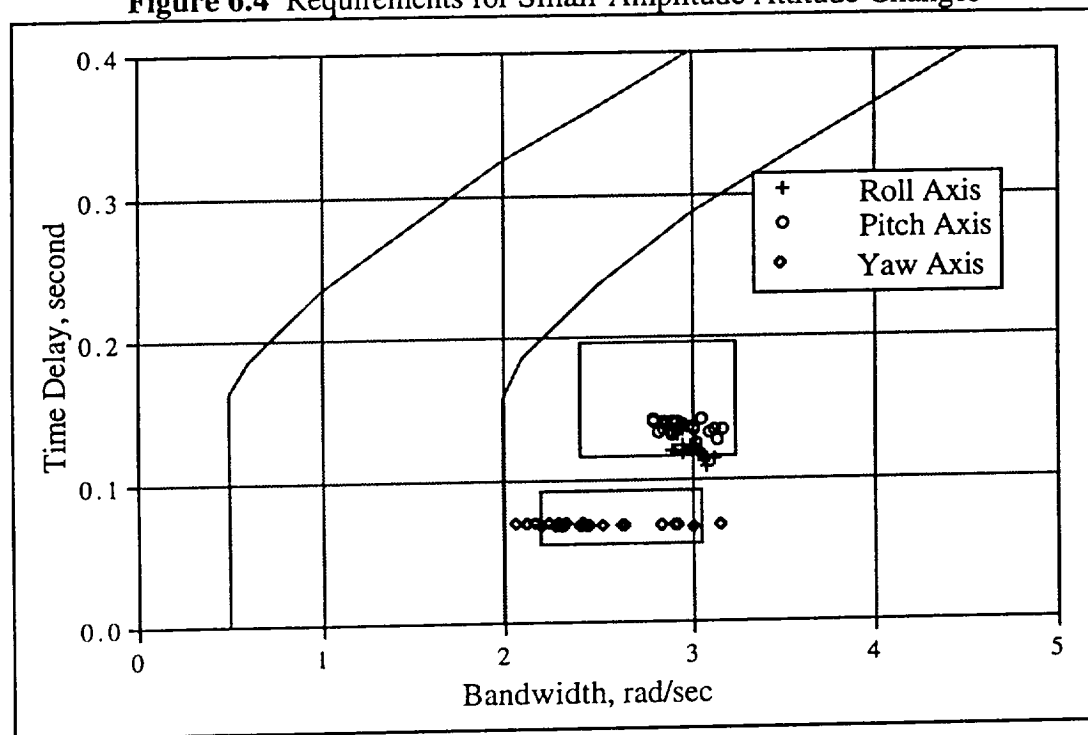
The handling quality analysis is based on the *Handling Qualities Requirements for Military Rotorcraft* (ADS-33C). In this study, three types of requirement are tested: Small-, Moderate-, Large-Amplitude Attitude Changes. All three requirements are evaluated by two variables: bandwidth and phase delay. The definitions (ref. 22)⁶ of these two variables are shown in Figure 6.3. Notice that the bandwidth of the system is the lesser one of $\omega_{BW_{gain}}$, $\omega_{BW_{phase}}$, and phase delay is calculated by following equation:

$$\tau_p = \frac{\Delta\phi_{2\omega_{180}}}{57.3 (2\omega_{180})}$$

⁶ ADS-33C, page 19, Figure 2(3.3)

Figure 6.3 Definitions of Bandwidth and Phase Delay**Small-Amplitude Attitude Change**

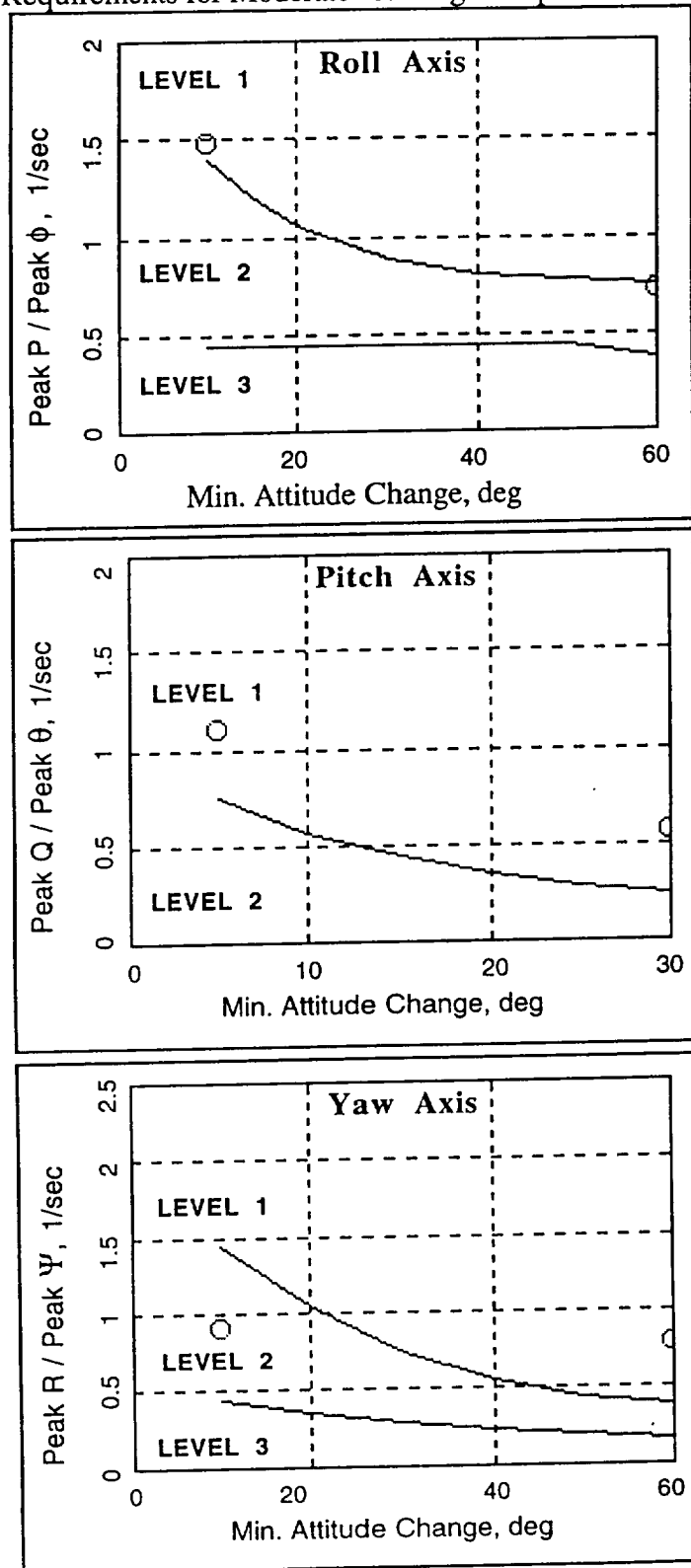
The handling qualities results of small-amplitude roll (pitch, yaw) attitude changes for hover and low speed is shown in Figure 6.4. The figures have shown that the handling qualities of small-amplitude change for all roll, pitch, and yaw axis are desirable (Level 1).

Figure 6.4 Requirements for Small-Amplitude Attitude Changes

Moderate-Amplitude Attitude Change

In the moderate-amplitude attitude change requirement (quickness), the aircraft must achieve a minimum attitude change of 10° in roll and yaw axis, and a minimum attitude change of 5° in pitch axis. The required attitude changes should be made as rapidly as possible from one steady attitude to another without significant reversals in the sign of the cockpit control input relative to the trim position. Most of the time the helicopter is able to perform this task but not quickly enough. The main reason for this slow reaction is excess time delay. The handling qualities results of moderate-amplitude roll (pitch, yaw) attitude changes for hover and low speed are shown in Figure 6.5. The figures have shown that the handling qualities of moderate-amplitude change for pitch axis are desirable (Level 1), but the roll and yaw axes are less desirable (Level 2).

Figure 6.5 Requirements for Moderate- & Large-Amplitude Attitude Changes



Large-Amplitude Attitude Change

From ADS-33C (ref. 22), the requirement for large-amplitude attitude changes is shown in Table XII. The handling quality study here is the level 1 aggressive maneuvering in rapid hovering turn. Under this requirement, the aircraft has to obtain a bank angle of $\pm 60^\circ$, pitch angle of $\pm 30^\circ$, and a yaw rate of ± 60 deg/sec, and their results are shown in Figure 6.5. Notice that the large-amplitude attitude change has lesser strict requirement compare to the moderate-amplitude one.

Table XII Requirements for Large-Amplitude Attitude Changes

	RATE RESPONSE-TYPE						ATTITUDE RESPONSE-TYPE			
	MINIMUM ACHIEVABLE ANGULAR RATE (deg/sec)						MINIMUM ACHIEVABLE ANGLE (deg)			
	LEVEL 1			LEVEL 2 & 3			LEVEL 1		LEVEL 2 & 3	
	q	p	r	q	p	r	θ	ϕ	θ	ϕ
<u>Limited Maneuvering</u> All MTEs not otherwise specified	± 6	± 21	± 6.5	± 3	± 15	± 5	± 15	± 15	± 7	± 10
<u>Moderate Maneuvering</u> Rapid transition to precision hover Slope Landing Shipboard landing	± 13	± 50	± 22	± 6	± 21	± 9.5	± 20 -30	± 60	± 13	± 30
<u>Aggressive Maneuvering</u> Rapid accel and decel Rapid sidestep Rapid hovering turn Rapid slalom Target acquisition and tracking Pullup/pushover Rapid bobup-bobdown	± 30	± 50	± 60	± 13	± 50	± 22	± 30	± 60	± 20 -30	± 30

Collective-to-Yaw Coupling Requirement

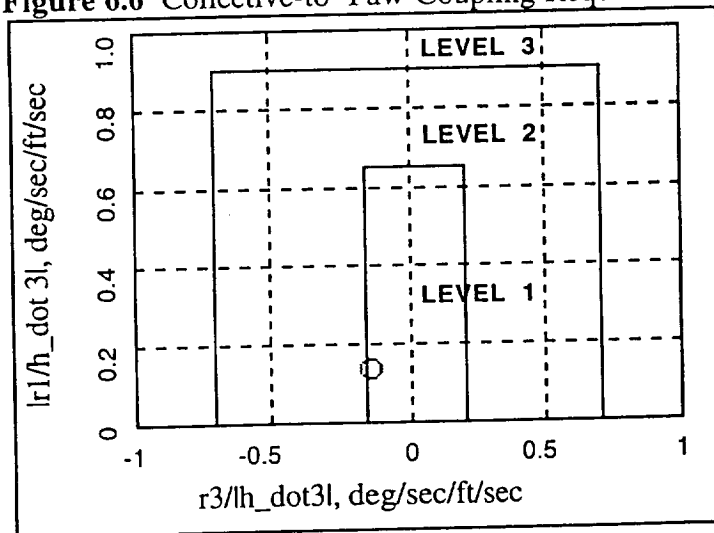
Unlike the roll, pitch, and yaw axis, the vertical axis (heave) does not have similar type of handling quality requirement. However, there is a collective-to-yaw coupling requirement which evaluates vertical axis performance. As it points out in ADS-33C, there should be no objectionable yaw oscillations following step or ramp collective changes in the positive and negative direction. Oscillations involving yaw rates greater than 5 deg/sec shall be deemed objectionable (ref. 22, Section 3.3.9.1, page 26). The evaluation of this requirement is based on following variables and their definition is shown below and analysis is present in Figure 6.6. Figure 6.6 shows that the collective-to-yaw coupling requirement is desirable (Level 1).

r_1 = first peak (before 3 seconds) or $r(1)$ if no peak occurs before 3 seconds

$r_3 = (r(3) - r_1)$ for $r_1 > 0$ or $(r_1 - r(3))$ for $r_1 < 0$

$r(1)$, $r(3)$ are yaw rate responses measured at 1 and 3 seconds, and $h(3)$ is altitude rate response measured at 3 seconds following a step collective input at $t = 0$.

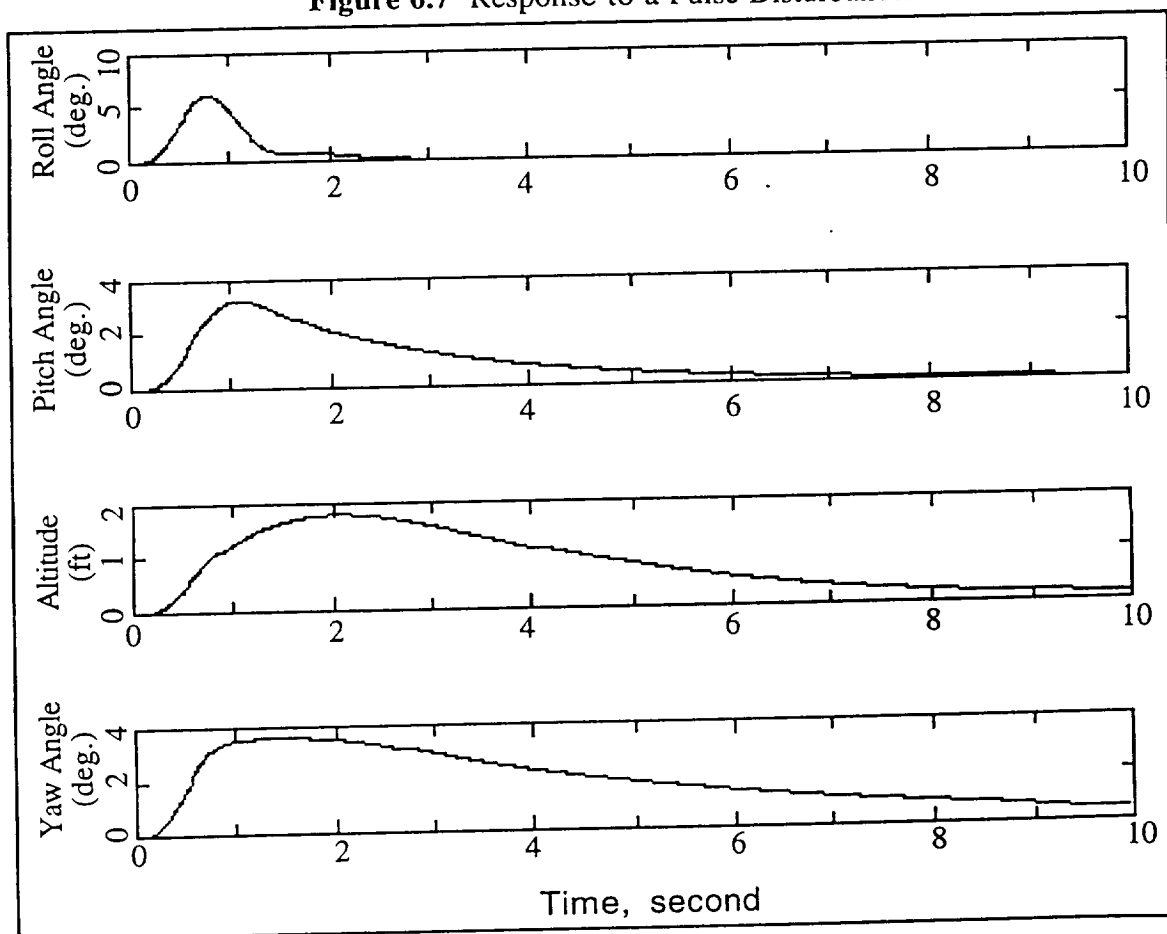
Figure 6.6 Collective-to-Yaw Coupling Requirements



Disturbance Rejection Performance

The objective of the feedback system is to attenuate undesired responses and disturbances. Disturbances are resulted from atmospheric and electrical inputs. A 1-inch pulse input of a 0.5 second duration is used to evaluate the disturbance rejection performance of the nominal plant closed-loop system. Time responses of the all four axes for the final closed-loop system is shown in Figure 6.7. The feedback control system is seen to achieve well damped closed-loop dynamics and good disturbance rejection in both roll and pitch axis, and less desirable results in heave and yaw axis. Overall, the QFT control system does yield a good disturbance rejection.

Figure 6.7 Response to a Pulse Disturbance.



CHAPTER VII

CONCLUSIONS & RECOMMENDATIONS

A four-input, four-output (roll, pitch, yaw, and heave) QFT controls design with robust crossfeeds was developed for a rotorcraft in near-hovering flight. The control system bandwidth allows the rotorcraft to be used as an inflight simulator. The resulting design proved to be superior to alternative control system designs using conventional fixed-gain crossfeeds and to feedback-only designs which rely on high gains to suppress undesired off-axis responses. The use of dynamic, robust crossfeeds prior to the QFT design conserved feedback gain and resulted in performance that meets current handling qualities specifications relative to the decoupling of off-axis responses. Handling qualities are level 1 for both low-gain tasks and high-gain tasks in roll, pitch, yaw axis except for the 10 deg/sec yaw command. It has a level 2 handling quality which is caused by phase lag.

Frequency dependent performance metrics focusing on piloted flight were developed, and decoupling criteria were implemented on 23 flight configurations. The decoupling criteria showed that only seven of the possible twelve crossfeeds were required. All but one of the resulting crossfeeds were implemented using transfer functions instead of fixed-gains to ensure robust decoupling. A weighting strategy was employed to ensure that the transfer functions were practical (i.e. stable and low order) and effective in the frequency range of piloted flight (0.2 to 2.0 rad/sec for the heave channel and 1.0 to 10.0 for the roll, pitch, and yaw channels).

The combined effect of the QFT feedback design following the implementation of low-order crossfeed compensators successfully decoupled ten of twelve off-axis channels more

than 20-dB (20 dB is 10% coupling between on-axis and off-axis responses). The remaining roll-from-elevator and heave-from-elevator channels resulted in 10.8 dB (29% coupling) and 17.2 dB (14% coupling) respectively. The relatively large coupling in these two channels was caused by abnormally large scatter in the frequency response data of the ideal decoupling crossfeeds for the 23 configurations, making it impossible to replace them with a single, low-order crossfeed.

It is recommended that a linear QFT controller tuned and digitized to the flight model be developed, implemented, and tested on an accurate non-linear flight simulation. Performance and disturbance specifications for this case remain to be developed. Finally, a new strategy of selecting low-order dynamic crossfeeds is needed when there is excessive scatter in the ideal crossfeed frequency response data.

REFERENCES

- 1) Catapang, D., Tischler, M. B., and D. J. Biezad, "Robust Crossfeed Design for Hovering Rotorcraft," Proceedings of the Quantitative Feedback Theory Symposium, USAF Document WL-TR-92-3036, Wright-Patterson AFB, Ohio, August 1992, pp. 190-211.
- 2) Tischler, M. B. "Digital Control of Highly Augmented Combat Rotorcraft." NASA-TM 88346 and USAAVSCOM TR 87-A-5. Ames Research Center, Moffett Field, May 1987.
- 3) Houppis, C. H. "Quantitative Feedback Theory (QFT): Technique for Designing Multivariable Control System." AFWAL-TR-86-3107. Air Force Wright Aeronautical Laboratories, Wright-Patterson AFB, Ohio, January 1987.
- 4) McRuer, D. T., Ashkenas, I. L., and Pass, H. R. "Analysis of Multi-loop vehicular Control Systems." ASR-TDR-62-1014. Wright-Patterson Air Force Base, Ohio, March 1964.
- 5) McRuer, D. T., Ashkenas, I. L., and Graham, D. Aircraft Dynamics and Automatic Control. Princeton University Press, New Jersey, 1973.
- 6) Hoh, R. H., Myers, T. T., Ashkenas, I. L., Ringland, R. R., and Craig, S. "Development of Handling Quality Criteria for Aircraft with Independent Control of six Degrees of Freedom." TR-81-3027, Air Force Wright Aeronautical Laboratories, Ohio, April 1981.
- 7) Anonymous. "Background Information and Handling Qualities Regiments for Military Rotorcraft." USAAVSCOM TR 89-A-008. 1989.8)
- 8) Kim, F. D., Celi, R. "Simulation Modeling for Combat Rotorcraft Flight Control System Design." Joint research Interchange NCA2-310. University of Maryland, College Park, June 1990.
- 9) Catapang, D. R., "Robust Crossfeed Design for hovering Rotorcraft," M. S. thesis, Cal Poly State University, April 1993.
- 10) Jewell, W. F., Clement, W. F., "Crossfeed compensation Techniques for Decoupling Rotorcraft Responses to Control Inputs, TR-1229-1, Systems Technology, Inc., Sept. 1985.
- 11) Lee, Eugene A. "LCAP2- Linear Controls Analysis Program." IEEE Control Systems Magazine. vol. 2, no. 4, December 1982, pp.15-18.
- 12) Hodgkinson, J., and Buckley, J. "NAVFIT- General Purpose Frequency Response Curve Fit Program (Arbitrary Order)." October 1978.
- 13) Yaniv, O., "Multiple-Input Single-Output (MISO) QFT-CAD User Manual," Dept. of Electrical Engineering systems, tel-Aviv University, Tel-Aviv, Israel, Dec 1991.

- 14) Hess, R. A., and P. J. Gorder, "Quantitative Feedback Theory applied to the Design of a Rotorcraft Flight control Systems," *Journal of Guidance, Control, and Dynamics*, Vol. 16, No. 4, July-August 1993, pp. 748-753.
- 15) Horowitz, I., *Quantitative Feedback Design Theory*, Vol. 1, QFT Publications, Boulder Colorado, 80303, 1992.
- 16) Horowitz, I., "Survey of Quantitative Feedback Theory (QFT), *International Journal of Control*, Vol. 53, No. 2, 1991, pp. 255-291.
- 17) Takahashi, M. D. "Flight-Control Design Using Rotor-State Feedback for an Articulated Rotor Helicopter in Hover." NASA-TM 103967 and USAATCOM TR 92-A-012. Ames Research Center, Moffett Field, January 1993.
- 18) Takahashi, M. D. "H infinity Flight Control Law Design with and without Rotor State Feedback." AIAA-93-3849. Ames Research Center, Moffett Field, August 1993.
- 19) Kim, F. D. "Forecast Manual", Ames Research Center, Moffett Field Contact Dr. Tischler for detail
- 20) Landis, Kenneth H. and Glusman, Steven I. "Development of ADOCS Controllers and Control Laws." NASA CR-177339, 1985
- 21) MATLAB SIMULINK, Math Works Corp.
- 22) United States Army Aviation Systems Command, "Handling Qualities Requirements for Military Rotorcraft", ADS-33C, ST. Louis, MO., August, 1989

APPENDIX A

State Vector used in the Forecast Model

Name	Description	State Index
u	Forward Velocity	0
v	Sideward Velocity	0
w	Heave	1
p	Roll Rate	2
q	Pitch Rate	3
r	Yaw Rate	4
Phi	Roll Angle	5
Theta	Pitch Angle	6
Psi	Yaw Angle	0
beta_0-dot	Collective Flap Rate	7
beta_1c-dot	Longitudinal Flap Rate	8
beta_1s-dot	Lateral Flap Rate	9
beta_2-dot	Differential Flap Rate	-1
beta_0	Collective Flap	10
beta_1c	Longitudinal Flap	11
beta_1s	Lateral Flap	12
beta_2	Differential Flap	-1
zeta_0-dot	Collective Lag Rate	-1
zeta_1c-dot	Longitudinal Lag Rate	-1
zeta_1s-dot	Lateral Lag Rate	-1
zeta_2-dot	Differential Lag Rate	-1
zeta_0	Collective Lag	-1
zeta_1c	Longitudinal Lag	-1
zeta_1s	Lateral Lag	-1
zeta_2	Differential Lag	-1
phi_dyn	Dynamic Twist	-1
phi_dyn-dot	Dynamic Twist Rate	-1
lambda	Constant Inflow	13

APPENDIX B

Group I : Most Probable

Flight Configuration 1	Hovering
Flight Configuration 2	15 Knots Forward
Flight Configuration 3	15 Knots Rearward
Flight Configuration 7	15 Knots, $\beta = 80^\circ$
Flight Configuration 9	15 Knots, $\beta = -80^\circ$

Group II : Less Probable

Flight Configuration 6	15 Knots, $\beta = 45^\circ$
Flight Configuration 8	15 Knots, $\beta = -45^\circ$
Flight Configuration 14	6 Knots, $\gamma = 80^\circ$
Flight Configuration 15	6 Knots, $\gamma = -70^\circ$

Group III : Least Probable

Flight Configuration 4	30 Knots Forward
Flight Configuration 5	30 Knots, $\beta = 180^\circ$
Flight Configuration 10	30 Knots, $\beta = 45^\circ$
Flight Configuration 11	30 Knots, $\beta = 80^\circ$ (Not Trimmed)
Flight Configuration 12	30 Knots, $\beta = -45^\circ$
Flight Configuration 13	30 Knots, $\beta = -80^\circ$
Flight Configuration 16	12 Knots, $\gamma = 80^\circ$
Flight Configuration 17	45 Knots, $\gamma = -7.06^\circ$, $\phi = 20^\circ$ (Not Trimmed)
Flight Configuration 18	45 Knots, $\gamma = -7.06^\circ$, $\phi = -20^\circ$
Flight Configuration 19	45 Knots, $\gamma = 7.06^\circ$, $\phi = 20^\circ$
Flight Configuration 20	Hovering, Main Rotor Speed = 24 rad/sec
Flight Configuration 21	Hovering, Main Rotor Speed = 30 rad/sec
Flight Configuration 22	Hovering, Weight = 20,000 lbs
Flight Configuration 23	45 Knots, $\gamma = -7.06^\circ$, $\phi = 20^\circ$, Weight = 20,000 lbs
Flight Configuration 24	Hovering, Forward CG
Flight Configuration 25	Hovering, Aft CG

APPENDIX C

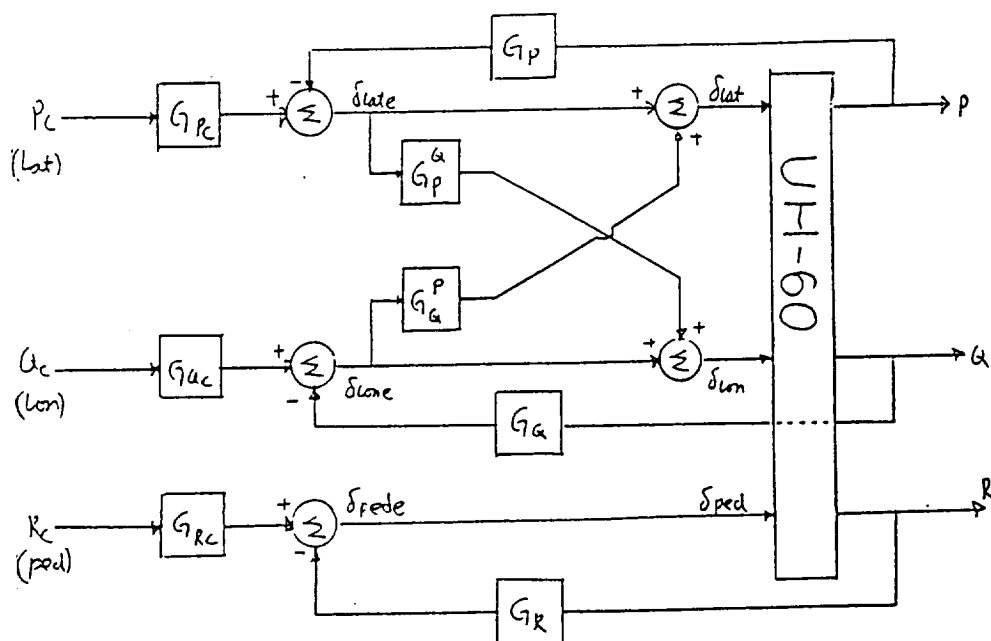
Derivation of Coupling Numerator For Pitch-from-Aileron Coupling

$$\begin{bmatrix} \delta_{lat} \\ \delta_{lon} \\ \delta_{ped} \end{bmatrix} = \begin{bmatrix} 1 & G_a^p & 0 \\ G_p^a & 1 & 0 \\ 0 & 0 & 1 \end{bmatrix} \begin{bmatrix} \delta_{lat}^* \\ \delta_{lon}^* \\ \delta_{ped}^* \end{bmatrix} \quad \text{--- Eqn (1)}$$

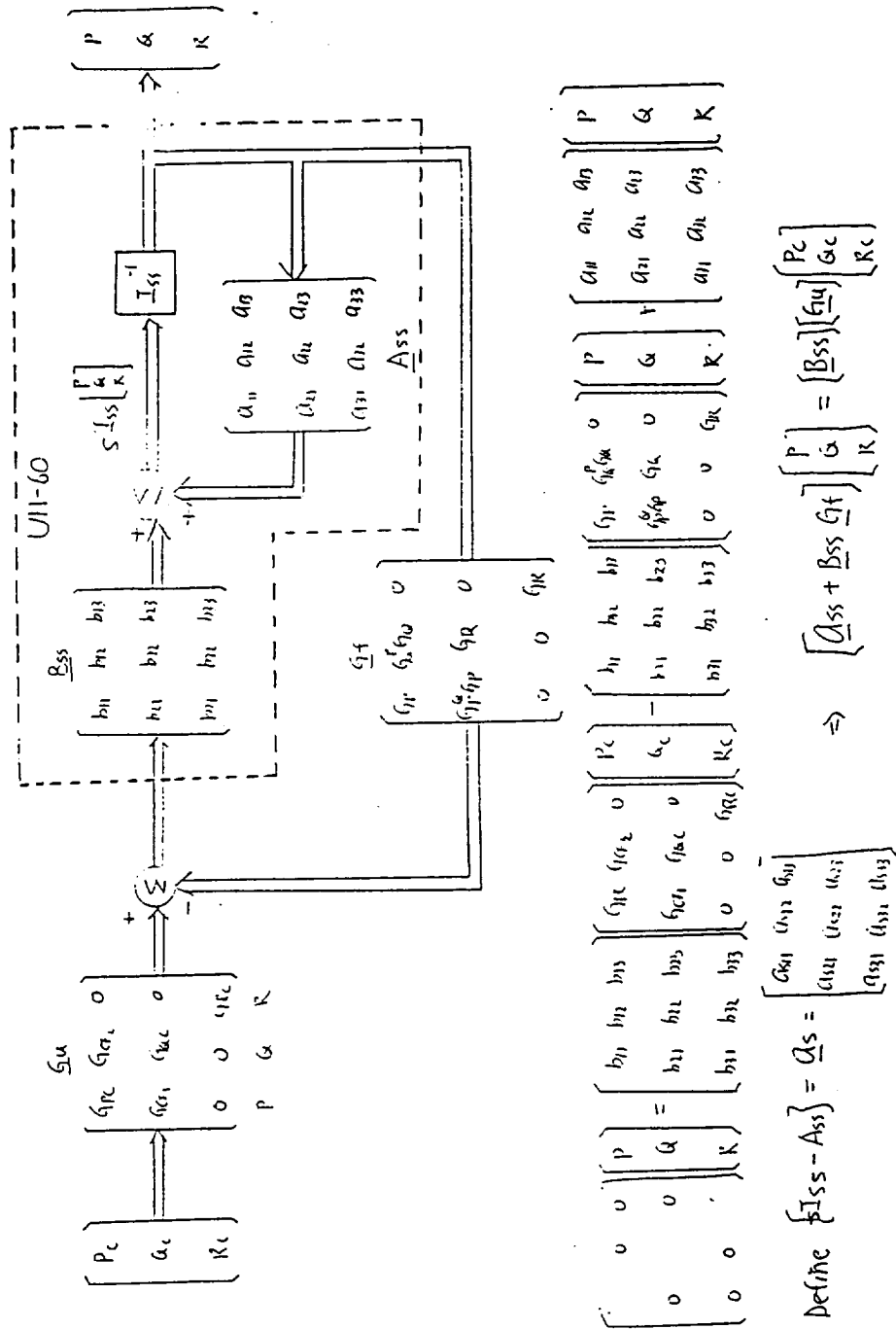
$$\begin{bmatrix} \delta_{lat}^* \\ \delta_{lon}^* \\ \delta_{ped}^* \end{bmatrix} = \begin{bmatrix} G_{pc} & 0 & 0 \\ 0 & G_{ac} & 0 \\ 0 & 0 & G_{rc} \end{bmatrix} \begin{bmatrix} P_c \\ Q_c \\ R_c \end{bmatrix} = \begin{bmatrix} G_p & 0 & 0 \\ 0 & G_a & 0 \\ 0 & 0 & G_R \end{bmatrix} \begin{bmatrix} P \\ Q \\ R \end{bmatrix} \quad \text{--- Eqn (2)}$$

Substitute Eqn (2) into Eqn (1)

$$\begin{aligned} \begin{bmatrix} \delta_{lat} \\ \delta_{lon} \\ \delta_{ped} \end{bmatrix} &= \begin{bmatrix} 1 & G_a^p & 0 \\ G_p^a & 1 & 0 \\ 0 & 0 & 1 \end{bmatrix} \begin{bmatrix} G_{pc} & 0 & 0 \\ 0 & G_{ac} & 0 \\ 0 & 0 & G_{rc} \end{bmatrix} \begin{bmatrix} P_c \\ Q_c \\ R_c \end{bmatrix} = \begin{bmatrix} 1 & G_a^p & 0 \\ G_p^a & 1 & 0 \\ 0 & 0 & 1 \end{bmatrix} \begin{bmatrix} G_p & 0 & 0 \\ 0 & G_a & 0 \\ 0 & 0 & G_R \end{bmatrix} \begin{bmatrix} P \\ Q \\ R \end{bmatrix} \\ &= \begin{bmatrix} G_{pc} & G_a^p G_{ac} & 0 \\ G_p^a G_{pc} & G_{ac} & 0 \\ 0 & 0 & G_{rc} \end{bmatrix} \begin{bmatrix} P_c \\ Q_c \\ R_c \end{bmatrix} = \begin{bmatrix} G_p & G_a^p G_a & 0 \\ G_p^a G_p & G_a & 0 \\ 0 & 0 & G_R \end{bmatrix} \begin{bmatrix} P \\ Q \\ R \end{bmatrix} \quad \begin{aligned} \text{let } G_{ca1} &= G_p^a G_{pc} \\ G_{ca2} &= G_a^p G_{ac} \end{aligned} \\ &= \begin{bmatrix} G_{pc} & G_{ca1} & 0 \\ G_{ca2} & G_{ac} & 0 \\ 0 & 0 & G_{rc} \end{bmatrix} \begin{bmatrix} P_c \\ Q_c \\ R_c \end{bmatrix} = \begin{bmatrix} G_p & G_a^p G_a & 0 \\ G_p^a G_p & G_a & 0 \\ 0 & 0 & G_R \end{bmatrix} \begin{bmatrix} P \\ Q \\ R \end{bmatrix} \end{aligned}$$



Derivation of Coupling Numerator For Pitch-from-Aileron Coupling (continued)



Derivation of Coupling Numerator For Pitch-from-Aileron Coupling (continued)

$$\begin{bmatrix} a_{s11} + g_p b_{11} + g_p^G g_p b_{12}, & a_{s12} + g_a^P b_{11} + g_a b_{12}, & a_{s13} + g_R b_{13} \\ a_{s21} + g_p b_{21} + g_p^G g_p b_{22}, & a_{s22} + g_a^P b_{21} + g_a b_{22}, & a_{s23} + g_R b_{23} \\ a_{s31} + g_p b_{31} + g_p^G g_p b_{32}, & a_{s32} + g_a^P b_{31} + g_a b_{32}, & a_{s33} + g_R b_{33} \end{bmatrix} \begin{bmatrix} P \\ Q \\ R \end{bmatrix} = \begin{bmatrix} b_{11} g_{pc} + b_{12} g_{ce}, & b_{11} g_{ce} + b_{12} g_{ce}, & g_{RC} b_{13} \\ b_{21} g_{pc} + b_{22} g_{ce}, & b_{21} g_{ce} + b_{22} g_{ce}, & g_{RC} b_{23} \\ b_{31} g_{pc} + b_{32} g_{ce}, & b_{31} g_{ce} + b_{32} g_{ce}, & g_{RC} b_{33} \end{bmatrix} \begin{bmatrix} P_c \\ Q_c \\ R_c \end{bmatrix}$$

* Solve for $\frac{Q}{P_c} =$

$$\begin{bmatrix} a_{s11} + g_p b_{11} + g_p^G g_p b_{12}, & b_{11} g_{pc} + b_{12} g_{ce}, & a_{s13} + g_R b_{13} \\ a_{s21} + g_p b_{21} + g_p^G g_p b_{22}, & b_{21} g_{pc} + b_{22} g_{ce}, & a_{s23} + g_R b_{23} \\ a_{s31} + g_p b_{31} + g_p^G g_p b_{32}, & b_{31} g_{pc} + b_{32} g_{ce}, & a_{s33} + g_R b_{33} \end{bmatrix} \begin{bmatrix} P \\ Q \\ R \end{bmatrix} = \frac{N}{D}$$

$$N = \begin{bmatrix} a_{s11} & b_{11} g_{pc} & a_{s13} \\ a_{s21} & b_{21} g_{pc} & a_{s23} \\ a_{s31} & b_{31} g_{pc} & a_{s33} \end{bmatrix} + \begin{bmatrix} a_{s11} & b_{11} g_{ce} & g_{RC} b_{13} \\ a_{s21} & b_{21} g_{ce} & g_{RC} b_{23} \\ a_{s31} & b_{31} g_{ce} & g_{RC} b_{33} \end{bmatrix} + \begin{bmatrix} a_{s11} & b_{12} g_{ce} & a_{s13} \\ a_{s21} & b_{22} g_{ce} & a_{s23} \\ a_{s31} & b_{32} g_{ce} & a_{s33} \end{bmatrix} + \begin{bmatrix} a_{s11} & b_{12} g_{ce} & g_{RC} b_{13} \\ a_{s21} & b_{22} g_{ce} & g_{RC} b_{23} \\ a_{s31} & b_{32} g_{ce} & g_{RC} b_{33} \end{bmatrix} + \begin{bmatrix} g_p b_{11} & b_{11} g_{pc} & a_{s13} \\ g_p b_{21} & b_{21} g_{pc} & a_{s23} \\ g_p b_{31} & b_{31} g_{pc} & a_{s33} \end{bmatrix} + \begin{bmatrix} g_p b_{11} & b_{11} g_{ce} & a_{s13} \\ g_p b_{21} & b_{21} g_{ce} & a_{s23} \\ g_p b_{31} & b_{31} g_{ce} & a_{s33} \end{bmatrix} + \begin{bmatrix} g_p b_{11} & b_{12} g_{ce} & g_{RC} b_{13} \\ g_p b_{21} & b_{22} g_{ce} & g_{RC} b_{23} \\ g_p b_{31} & b_{32} g_{ce} & g_{RC} b_{33} \end{bmatrix} + \begin{bmatrix} g_p^G g_p b_{12} & b_{11} g_{ce} & a_{s13} \\ g_p^G g_p b_{22} & b_{21} g_{ce} & a_{s23} \\ g_p^G g_p b_{32} & b_{31} g_{ce} & a_{s33} \end{bmatrix} + \begin{bmatrix} g_p^G g_p b_{12} & b_{12} g_{ce} & g_{RC} b_{13} \\ g_p^G g_p b_{22} & b_{22} g_{ce} & g_{RC} b_{23} \\ g_p^G g_p b_{32} & b_{32} g_{ce} & g_{RC} b_{33} \end{bmatrix} + \begin{bmatrix} g_p^G g_p b_{12} & b_{11} g_{ce} & a_{s13} \\ g_p^G g_p b_{22} & b_{21} g_{ce} & a_{s23} \\ g_p^G g_p b_{32} & b_{31} g_{ce} & a_{s33} \end{bmatrix} + \begin{bmatrix} g_p^G g_p b_{12} & b_{12} g_{ce} & g_{RC} b_{13} \\ g_p^G g_p b_{22} & b_{22} g_{ce} & g_{RC} b_{23} \\ g_p^G g_p b_{32} & b_{32} g_{ce} & g_{RC} b_{33} \end{bmatrix} \neq \frac{1}{4}$$

$$\begin{aligned} &= \left[g_{pc} N_{\delta_{lat}}^Q + g_{ce} g_R N_{\delta_{lat} \delta_{ped}}^Q + g_{ce} N_{\delta_{lat}}^Q + g_{ce} g_R N_{\delta_{lat} \delta_{ped}}^Q + g_p g_{pc} N_{\delta_{lat} \delta_{ped}}^Q + g_p g_{ce} g_R N_{\delta_{lat} \delta_{ped}}^Q \right. \\ &\quad + g_p g_{ce} N_{\delta_{lat} \delta_{ped}}^Q + g_p g_{ce} g_R \Delta_{\delta_{lat}} + g_p^G g_p g_{ce} N_{\delta_{lat} \delta_{ped}}^Q + g_p^G g_p g_{ce} g_R N_{\delta_{lat} \delta_{ped}}^Q \\ &\quad \left. + g_p^G g_p g_{ce} N_{\delta_{lat} \delta_{ped}}^Q + g_p^G g_p g_{ce} g_R N_{\delta_{lat} \delta_{ped}}^Q \right] \neq \frac{1}{4} \end{aligned}$$

* No P, Q feed back so $g_p = 0, g_a = 0$

$$N = \left[g_{pc} N_{\delta_{lat}}^Q + g_{ce} g_R N_{\delta_{lat} \delta_{ped}}^Q + g_{ce} N_{\delta_{lat}}^Q + g_{ce} g_R N_{\delta_{lat} \delta_{ped}}^Q \right] \neq \frac{1}{4}$$

Derivation of Coupling Numerator For Pitch-from-Aileron Coupling (continued)

$$D = \begin{bmatrix} \begin{vmatrix} a_{s11} & a_{s12} & a_{s13} \\ a_{s21} & a_{s22} & a_{s23} \\ a_{s31} & a_{s32} & a_{s33} \end{vmatrix} & + & \begin{vmatrix} a_{s11} & a_{s12} & g_{rb13} \\ a_{s21} & a_{s22} & g_{rb23} \\ a_{s31} & a_{s32} & g_{rb33} \end{vmatrix} & + & \begin{vmatrix} a_{s11} & g_a^p g_{ab11} & a_{s13} \\ a_{s21} & g_a^p g_{ab21} & a_{s23} \\ a_{s31} & g_a^p g_{ab31} & a_{s33} \end{vmatrix} & + & \begin{vmatrix} a_{s11} & g_a^p g_{ab11} & g_{rb13} \\ a_{s21} & g_a^p g_{ab21} & g_{rb23} \\ a_{s31} & g_a^p g_{ab31} & g_{rb33} \end{vmatrix} \\ + & \begin{vmatrix} a_{s11} & g_a b_{12} & a_{s13} \\ a_{s21} & g_a b_{22} & a_{s23} \\ a_{s31} & g_a b_{32} & a_{s33} \end{vmatrix} & + & \begin{vmatrix} a_{s11} & g_a b_{12} & g_{rb13} \\ a_{s21} & g_a b_{22} & g_{rb23} \\ a_{s31} & g_a b_{32} & g_{rb33} \end{vmatrix} & + & \begin{vmatrix} g_{pb11} & a_{s12} & a_{s13} \\ g_{pb21} & a_{s22} & a_{s23} \\ g_{pb31} & a_{s32} & a_{s33} \end{vmatrix} & + & \begin{vmatrix} g_{pb11} & a_{s12} & g_{rb13} \\ g_{pb21} & a_{s22} & g_{rb23} \\ g_{pb31} & a_{s32} & g_{rb33} \end{vmatrix} \\ + & \begin{vmatrix} g_{pb11} & g_a^p g_{ab11} & a_{s13} \\ g_{pb21} & g_a^p g_{ab21} & a_{s23} \\ g_{pb31} & g_a^p g_{ab31} & a_{s33} \end{vmatrix} & + & \begin{vmatrix} g_{pb11} & g_a^p g_{ab11} & g_{rb13} \\ g_{pb21} & g_a^p g_{ab21} & g_{rb23} \\ g_{pb31} & g_a^p g_{ab31} & g_{rb33} \end{vmatrix} & + & \begin{vmatrix} g_{pb11} & g_a b_{12} & a_{s13} \\ g_{pb21} & g_a b_{22} & a_{s23} \\ g_{pb31} & g_a b_{32} & a_{s33} \end{vmatrix} & + & \begin{vmatrix} g_{pb11} & g_a b_{12} & g_{rb13} \\ g_{pb21} & g_a b_{22} & g_{rb23} \\ g_{pb31} & g_a b_{32} & g_{rb33} \end{vmatrix} \\ + & \begin{vmatrix} g_{p^a p^a} g_{p^a} g_{p^a} a_{s12} & a_{s13} \\ g_{p^a p^a} g_{p^a} a_{s22} & a_{s23} \\ g_{p^a p^a} g_{p^a} a_{s32} & a_{s33} \end{vmatrix} & + & \begin{vmatrix} g_{p^a p^a} g_{p^a} a_{s12} & g_{rb13} \\ g_{p^a p^a} g_{p^a} a_{s22} & g_{rb23} \\ g_{p^a p^a} g_{p^a} a_{s32} & g_{rb33} \end{vmatrix} & + & \begin{vmatrix} g_{p^a p^a} g_{p^a} g_a^p g_{ab11} & a_{s13} \\ g_{p^a p^a} g_{p^a} g_a^p g_{ab21} & a_{s23} \\ g_{p^a p^a} g_{p^a} g_a^p g_{ab31} & a_{s33} \end{vmatrix} & + & \begin{vmatrix} g_{p^a p^a} g_{p^a} g_a^p g_{ab11} & g_{rb13} \\ g_{p^a p^a} g_{p^a} g_a^p g_{ab21} & g_{rb23} \\ g_{p^a p^a} g_{p^a} g_a^p g_{ab31} & g_{rb33} \end{vmatrix} \\ + & \begin{vmatrix} g_{p^a p^a} g_{p^a} g_a^p g_{ab11} & a_{s13} \\ g_{p^a p^a} g_{p^a} g_a^p g_{ab21} & a_{s23} \\ g_{p^a p^a} g_{p^a} g_a^p g_{ab31} & a_{s33} \end{vmatrix} & + & \begin{vmatrix} g_{p^a p^a} g_{p^a} g_a^p g_{ab11} & g_{rb13} \\ g_{p^a p^a} g_{p^a} g_a^p g_{ab21} & g_{rb23} \\ g_{p^a p^a} g_{p^a} g_a^p g_{ab31} & g_{rb33} \end{vmatrix} & + & \begin{vmatrix} g_{p^a p^a} g_{p^a} g_a^p g_{ab11} & g_{rb13} \\ g_{p^a p^a} g_{p^a} g_a^p g_{ab21} & g_{rb23} \\ g_{p^a p^a} g_{p^a} g_a^p g_{ab31} & g_{rb33} \end{vmatrix} & + & \begin{vmatrix} g_{p^a p^a} g_{p^a} g_a^p g_{ab11} & g_{rb13} \\ g_{p^a p^a} g_{p^a} g_a^p g_{ab21} & g_{rb23} \\ g_{p^a p^a} g_{p^a} g_a^p g_{ab31} & g_{rb33} \end{vmatrix} \end{bmatrix} \frac{1}{6}$$

$$= \frac{1}{6} \left[\Delta_A + g_{ra} N_{\delta_{lat}}^K + g_a^p g_a N_{\delta_{lat}}^Q + g_a^p g_a g_{ra} N_{\delta_{lat} \delta_{roll}}^K + g_a N_{\delta_{lat}}^Q + g_a g_{ra} N_{\delta_{lat} \delta_{roll}}^K \right. \\ + g_p N_{\delta_{lat}}^P - g_p g_a N_{\delta_{lat} \delta_{roll}}^P + g_p g_a g_a N_{\delta_{lat} \delta_{roll}}^P + g_p g_a g_a g_{ra} N_{\delta_{lat} \delta_{roll} \delta_{roll}}^P \\ + g_{ra} g_a N_{\delta_{lat} \delta_{roll}}^P + g_p g_{ra} g_{ra} \Delta_B + g_p g_a N_{\delta_{lat}}^P + g_p g_a g_{ra} N_{\delta_{lat} \delta_{roll}}^P \\ + g_p g_a g_a N_{\delta_{lat} \delta_{roll}}^P + g_p g_a g_a g_{ra} N_{\delta_{lat} \delta_{roll} \delta_{roll}}^P + g_p g_a g_a N_{\delta_{lat} \delta_{roll}}^P \\ \left. + g_p g_a g_a g_{ra} N_{\delta_{lat} \delta_{roll} \delta_{roll}}^P \right]$$

Derivation of Coupling Numerator For Pitch-from-Aileron Coupling (continued)

* NO F_z feedback. $\therefore G_{fp} = 0, G_{fq} = 0$

$$D = \frac{1}{6} [\Delta A_s + G_R N_{\delta_{ped}}^R]$$

$$\frac{Q}{P_c} = \frac{\frac{1}{4} [G_{pe} N_{\delta_{lat}}^Q + G_{pe} G_R N_{\delta_{lat}}^Q N_{\delta_{ped}}^R + G_{cr} N_{\delta_{lat}}^Q + G_{cr} G_R N_{\delta_{lat}}^Q N_{\delta_{ped}}^R]}{\frac{1}{6} [\Delta A_s + G_R N_{\delta_{ped}}^R]}$$

* When the yaw feedback loop is tight ($G_R \gg 1$), G_R terms weight more

$$\frac{Q}{P_c} \approx \frac{G_{pe} G_R N_{\delta_{lat}}^Q N_{\delta_{ped}}^R + G_{cr} G_R N_{\delta_{lat}}^Q N_{\delta_{ped}}^R}{G_R N_{\delta_{ped}}^R}$$

* For ideal cross feed, $\frac{Q}{P_c} = 0 \quad \therefore 11 = 0$

$$G_{pe} G_R N_{\delta_{lat}}^Q N_{\delta_{ped}}^R + G_{cr} G_R N_{\delta_{lat}}^Q N_{\delta_{ped}}^R = 0$$

* Let $G_{pe} = 1 \Rightarrow G_{cr} = G_{pe} G_p^Q = G_p^Q$

$$G_p^Q = - \frac{N_{\delta_{lat}}^Q N_{\delta_{ped}}^R}{N_{\delta_{lat}}^Q N_{\delta_{ped}}^R}$$

* By apply similar way, G_q^P can be determine

$$G_q^P = - \frac{N_{\delta_{lat}}^P N_{\delta_{ped}}^R}{N_{\delta_{lat}}^P N_{\delta_{ped}}^R}$$

where $G_{qc} = 1$